FRACTURE CHARACTERISTICS AND DISTRIBUTION IN EXPOSED CRETACEOUS ROCKS NEAR THE UMIAT ANTICLINE, NORTH SLOPE OF ALASKA

By

Raelene Wentz

RECOMMENDED:

Dr. Paul McCarthy

Dr. Wesley Wallace

Dr. Catherine Hanks
Advisory Committee Chair

Dr. Paul McCarthy
Chair, Department of Geology and Geophysics

APPROVED:

Dr. Paul Layer
Dean, College of Natural Science and Mathematics

Dr. John Eichelberger
Dean of Graduate School

8/15/14
Date

FRACTURE CHARACTERISTICS AND DISTRIBUTION IN CRETACEOUS ROCKS NEAR THE UMIAT ANTICLINE, NORTH SLOPE OF ALASKA

A

THESIS

Presented to the Faculty

of the University of Alaska Fairbanks

in Partial Fulfillment of the Requirements

for the Degree of

MASTER OF SCIENCE

By

Raelene Wentz, B.S.

Fairbanks, Alaska

August 2014

ABSTRACT

Umiat oil field in the southeast part of the National Petroleum Reserve–Alaska is a shallow, thrust-related anticline in the northern foothills of the Brooks Range and was one of the earliest discovered oil fields on the North Slope of Alaska. Despite significant reserves of light oil, Umiat has remained undeveloped because the reservoirs are located at shallow depths within the permafrost. Recent development of horizontal drilling techniques could provide access to this shallow reservoir with a minimal surface footprint, and has caused industry to take a second look at Umiat.

Fracture networks are valuable in petroleum systems because they can enhance both porosity and permeability in a reservoir and they act as migration pathways from source rocks to reservoir. At Umiat, natural fractures, if open, could enhance reservoir permeability or, if filled with cement or ice, could impede fluid flow. In order to determine the potential of fractures at Umiat, I examined core from older Umiat wells and surveyed fractures at four exposed anticlines similar to Umiat anticline. Three fracture sets were observed in the surface anticlines: an early north-south set of calcite-filled regional extension fractures that predate folding and are interpreted as due to elevated pore pressures during burial and under north-south compression; east-west oriented, unfilled hinge-parallel extension fractures that formed during folding due to outer arc tangential longitudinal strain in fold hinges; and a set of unfilled, vertical conjugate shear fractures oriented perpendicular to fold hinges that is interpreted as having developed on the fold limbs.

Several natural fractures were identified in unoriented core from Umiat wells. These natural fractures dip steeply with respect to bedding and are calcite cemented and/or open. Lack of orientation data precludes assigning these fractures directly to a fracture set observed in

surface exposures, but the presence of, calcite cement suggest that these fractures belong to the early, north-south oriented calcite-filled fracture set seen in nearby surface exposures.

These observations suggest that production in horizontal legs could vary depending on the azimuth of the borehole. North-south, calcite-filled fractures could serve as permeability baffles and reduce flow in north-south oriented legs. Alternatively, horizontal legs that encounter the open hinge-parallel fractures or hinge perpendicular conjugate set could experience early water breakthrough or loss of circulation.

TABLE OF CONTENTS

Page

Signature Page i

Title Page iii

Abstract v

Table of Contents vii

List of Figures xi

List of Tables xv

Acknowledgments xvii

Chapter 1: Introduction 1

Chapter 2: Fractures in Foreland Basin Systems 5

2.1 Introduction 5

2.2 Fracture formation and types of fractures 6

2.3 Mechanical stratigraphy and fractures 8

2.4 Fractures in flat-lying rocks 9

2.5 Fold-related fractures 10

2.6 Fracture evolution in foreland fold-and-thrust belts and fluid flow 15

Chapter 3: Regional Geology 19

3.1 Geologic setting 19

3.2 Stratigraphy 24

3.2.1. Colville basin stratigraphy 26

3.2.2 Brookian Sequence, Torok Formation 27

3.2.3 Brookian Sequence, Nanushuk Formation 28

3.2.4. Brookian Sequence, Seabee Formation 29

3.2.5 Brookian Sequence, Tuluvak Formation 30

3.3 General structural style of the Brooks Range foothills 30

3.4 Previous fracture studies in northern Alaska 33

3.5 Age of deformation of the central Brooks Range foothills in the southern Colville basin 36

3.6 Umiat anticline and oil field 38

3.7 Geology of the study area 41

Chapter 4: Methods 45

4.1 Introduction 45

4.2 Identification of fractures in cores 45

4.3 Surface fracture mapping 47

Chapter 5: Observations 49

5.1 Fracture distribution and characteristics in Umiat core 49

5.2 Fracture character and distribution in the field 55

5.2.1 Structural data 59

5.2.2 Colville incision observations 63

5.2.3 Fossil Creek anticline: south limb observations 70

5.2.4 Big Bend south anticline observations 75

5.2.5 Big Bend north anticline observations 78

Chapter 6: Statistical Analysis of Fracture Spacing Data 83

6.1 Statistical analysis of fracture spacing data 83

6.2 Fracture sets observed in field 83

6.3 Predicting fracture spacing in the subsurface 91

Chapter 7: Discussion 101

7.1 Summary of observations and preliminary interpretation 101

7.2 Relations between fractures and structural/stratigraphic position 104

Chapter 8: Fracture Model for the Umiat Anticline.....107

8.1 Model introduction.....107

8.2 Primary elements of all Umiat fracture models 107

8.3 Model 1: All fractures are associated with regional stresses 108

8.3.1 Model 1: Implications for fracture distribution at Umiat.....111

8.3.2 Model 1 deficiency 112

8.4 Model 2: All fractures are associated with local fold-related stresses.....112

8.4.1 Model 2: Implications for fracture distribution at Umiat.....116

8.4.2 Model 2 deficiency 117

8.5 Model 3: Composite fracture model 117

8.5.1 Model 3: Implications for fracture distribution at Umiat.....120

8.5.2 Model 3 deficiency 121

Chapter 9: Discussion 123

Chapter 10: Conclusions.....127

10.1 Future work.....130

Chapter 11: References.....131

Appendix A: Fracture Transects Data Tables from Each Field Location.....139

Appendix B: Results of Statistical Tests Performed on Fracture Spacing.....151

LIST OF FIGURES

Page

Figure 1: Arctic Alaska Petroleum Province, showing locations of principal geologic features ...3

Figure 2: Big Bend anticline, Fossil Creek anticline, and the Colville incision and their relationship to the Umiat anticline to the north. 4

Figure 3: Schematic drawing illustrating three ways that fractures propagate 7

Figure 4: Schematic drawings showing simplified fracture-stress state relationships 7

Figure 5: Fundamental fracturing using Mohr's Circle 8

Figure 6: Schematic representation of possible fold mechanisms 11

Figure 7: Schematic representation showing the tangential longitudinal strain associated with buckling of mechanically competent beds 12

Figure 8: Schematic drawings showing simplified fracture-stress state relations in a fold....14

Figure 9: Schematic drawing depicting the four fracture sets that are commonly associated with folding 15

Figure 10: Tectonic map of northern Alaska 21

Figure 11: Schematic illustration of the North Slope of Alaska 22

Figure 12: Schematic regional cross section....23

Figure 13: Stratigraphy of the National Petroleum Reserve in Alaska....25

Figure 14: West-east segment of seismic line across the Nanushuk shelf margin 27

Figure 15: Panoramic photo view and schematic cross section showing thrust fault....32

Figure 16a: Kinematic model proposed by Hayes....35

Figure 16b: Stages 4–5A: Set 2 fractures continue to form by tangential longitudinal strain and cut through multiple mechanical units. 36

Figure 17: Schematic time-temperature history curve 37
Figure 18: False-color infrared aerial photomosaic of Umiat area, northern Alaska 39
Figure 19: Schematic diagram showing approximate stratigraphic level 42
Figure 20: Near-vertical natural fracture identified in core 144 of Umiat well 1 52
Figure 21: Fracture with a 79° dip in Umiat well 2, core 38 53
Figure 22: Fracture with an 82° dip in Umiat well 11, core 14 54
Figure 23: Significantly gentler dipping fracture (~45°) 54
Figure 24: Map showing the Colville incision, Fossil Creek, and the Big Bend anticline with the location and relative orientations of each fracture transect 57
Figure 25: Map showing the Colville incision, Fossil Creek, and the Big Bend anticline with fracture stereonets 58
Figure 26a: Raw data stereonets and rose diagrams for four scan-line fracture surveys at Big Bend anticline, Fossil Creek anticline, and the Colville incision 60
Figure 26b: Raw data stereonets and rose diagrams for fracture surveys taken at Big Bend north anticline 61
Figure 27: Poles to planes, contoured, and contoured-bed horizontal stereonets 62
Figure 28: Photo of the eastern Colville incision 65
Figure 29: Photo of plumose structures at Colville incision 67
Figure 30: Photo of northwest striking set Cnw fractures at the Colville incision 68
Figure 31: Photo of north to north-northwest striking Ao fractures and Af partially filled fractures at the Colville incision 69
Figure 32: Bed horizontal stereonet for partially filled to completely filled fracture set Af at the Colville incision 70

Figure 33: Photo of the south limb of the Fossil Creek anticline and the location of transect 8 ..72
Figure 34: Photo of fracture set Cnw at Fossil Creek 73
Figure 35: Photo of Fossil Creek set Cne fractures that are vertically extensive 74
Figure 36: Photo of the south limb of the south branch of Big Bend anticline and the location of transect 2 (red dashed line) 76
Figure 37: Photo of fracture set Cnw and Cne in the south limb of the south branch of Big Bend anticline 77
Figure 38: Photo of fracture set Cnw and Cne in the south limb of the south branch of Big Bend anticline 78
Figure 39: Photo of the north Big Bend anticline and the location of four fracture transects 81
Figure 40: Photo of fracture sets Cnw and Cne in transect 6 on the north Big Bend anticline 82
Figure 41: Photo of bedding surface with slickenlines on exposed set Cne fracture faces in north Big Bend anticline 82
Figure 42: Boxplots of fracture spacing of sets A, B, and C 84
Figure 43: Histogram plots of set A, B, and C fracture spacing distribution 86
Figure 44: Log normal and detrended log normal Q-Q plots for fracture set A 87
Figure 45: Log normal and detrended log normal Q-Q plots for fracture set B 89
Figure 46: Log normal and detrended log normal Q-Q plots for fracture set C 90
Figure 47: Y is the fracture spacing parallel to bedding 94
Figure 48: Relationship of observed fracture spacing in a borehole 96
Figure 49: Regional schematic model of the distribution and orientations of fractures associated with regional stress states at Umiat field 109

Figure 50: Local schematic model of the distribution and orientations of fractures associated with folding 114
Figure 51: Schematic model of the orientation of fracture set B 115
Figure 52: Schematic composite model of the Umiat field 119

LIST OF TABLES

Table 1: Fracture classification scheme 47

Table 2: Characteristics and classification of the natural fractures identified in Umiat well 1, 2, and 11 cores 51

Table 3: Well depth, amount of recovered and examined core, and number of natural fractures identified in Umiat wells 1, 2, and 11 55

Table 4: Characteristics, orientations, and relative ages of fracture sets observed at the Big Bend anticline, Colville incision, and Fossil Creek 66

Table 5: Average fracture spacing parallel to bedding and vertical distance between fractures calculated for the subsurface 95

Table 6: The Colville incision showing the predicted fracture spacing for set Ao and Af 97

Table 7: Fossil Creek anticline showing the predicted fracture spacing for set B 98

Table 8: Big Bend anticline showing the predicted fracture spacing for set C 99

Table A1: Transect 1. Location: Big Bend south anticline 140

Table A2: Transect 2. Location: Big Bend south anticline 141

Table A3: Transect 3. Location: Big Bend north anticline 142

Table A4: Transect 4. Location: Big Bend north anticline 143

Table A5: Transect 5. Location: Big Bend north anticline 144

Table A6: Transect 6. Location: Big Bend north anticline 145

Table A7: Transect 7. Location: Colville incision 146

Table A8: Transect 8. Location: Fossil Creek (south limb) 149

Table A9: GPS location, transect orientations, and bedding strike/dip for each transect location 150

Table B1: Descriptive statistics. Fracture sets A, B, and C 152

Table B2: Kolmogorov-Smirnov Test. Fracture Sets A, B, and C 153

Table B3: ANOVA Test. Fracture sets A, B, and C 153

Table B4: Post Hoc Test. Fracture sets A, B, and C 154

ACKNOWLEDGEMENTS

I would like to acknowledge the following organizations for their support in this research: the University of Alaska Fairbanks (UAF) Department of Geology and Geophysics, the UAF Geophysical Institute, the UAF Graduate School, and Renaissance Alaska, Inc. This study was funded by Department of Energy contract NT005641 and was a cooperative study between UAF and Renaissance Alaska and Linc Energy.

I would like to thank my advisor and committee members for their guidance and support during the composition of this thesis. I thank Ellen Craig and June Champlin for keeping me in line with important dates and deadlines.

This research would not have been possible without the discussion and support from my colleagues. Thank you all.

Special thanks to Barbara Wentz, Susana Salazar, and my wonderful husband Alex Shapiro for all your love and support. Many thanks to the friends I've made while in Fairbanks. Hayduke lives!

Chapter 1

INTRODUCTION

Fracture networks are valuable elements of petroleum systems in foreland basins because they can enhance both porosity and permeability in a reservoir and they act as migration pathways from source rocks to reservoir (Hanks et al., 2006). Regionally, open fractures can enhance both fluid flow and heat transfer in foreland basin systems (Allen and Allen, 2005; Hanks et al., 2006; Duncan et al., 2006). At the scale of a petroleum reservoir, identifying fractures is essential for predicting orientation of overall fracture populations that will potentially aid in fluid migration and for building three-dimensional reservoir porosity and permeability models. In turn, fracture populations are key to constraining the thermal evolution and the timing of structures in a basin. Examining the overall fracture pattern and its orientation can help to constrain the hydrocarbon maturation and migration history and identify potential oil source and reservoir (Moore et al., 2004; Hanks et al., 2006).

This project is aimed at constraining fluid migration pathways for the Umiat oil field on the North Slope of Alaska. The Umiat oil field is located in the southeastern part of the National Petroleum Reserve–Alaska (NPRA) on the north side of the Colville River, within the northern Arctic foothills physiographic province of Alaska (Fig. 1; Molenaar, 1982). Umiat hasn't been developed to date because the oil is light, but the reservoir is shallow and partially in permafrost, making the recovery factor low; fractures may be critical for improving recovery factor, thus making it economic. Understanding and mapping the distribution and character of both regional fractures and local fractures related to the Umiat anticline specifically will help determine the role that fractures played in migration of petroleum into the structure and how they may influence production. This is particularly important because the field is shallow and the

petroleum development scenario proposed by industry calls for several horizontal wells in order to access the shallow reservoir. This study documents fractures in unoriented core from Umiat anticline, but poor exposures precluded study of fractures in outcrop at Umiat anticline itself. The Big Bend anticline is a thrust-related anticline 33 km southeast of Umiat in the foothills of the North Slope that offers the opportunity to document the fracture patterns in Cretaceous-age rocks near the Umiat anticline (Fig. 2). Big Bend anticline is exposed in three dimensions, making it useful for field study of fractures. Exposures on the limbs of other anticlines at Colville incision and Fossil Creek were also visited (Fig. 2).

This study documents the fracture orientation, distribution, and character in surface analogs to the Umiat structure in age-equivalent rocks. These data are incorporated into fracture observations in Umiat core to a fracture model of the reservoir that will be used to develop a simulation model of the Umiat field. The aim is to better understand how fractures at Umiat field contribute to reservoir permeability. The results of these subsurface and surface observations were integrated into multiple models of fracture distribution at Umiat oil field.

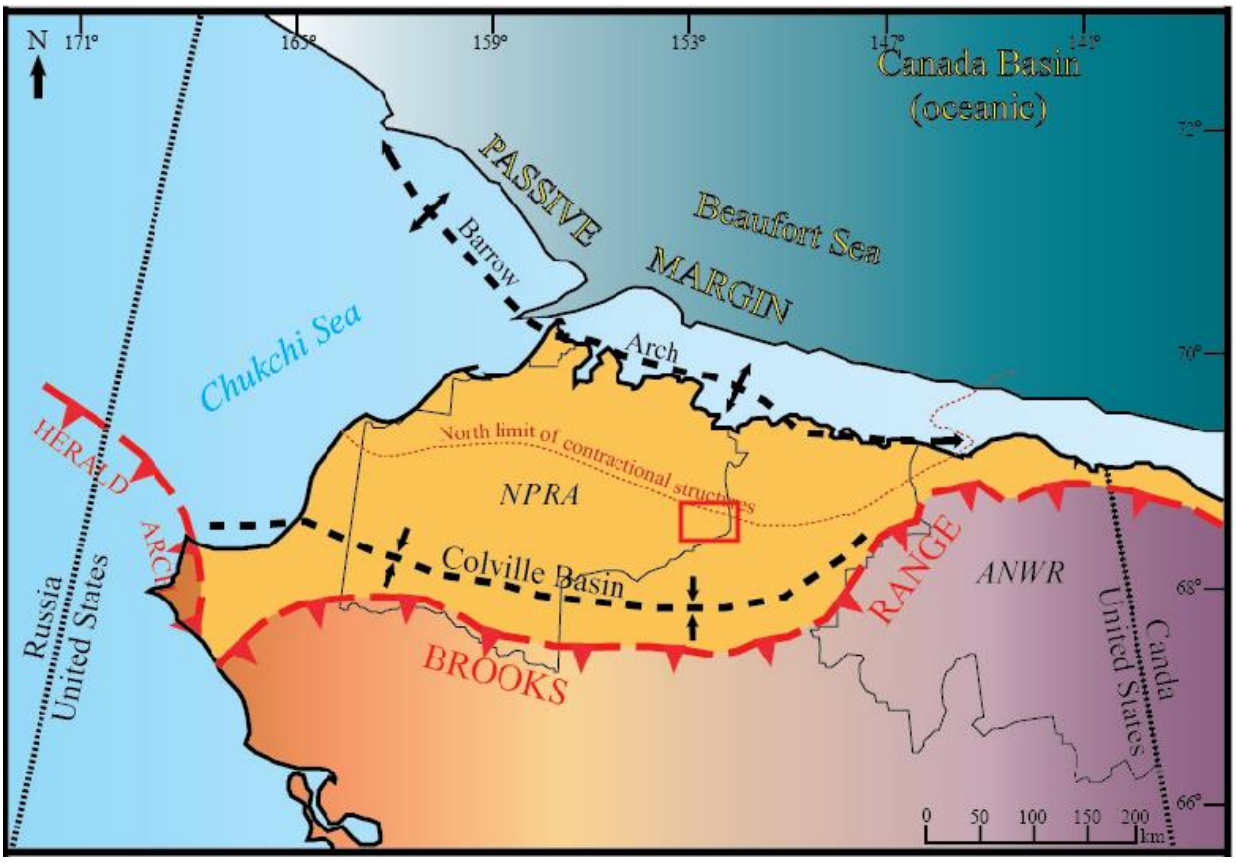

Figure 1: Arctic Alaska Petroleum Province, showing locations of principal geologic features. ANWR = Arctic National Wildlife Refuge; NPRA = National Petroleum Reserve–Alaska; Umiat location marked by red star. Units in km. Modified from Bird (1999).

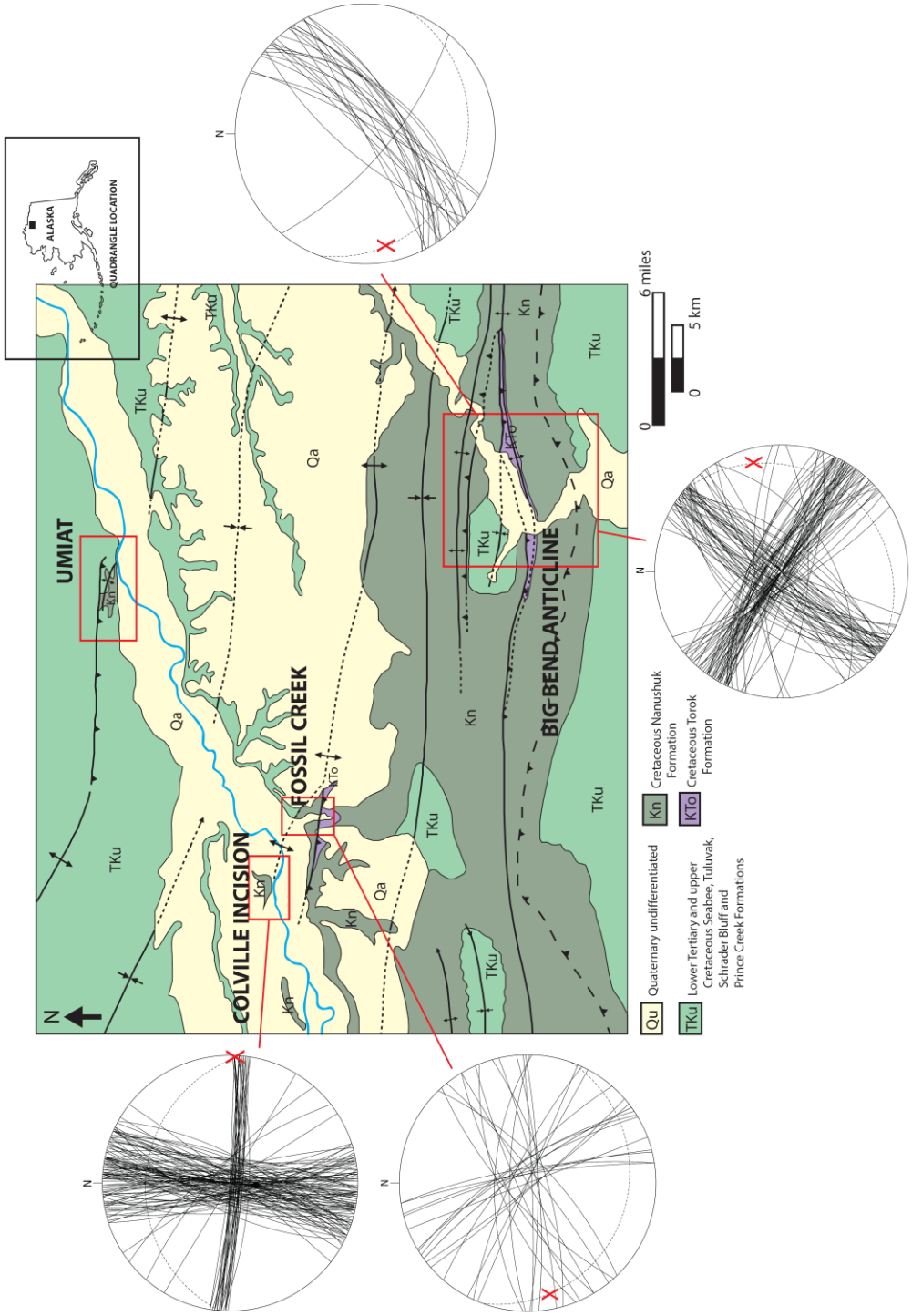

Figure 2: Location map of the Big Bend anticline, Fossil Creek anticline, and the Colville incision and their relationship to the Umiat anticline to the north. Stereonets indicate general trend of the anticlines and fracture patterns located at each site. Modified from Mull et al. (2004).

Chapter 2

FRACTURES IN FORELAND BASIN SYSTEMS

2.1 Introduction

Fractures form in foreland basins as a result of regional and localized stresses associated with burial, fault slip, folding, and unroofing (Engelder, 1985; Stearns, 1968; Atkinson, 1987; Lorenz et al., 1991; Hanks et al., 1997). Bach Ho field in southeast Vietnam is a prime example of how fracture studies yield profitable insight into petroleum reservoirs. An increasing percentage of the world's hydrocarbon reserves are found in fractured reservoirs like Bach Ho and the Asmari Formation in the Zagros Mountains of southwest Iran (Adabi et al., 2009; Cuong and Warren, 2009; Nelson, 2009). Because of their complex nature, fractured reservoirs require longer time and more expensive investigations to be understood completely and evaluated for potential exploration. The origin of natural fractures and their effect in controlling petroleum distribution in reservoirs must be determined in the early stages of exploration so reservoir evaluations and planning can be done accurately and efficiently (Nelson, 2009).

It is essential to understand the anisotropy and heterogeneity introduced in the subsurface by regional fracture networks to accurately predict reservoir quality in low-porosity rocks. Fractures in outcrops can be used to predict subsurface fracture networks. This study is aimed at assessing outcrop fractures as a means to determine subsurface migration pathways. Recent fracture studies by Hanks et al. (2004) and Duncan et al. (2006) have focused on distinguishing pre- and post-fold fractures from fold-related fractures. Identifying the multiple generations of fractures can yield important clues to the mechanisms of deformation and the conditions under

which folds evolved (Hanks et al., 2006). This information can be used to understand the timing of hydrocarbon migration and trap development.

2.2 Fracture formation and types of fractures

Fractures form when the differential stress between the greatest principal stress (σ1) and the least principal stress (σ3) overcomes the cohesive strength of a rock (Atkinson, 1987; Davis and Reynolds, 1996). The cohesive strength of a rock can be controlled by several factors, such as mineralogy, temperature, lithostatic pressure, pore fluid pressure, and the rate of deformation (Atkinson, 1987; Ramsay and Huber, 1987; Shackleton, 2003).

Mode I fractures form when the formation walls move away from the fracture plane at a right angle as the fracture opens (Fig. 3). Mode I fractures can form by one or more mechanisms such as thermal contraction, hydraulic fracturing, and/or diagenetic shrinkage (Stearns and Friedman, 1972; Bergbauer and Pollard, 2004). Mode I extension fractures form perpendicular to the least minimum compressive stress (σ3) and parallel to the maximum stress (σ1) (Figs. 4, 5; Griggs and Handin, 1960; Stearns and Friedman, 1972; Bergbauer and Pollard, 2004). If the magnitude of σ3 is equal to or exceeds the tensile strength of a rock under low differential stress, the result will be an extension fracture that forms parallel to σ1 (Figs. 4, 5; Atkinson, 1987; Davis and Reynolds, 1996; Hayes and Hanks, 2008).

In contrast, mode II shear fractures form due to shear stress, which acts parallel to the plane of the fracture and perpendicular to the fracture front (Fig. 3). Mode II fractures form obliquely to σ1 and parallel to the intermediate stress σ2 (Figs. 4, 5; Griggs and Handin, 1960; Stearns and Friedman, 1972; Bergbauer and Pollard, 2004). The greater the differential stress is between σ3 and σ1, the greater the potential for shear failure (Fig. 5). Shear fractures generally

form at higher effective mean and differential stress than extension fractures, as illustrated in Figure 5.

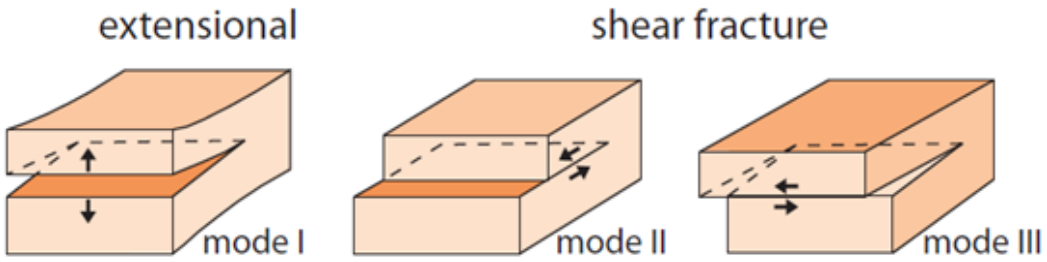

Figure 3: Schematic drawing illustrating three ways that fractures propagate: mode I, opening, and mode II and III, shearing. Modified from Bons et al. (2012).

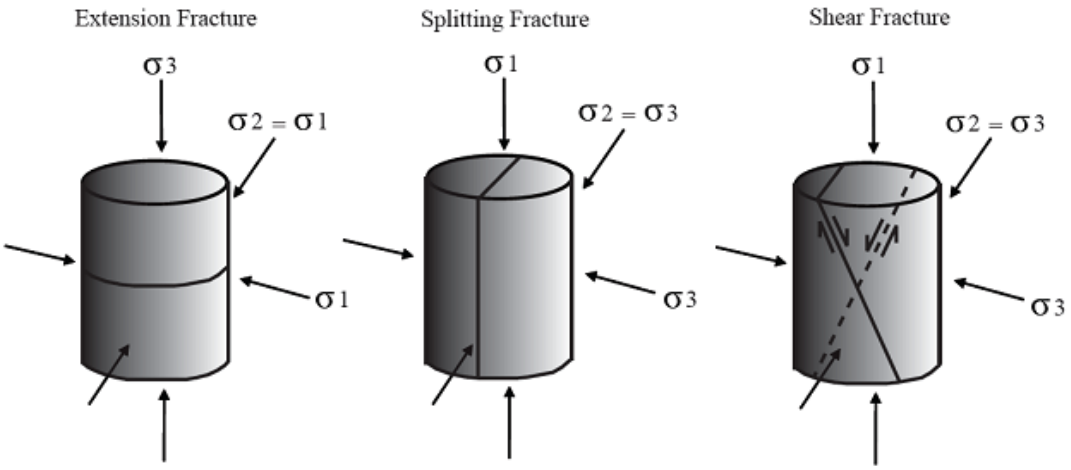

Figure 4: Schematic drawings showing simplified fracture-stress state relationships based on laboratory rock mechanic testing of cylindrical samples performed by Griggs and Handin (1960). Modified from Bergbauer and Pollard (2004).

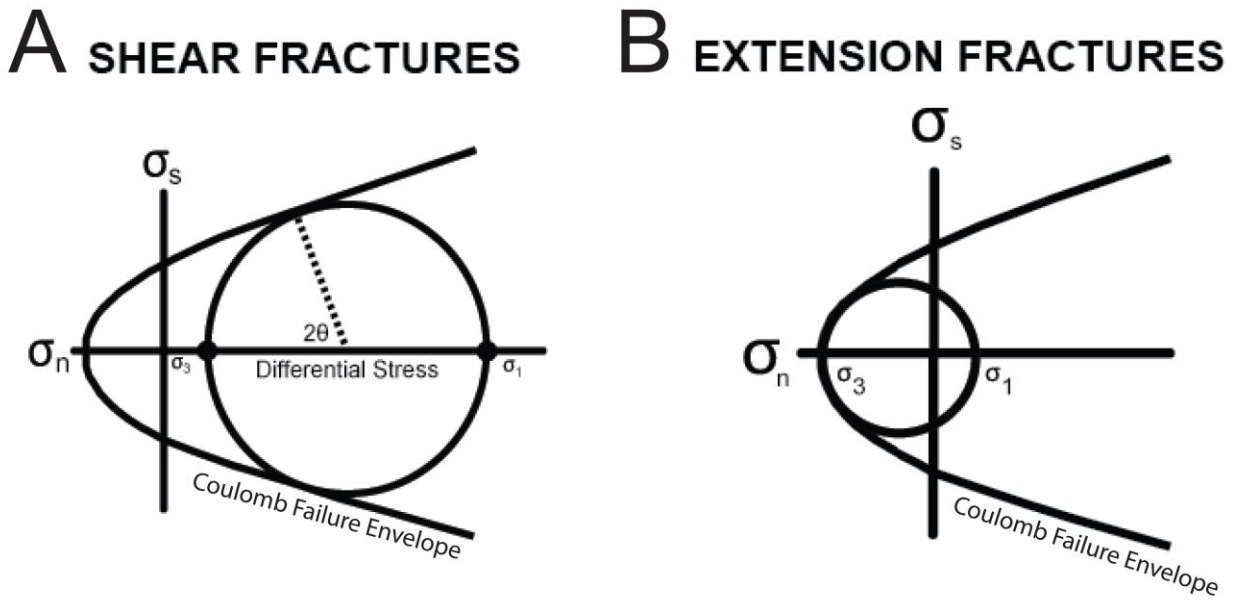

Figure 5: Fundamental fracturing using Mohr's Circle. The differential stress (σ1–σ3) controls the size of the circle. (A) Shear fracturing occurs when the differential stress is sufficient to overcome the strength of the rock under compressive stress. The orientation of the fractures is determined by 2θ, the angle between the horizontal normal stress axis and the line connecting the center of the circle with the point where the circle meets the failure envelope. The fracture is at θ from σ1, so shear fractures are inclined at some significant angle from σ1 while extension fractures parallel σ1. The site at which the initial propagation of a fracture begins is referred to as the origin and typically coincides with an internal flaw or irregularity in the rock, such as a fossil or inclusion (B) Extension fractures form when the differential stress between σ3 and σ1 is low and σ3 is normally negative. (Helgeson and Aydin, 1991; Davis and Reynolds, 1996).

2.3 Mechanical stratigraphy and fractures

The mechanical properties of individual strata within a multilayered package of heterogeneous rock control the scale and style of deformation (Ramsay and Huber, 1987; Narr and Suppe, 1991). Mechanical stratigraphy describes the behavior of individual sedimentary layers within a stratigraphic sequence of rocks in response to stress (Ramsay and Huber, 1987; Hanks et al., 2004; Hayes, 2004; Duncan et al., 2006). The character of bedding, relative thickness of individual layers, and lithologic composition within a deforming package of

heterogeneous rocks will have significant effects on the fracture spacing in flat-lying rocks as well as on the overall fold geometry and the character and distribution of fractures (Ramsay and Huber, 1987; Tanner, 1989; Narr and Suppe, 1991).

Fracture height and distribution are controlled by the thickness of individual beds of both incompetent and competent nature as well as composite "mechanical units" that consist of multiple bed units (Ramsay and Huber, 1987; Narr and Suppe, 1991; Hanks et al., 2004; Hayes and Hanks, 2008). The competency of a mechanical unit is controlled by the lithology: shale tends to be mechanically incompetent whereas carbonate and sandstone are more mechanically competent (Hanks et al., 2004; Hayes and Hanks, 2008). Weak units such as shale thus allow for regional displacement on décollements or detachment horizons.

Fracture spacing is controlled by mechanical layer thickness in well-defined mechanical layering (Narr and Suppe, 1991). Lower fracture densities are documented in thick competent beds with longer wavelength folds (Ramsay and Huber, 1987). Hayes and Hanks (2008) identified higher fracture densities in shorter wavelength folds formed in thin competent layers. The local stress field can be potentially altered depending on the mechanical interaction between different deforming layers with different lithologies and in response to varying temperature, pressure, and fluid changes (Bergbauer and Pollard, 2004).

2.4 Fractures in flat-lying rocks

Regional, prefolding, mode I extension fractures are common in flat-lying rocks and can form in undeformed foreland basins ahead of advancing thrust belts (Hanks et al., 1997). These regional extension fractures are interpreted to form either at depth with high fluid pressures and low differential effective *in situ* stress or as a result of removal of a lithostatic load by uplift and

erosion (Hancock and Engelder, 1989; Lorenz et al., 1991; Engelder and Lacazette, 1990; Engelder and Fischer, 1996; Hanks et al., 2004; Hanks et al., 2006). When formed at depth, regional extensional fractures or joints commonly develop prior to folding or faulting in flat-lying strata under low differential stress and high fluid pressure, and these fractures are thus oriented parallel to $\sigma 1$ and sub-perpendicular to the thrust front (Stearns, 1968; Lorenz et al., 1991).

2.5 Fold-related fractures

Fracture density and orientation in folded strata are controlled by bending stresses within a fold as it evolves (Szilard, 1974; Fischer and Wilkerson, 2000). Early conceptual models for fold-related fracturing were based on final fold geometry and neglected preexisting fracture patterns and the evolution of fold geometry (Fischer and Wilkerson, 2000; Bergbauer and Pollard, 2004). Fold-related fractures are commonly grouped into two categories based on their timing relative to folding. These are termed "early folding" or "late folding" but give little direct evidence for fracture timing during specific folding events (Cooper, 1992; Engelder et al., 1997; Hanks et al., 1997; Hennings et al., 2000; Shackleton, 2003; Bergbauer and Pollard, 2004). It is critical to establish the timing of fracture development because this allows determination of when a petroleum reservoir/permeable network was established (Hanks et al., 1997).

Flexural slip and flexural flow are two primary mechanisms for folding of a multilayered sequence of rocks (Davis and Reynolds, 1996). In flexural slip folding, layer-parallel slip along bedding surfaces occurs where mechanical layers are separated by well-developed bedding surfaces (Fig. 6; Ramsay and Huber, 1987; Narr and Suppe, 1991; Hayes and Hanks, 2008). Slickenlines along bedding surfaces are evidence for slip along bedding surfaces. Competent

sandstone, siltstone, and limestone tend to retain their primary thicknesses during flexural slip (Davis and Reynolds, 1996). In contrast, flexural flow folding occurs where layer-parallel displacement is evenly distributed throughout thick intervals of incompetent rock types such as shale (Fig. 6; Ramsay and Huber, 1987; Davis and Reynolds, 1996). In flexural flow folding, original bedding thickness is still maintained.

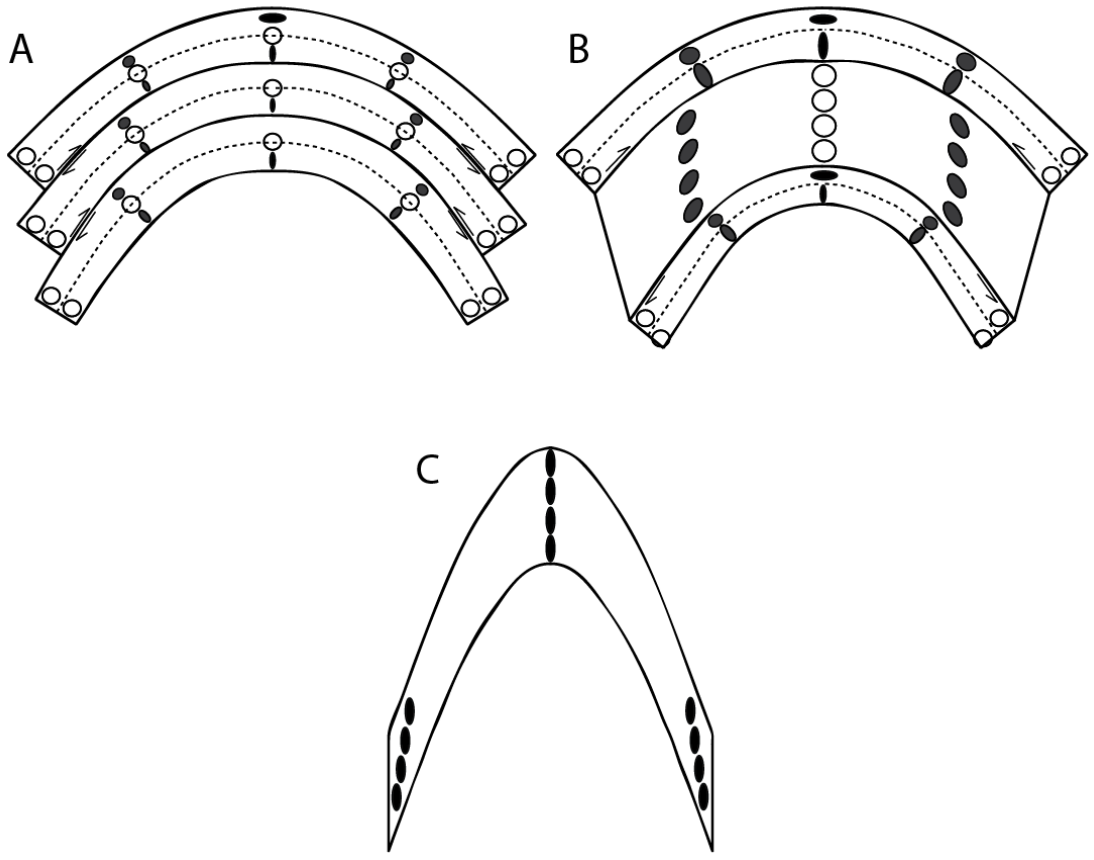

Figure 6: Schematic representation of possible fold mechanisms. Open circles represent unstrained original circular markers; originally circular markers are represented by ovals filled by grey that indicate increasing strain. (A) flexural slip folding, (B) flexural flow folding, (C) homogeneous flattening. Bed thickness remains constant as rigid layers deform by tangential longitudinal strain in A and B. In C, beds thicken in the fold hinges and thin on the limbs. Modified from Ramsay and Huber (1987).

Tangential longitudinal strain occurs in competent mechanical layers that are actively folding (Fig. 7; Ramsay and Huber, 1987; Davis and Reynolds, 1996; Hanks et al., 2004; Duncan et al., 2006; Hayes and Hanks, 2008). Maximum strain occurs at fold hinges. The outer arc of a competent layer undergoes layer-parallel extension in the fold hinge, while layer-parallel contraction occurs in the inner arc (Fig. 7; Davis and Reynolds, 1996). The neutral surface separates layer-parallel extension in the outer arc from layer-parallel contraction in the inner arc and represents a surface of no finite strain (Fig. 7; Davis and Reynolds, 1996). The neutral surfaces within multilayered mechanical packages migrate within the fold as it evolves and the thickness of mechanical layers changes (Ramsay and Huber, 1987; Shackleton et al., 2005; Hayes and Hanks, 2008).

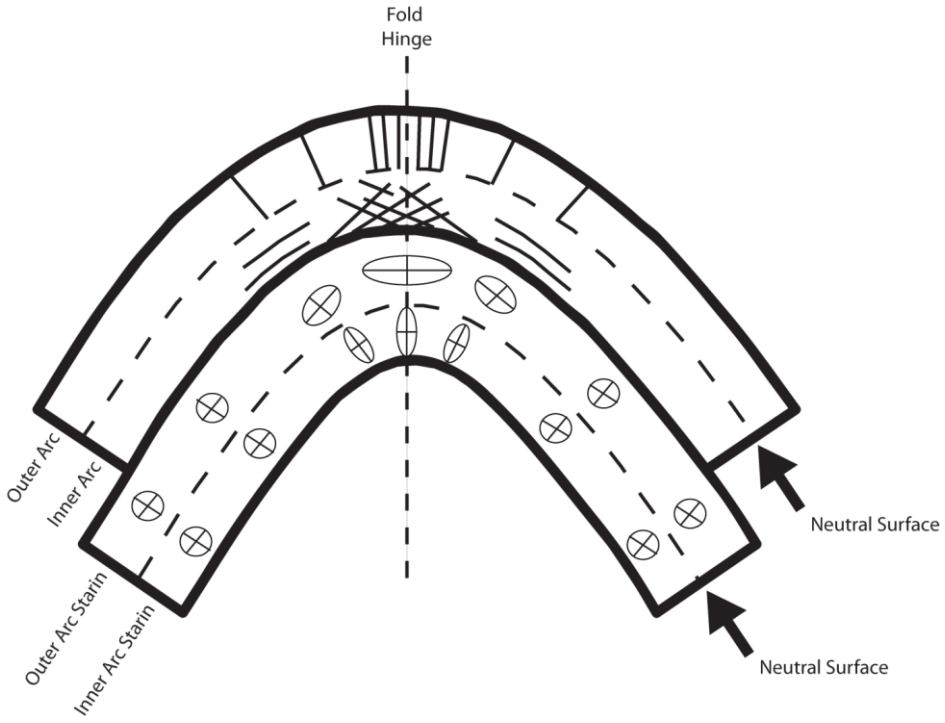

Figure 7: Schematic representation showing the tangential longitudinal strain associated with buckling of mechanically competent beds. The upper bed illustrates how fracturing can accommodate strain with low-angle shear fractures and layer-parallel extensional fractures in the inner arc and extensional fractures in the outer arc. The lower bed illustrates the distribution of strain in the outer and inner arc separated by a neutral surface. Modified from Hayes (2004).

Several different stress states can exist in a particular volume of rock throughout fold evolution (Stearns and Friedman, 1972) and may yield four possible fracture patterns that are systematically related to the orientation of the fold axis and bedding, as proposed by Stearns (1968) (Fig. 8). Stearns (1968) and Bergbauer and Pollard (2004) have proposed fracture sets that include both shear and extension fractures (Fig. 8). Shear and extension fractures cannot normally form at the same time under the same stress magnitude (Fig. 5). Fracture sets were interpreted by Stearns (1968) to result from inner arc limb contraction (sets 1 and 4) and outer arc limb extension (sets 2 and 3) during tangential longitudinal strain (Figs. 8, 9). Fracture set 1 includes two conjugate shear fractures and one extension fracture that form when $\sigma 1$ is parallel to the bedding dip direction, $\sigma 3$ is parallel to the fold axis, and $\sigma 2$ is normal to bedding (Figs. 8, 9; Stearns, 1968). This overall pattern of fracturing indicates extension parallel to the fold axis and shortening in the dip direction, with no movement normal to bedding (Stearns, 1968).

Fracture set 2 consists of two conjugate shear fractures and an extension fracture with $\sigma 1$ parallel to the strike of the bed, $\sigma 3$ parallel to the dip direction, and $\sigma 2$ normal to bedding (Figs. 8, 9; Stearns, 1968). Fracture set 2 patterns are interpreted to result from shortening parallel to the fold axis and elongation parallel to the bed dip (Stearns, 1968).

Fracture set 3 includes an extension fracture and two conjugate shear fractures oriented parallel to the fold axis and sub-perpendicular to bedding, indicating extension parallel to dip with $\sigma 1$ normal to bedding and $\sigma 2$ parallel to the fold axis (Figs. 8, 9; Stearns, 1968). Fracture set 4 characteristically consists of shear fractures that are at a low angle with respect to bedding and bed-parallel extension fractures that indicate extension perpendicular to bedding and compression parallel to the dip direction. This indicates that $\sigma 1$ was oriented parallel to the dip

direction, σ3 was normal to bedding, and σ2 was oriented parallel to strike (Fig. 9; Stearns, 1968). None of these four fracture patterns necessarily reflects the regional stress field, but they are controlled by a local stress field as folding occurs.

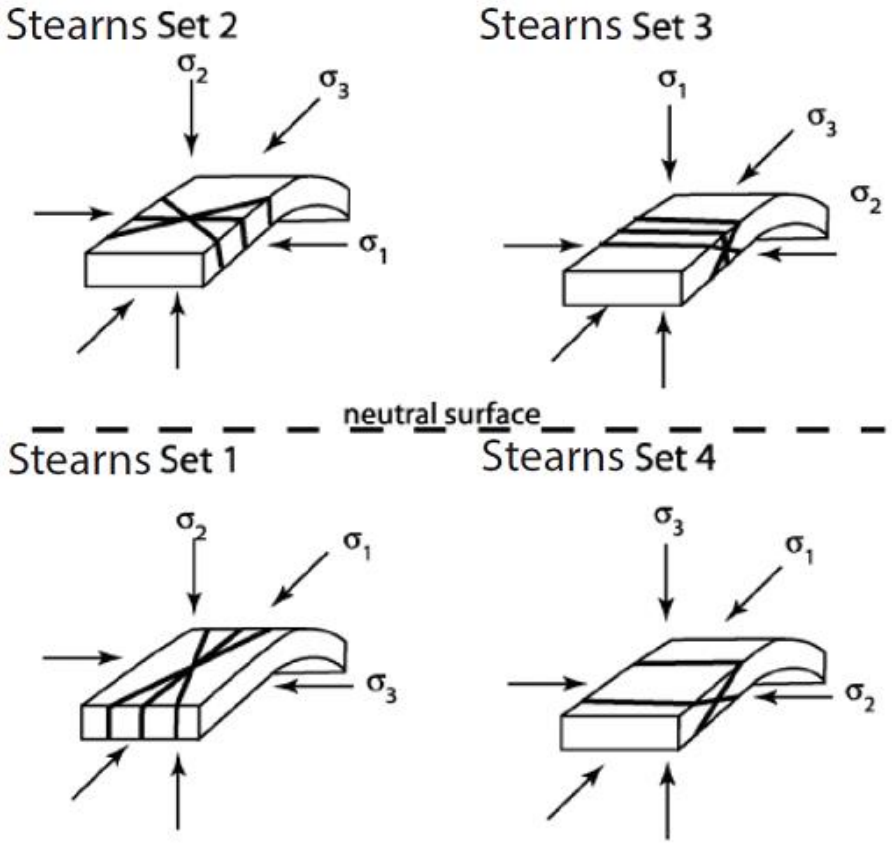

Figure 8: Schematic drawings showing simplified fracture-stress state relations in a fold. Shear fractures and extension fractures do not normally form under the same stress state and hence do not form synchronously. This diagram assumes that the fractures form by tangential longitudinal strain in a fold, which results in σ1 oriented down-dip in the inner arc (below the neutral surface) and σ3 oriented down-dip in the outer arc (above the neutral surface). Two sets of fractures are possible in both inner and outer arc, depending on whether σ2 is parallel to the fold axis or perpendicular to bedding. Modified from Stearns (1968) and Bergbauer and Pollard (2004).

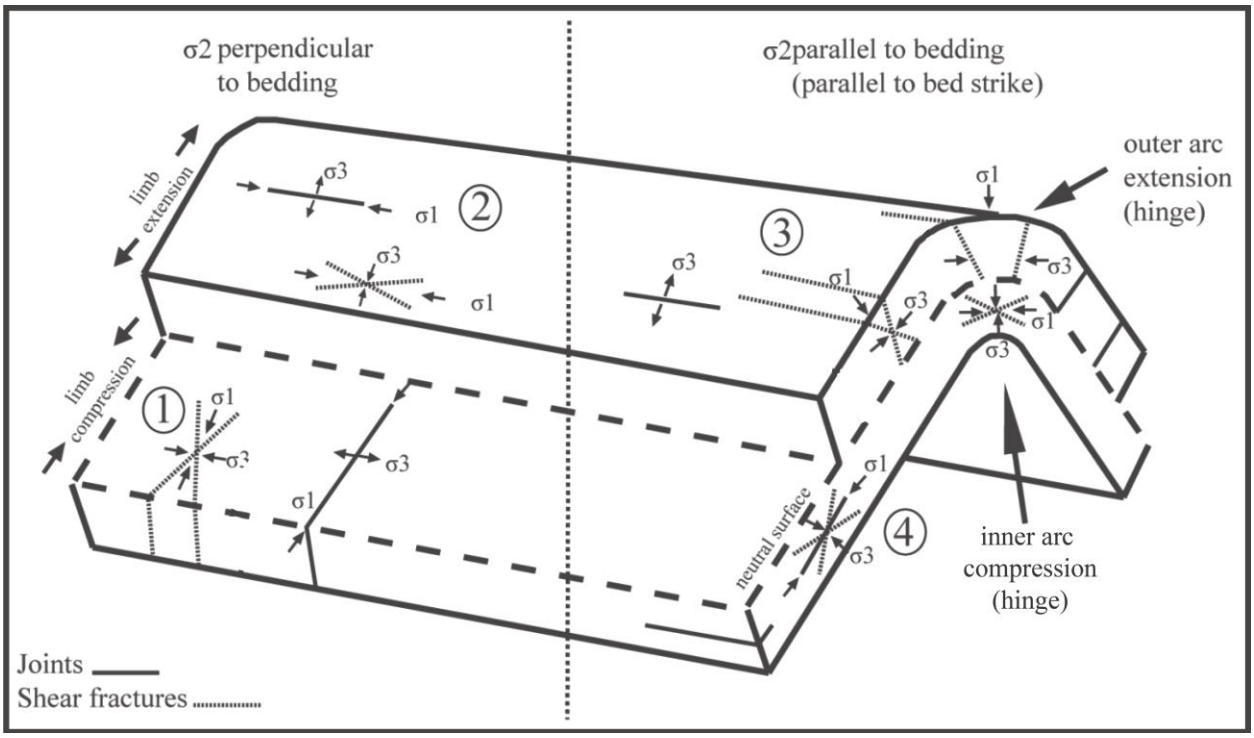

Figure 9: Schematic drawing depicting the four fracture sets that are commonly associated with folding. Sets 1 and 2 represent inner and outer arc tangential longitudinal strain, respectively, and have σ2 oriented normal to bedding. Sets 3 and 4 have σ2 oriented parallel to the fold axis and represent inner and outer tangential longitudinal strain, respectively. Modified from Hayes (2004).

Engelder (1985) proposed a fifth post-fold fracture or unloading joint pattern. These fractures will be oriented parallel to the overlying ground surface and will exploit any bedding or preexisting fractures that are near that orientation (Engelder, 1985; Hancock and Engelder, 1989). These fractures are interpreted to form after removal of more than half of the overburden.

2.6 Fracture evolution in foreland fold-and-thrust belts and fluid flow

During early stages in the evolution of a fold-and-thrust belt, strata are commonly subjected to compression (σ1) that is oriented sub-perpendicular or perpendicular to the thrust front and extension (σ3) sub-parallel to the developing thrust front (Engelder, 1985; Lorenz et

al., 1991). For example, assuming maximum regional stress on the Alaska North Slope was oriented north-south, normal to the present thrust front, early extension fractures would be oriented north-south, and later shear fractures would be oriented north-east and north-west (Fig. 5).

The fracture density and orientation affect the permeability of a rock and its effective drainage of fluids from a basin near the surface (Narr et al., 2006). Various rock types within a basin behave differently with regard to fluid flow (Bachu, 1995). For example, sandstones and carbonates will generally aid in fluid migration while shales impede fluid flow. Formation water may also contribute to the migration and accumulation of hydrocarbons (Bachu, 1995). Fluid migrates through porous rocks through permeable layers as a result of (1) density differences, (2) hydraulic head gradients, or (3) variations in chemical concentrations or thermal fields. The two dominant flow mechanisms in foreland basins are hydraulic-head gradients (hydrostatic flow) and density differences (buoyancy flow) between formation waters and hydrocarbons (Bachu, 1995). Hydraulic flow is often a result of elevation differences where formation waters in the basin flow in local, intermediate, and regional systems driven by topography (Bachu, 1995). Hydraulic-head gradients may fluctuate due to a change in fluid or pore volume as a result of mechanical processes like compaction or erosional unloading. The various flow mechanisms are active both areally and stratigraphically in different parts of the basin (Bachu, 1995). After hydrocarbons are expelled from the source beds, migration occurs along bedding of more permeable strata. The driving force of hydrocarbon migration is a combination of buoyancy and entrainment by formation water flow (Hubbert, 1940, 1953; Bachu, 1995).

Numerous fracture studies (e.g., Narr et al., 2006) suggest that only a slight decrease in fracture density and a little variation of fracture orientations occurs at depth. If so, then surface

fracture patterns and densities are a good indication of the orientation of fractures in the subsurface. Understanding the distribution and patterns of fractures in the subsurface will help determine how fractures may influence production.

Chapter 3

REGIONAL GEOLOGY

3.1 Geologic setting

The Brooks Range is a generally east-west trending mountain range with elevations greater than 3,000 m in the east and gradually decreasing elevation toward the west (Figs. 1, 10) (Moore et al., 1994). The first phase in the evolution of the Brooks Range was during Late Jurassic to Early Cretaceous in response to a collision of an island arc to the south with the continental margin of arctic Alaska (Moore et al., 1994). A late Paleozoic to early Mesozoic south-facing passive margin collapsed, and seven regionally extensive allochthons were emplaced as a result of this collision (Moore et al., 1994).

The North Slope, north of the Brooks Range, is underlain by the large, east-west trending Colville basin (Fig. 1), a foreland basin of Cretaceous-Tertiary age that resulted from loading of lithosphere as the allochthons were emplaced and the crust thickened during continued growth of the range (Fig. 10). The north flank of the asymmetric Colville basin dips gently toward a structural high near the present coastline called the Barrow Arch (Coakley and Watts, 1991; Moore et al., 1994, 2004). The Barrow arch is the combined result of the south flank that dips into the Colville basin and a steeper flank that dips north and forms the present-day passive margin of the Arctic basin. As the Brooks Range and Herald arch (Fig. 11) evolved and uplifted in the mid-Cretaceous, sediments were shed into the Colville basin foredeep from the west in a series of east-northeastward prograding topset-to-deep-water clinoform sequences, resulting in predominantly axial basin deposits (Fig. 11; Molenaar, 1982; Mull, 1982; Moore et al., 1994; Mull et al., 2003; Decker, 2007; Houseknecht et al., 2009). Throughout the Late Cretaceous and

Tertiary, the Colville basin continued to fill. Some locations preserve in excess of 4,000 m of marine, marginal marine, and nonmarine sediments (Molenaar et al., 1988; Decker, 2007).

Renewed deformation during the Paleocene resulted in creation of the present Brooks Range mountain front and folding and thrust faulting of foreland basin deposits to form the foothills to the north (Moore et al., 1994, 2004; Wallace, 2009; Wallace et al., 2011). Umiat field is in folded and thrust-faulted Cretaceous sedimentary rocks at the leading edge of the Brooks Range fold-and-thrust belt (Fig. 12). The reservoir consists of mid-Cretaceous clastic sediments deposited into the foreland basin of the Brooks Range. Eventual incorporation of these sedimentary rocks into the leading edge of the Brooks Range thrust belt resulted in the Umiat anticline, a doubly plunging, north-vergent, thrust-faulted detachment fold (Molenaar, 1982; Wallace, 2009). The anticline is classified as a detachment fold by Molenaar (1982), Moore et al. (2004), and Wallace (2011) because the fold was formed by thickening of the incompetent Torok Formation as a result of a gently south-dipping detachment in or below the lower Torok Formation. The Umiat anticline trends east-west and is approximately 10 miles long by 3 miles wide. The source rocks for the Umiat petroleum system are thought to be Cretaceous organic-rich shales of the Torok Formation (Magoon and Bird, 1985; Potter and Moore, 2003). The internal shales throughout the Nanushuk Formation provide the seal to the Umiat system (Magoon et al., 2003).

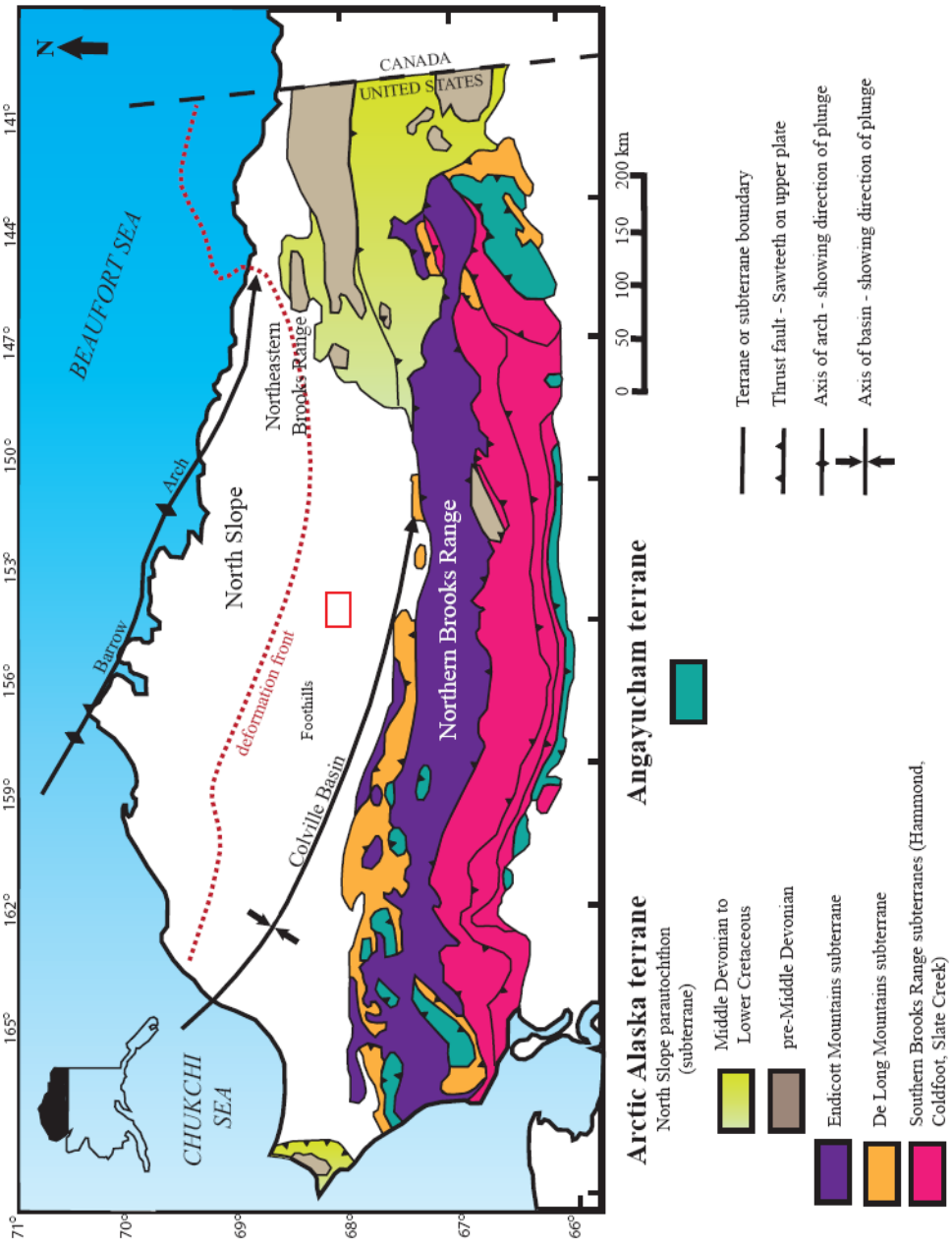

Figure 10: Tectonic map of northern Alaska showing the distribution of major structural features. The red box outlines the location of the study area. Modified from Moore et al. (1994) and Wallace (1997).

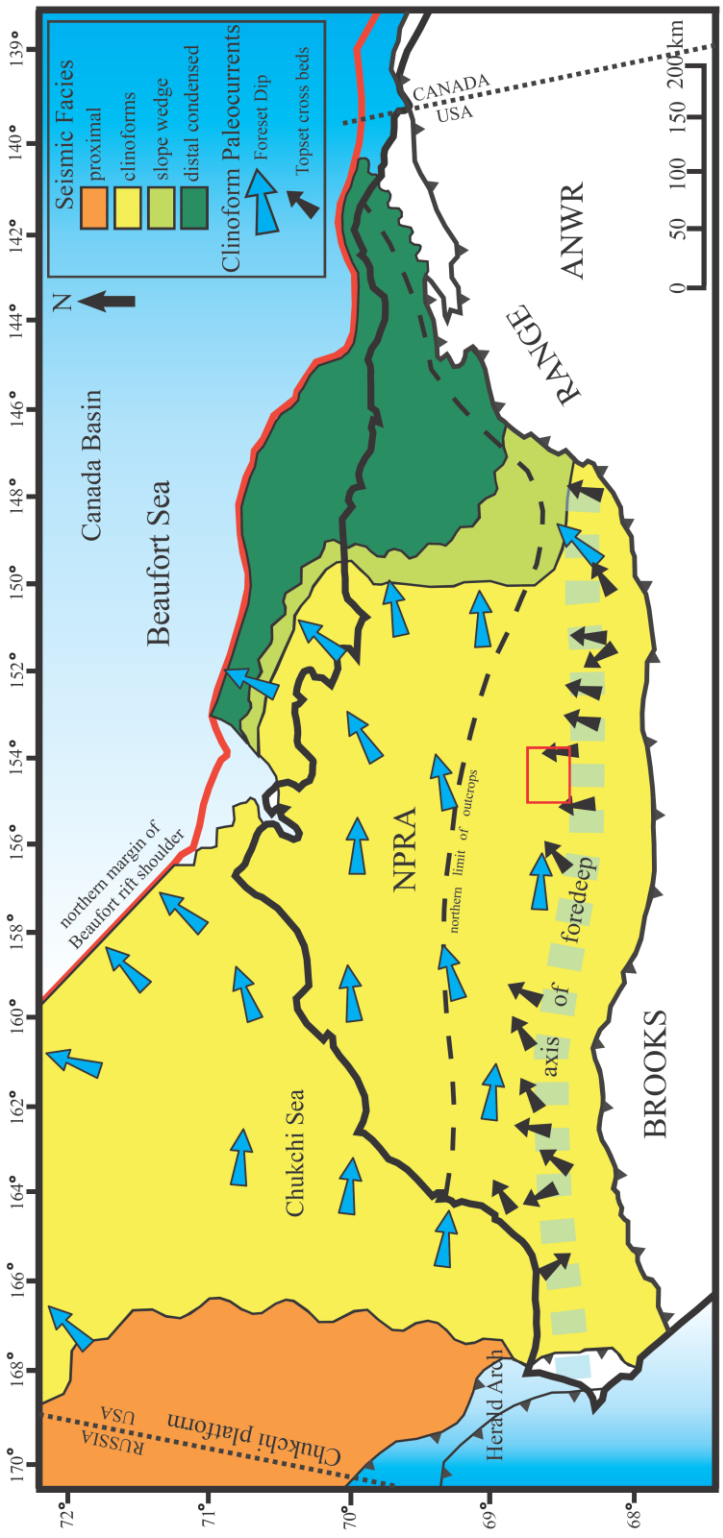

Figure 11: Schematic illustration of the North Slope of Alaska showing the Colville foreland basin and the facies distribution of the basin fill. The Colville basin generally filled from west to east. Study area outlined in a red box. Modified from Houseknecht et al. (2009).

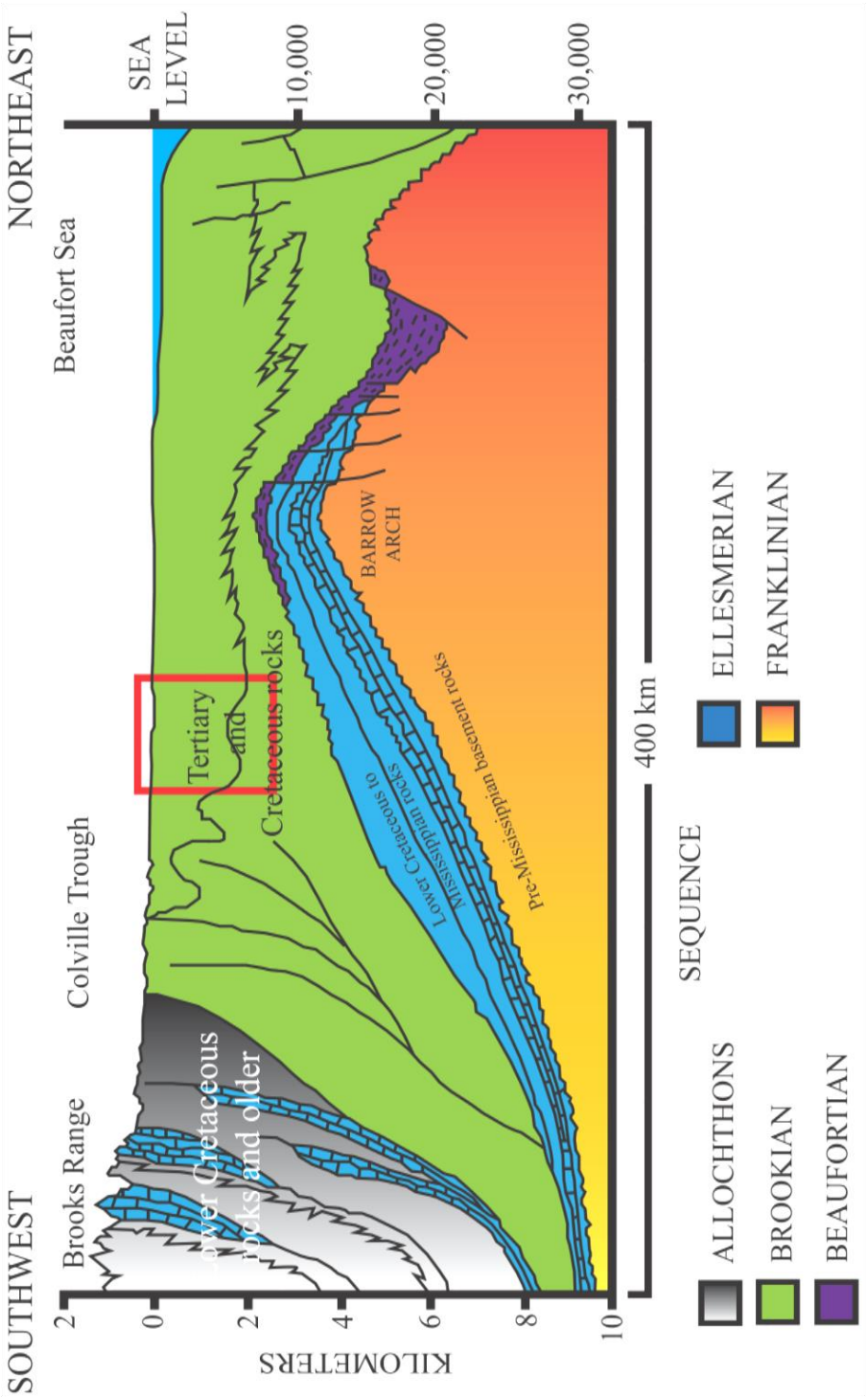

Figure 12: Schematic regional cross section showing the leading edge of the Brooks Range fold-and-thrust belt. Blue packages shown in the allochthon are equivalent to the carbonate within the Ellesmerian. Location of Umiat field outlined with red box. Modified from Bird and Bader (1987).

3.2 Stratigraphy

The regional stratigraphy of the North Slope of Alaska is composed of four main sequences: the pre-Middle Devonian Franklinian sequence, the Mississippian to Jurassic Ellesmerian sequence, the Jurassic and Lower Cretaceous Beaufortian sequence, and the Lower Cretaceous to Tertiary Brookian sequence (Figs. 12, 13). The Franklinian sequence consists of weakly metamorphosed sedimentary and volcanic rocks that form the basement to the region and are unconformably overlain by the Ellesmerian sequence (Fig. 13; Bird, 1999). The Ellesmerian sequence is a northerly-derived sequence of clastic and carbonate rocks (Fig. 13; Bird, 1999). The Beaufortian sequence consists of deposits related to the rifting and rift-margin uplift associated with opening of the Arctic Ocean basin (Bird, 1999). The Brookian sequence is derived from the Brooks Range to the south and downlaps northward onto the Ellesmerian and Beaufortian sequences. It prograded to the east-northeast, filling the Colville basin and spilling over the Beaufort passive margin to the northeast (Fig. 11, 12; Houseknecht et al., 2009).

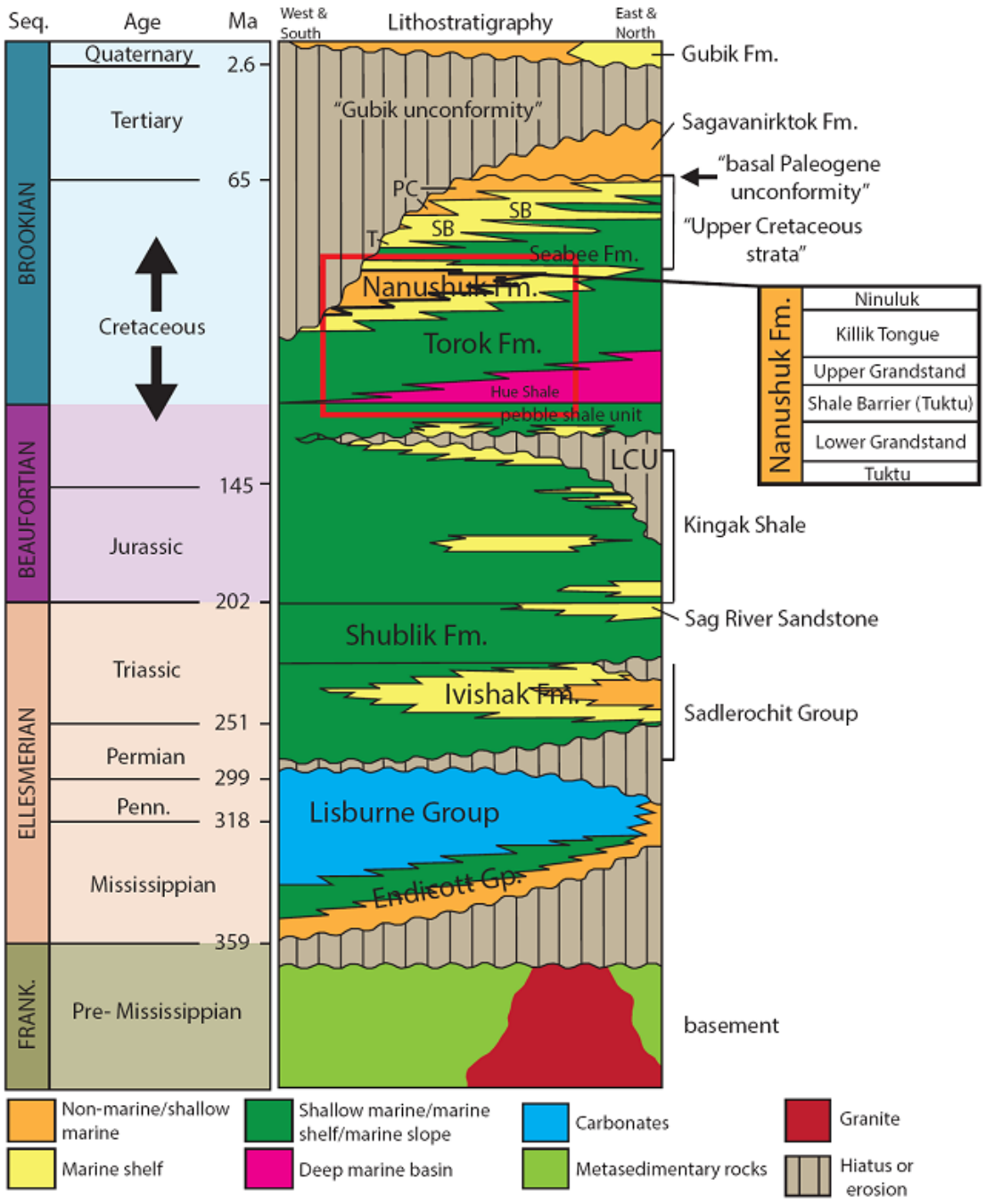

Figure 13: Stratigraphy of the National Petroleum Reserve in Alaska. Stratigraphy in the Umiat anticline area is composed of two major depositional sequences: the Torok-Nanushuk sequence and the Seabee-Tuluvak sequence. The stratigraphy represented in Umiat field is outlined in a red box. The Nanushuk Formation is outlined in bold with the informal subsurface stratigraphy used at Umiat Field in the small box. Modified from Houseknecht et al. (2011) and Shimer et al. (2014).

3.2.1. Colville basin stratigraphy

The Colville basin stratigraphy consists of an upper Mesozoic and Cenozoic north-facing foreland-basin sequence (Bird and Molenaar, 1992; Moore et al., 1994; Houseknecht et al., 2009; Fig. 13). The Colville basin was filled from west to east with clastic sedimentary rocks derived from the Herald arch to the west and the Brooks Range to the south and overlies a Mississippian to Lower Cretaceous continental margin sequence (the Ellesmerian sequence) (Figs. 12, 13).

Stratigraphy in the Umiat area consists of two major depositional sequences: the Aptian to Cenomanian Torok-Nanushuk sequence and the Turonian to Santonian Seabee-Tuluvak sequence (Figs. 2, 14). Previous work by Molenaar et al. (1988), Bird and Molenaar (1992), Houseknecht and Schenk (2004), and Houseknecht et al. (2009) established that the geometry of the Torok and Nanushuk Formations displays an east-to-northeast progradation of bottomset-clinoform-topset strata (Fig. 14). The Torok Formation and Seabee Formation define the slopes and bottomsets of the clinoform reflections and grade into the overlying topset reflectors that define the lower Nanushuk Formation and the Tuluvak Formation (Mull et al., 2003). The depositional system includes deep-marine environments with the Torok Formation deposited in a deep-marine basin, marine slope, and outer shelf. The Nanushuk Formation represents a thick deltaic unit. The Seabee Formation was deposited in a marine slope, offshore marine shelf, and basin environment. The Tuluvak Formation was deposited in a marine to marginal marine depositional environment.

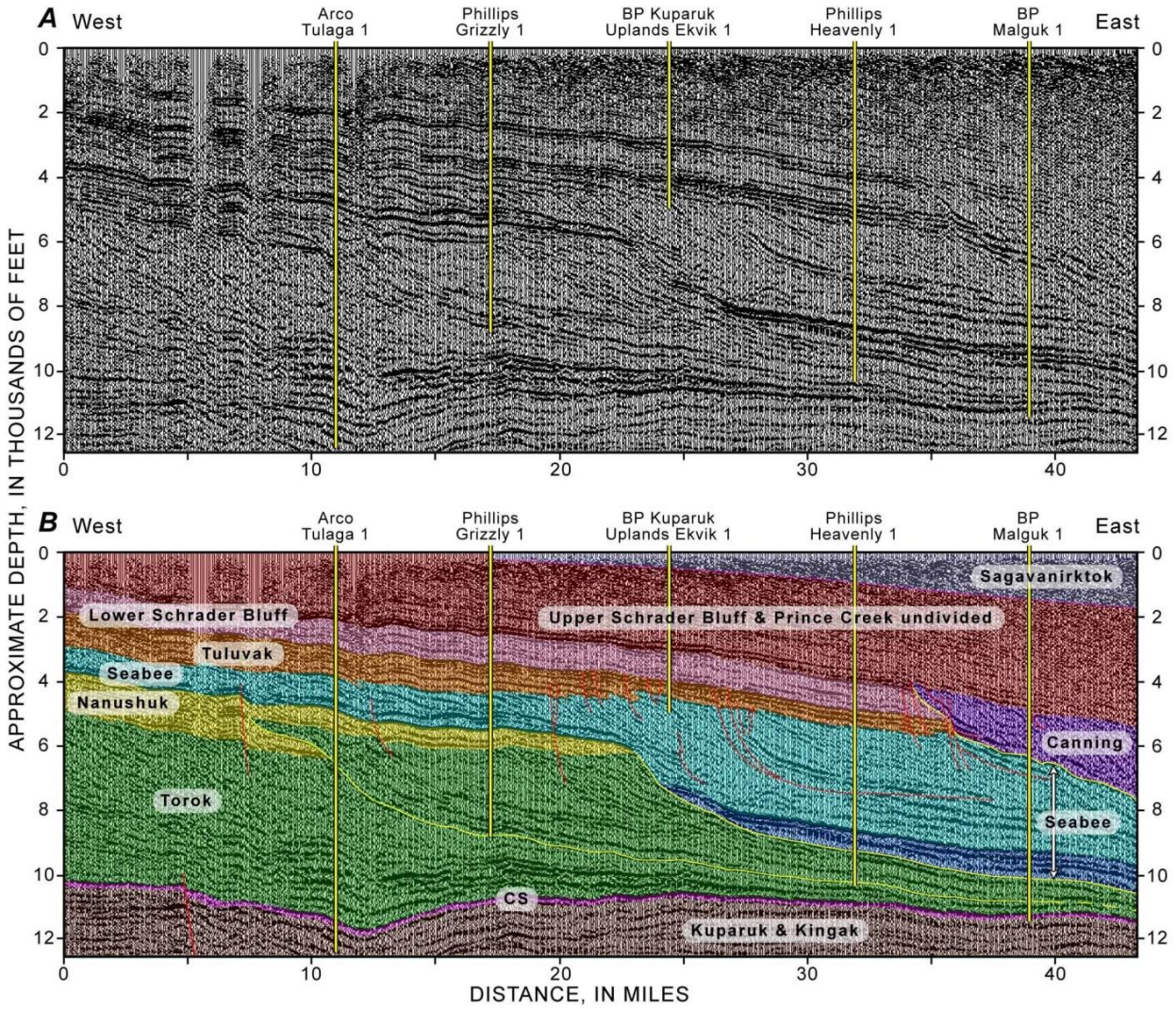

Figure 14: West-east segment of seismic line across the Nanushuk shelf margin illustrating the geometry of the Torok-Nanushuk and the Seabee-Tuluvak depositional sequences. Modified from Houseknecht and Schenk (2004).

3.2.2 Brookian Sequence, Torok Formation

The Torok Formation was deposited in a deep-marine-basin, marine-slope and outer-shelf environment during Aptian-Cenomanian time (Molenaar et al., 1988; Houseknecht and Schenk, 2004; Shimer et al., 2014) (Figs. 13, 14). The Torok Formation defines the slope and bottomset

of the clinoform reflections and grades into the overlying topset reflectors that define the lower Nanushuk Formation (Fig. 14) (Mull et al., 2003). The Torok Formation downlaps onto the top of the Ellesmerian sequence, including the pebble shale unit and Kingak Shale, and grades basinward into the Hue Shale (Fig. 14). The Torok Formation is composed of grey-to-black recessive silty shale, mudstone, and clay shale with interbedded medium-to-fine grained sandstone (Figs. 13, 14). The Torok Formation has a maximum thickness of approximately 18,500 feet in the deepest part of the basin to the south and less than 3,100 feet beneath the northern part of the Colville basin (Molenaar, 1982; Bird, 1988; Mull at al., 2003). The Torok Formation is commonly folded in surface exposures, and subsurface seismic data suggest substantial amounts of tectonic thickening (Mull et al., 2003).

3.2.3 Brookian Sequence, Nanushuk Formation

The Nanushuk Formation was originally defined as the Nanushuk Group but has been lowered to formation status to comply with international guidelines (Mull et al., 2003; Shimer et al., 2014). The informal units of the former Nanushuk Group are commonly used in the subsurface at Umiat and include the marine Tuktu, shallow marine to deltaic Grandstand, marginal marine to nonmarine Killik tongue of the Chandler, and the shallow marine Ninuluk (Fig. 13; Shimer et al., 2014). At Umiat, the Grandstand contains two distinct, sand-rich intervals (Upper and Lower Grandstand) separated by a tongue of marine mudstone of the Tuktu, commonly referred to as the Shale Barrier (Fig. 13; Shimer et al., 2014).

The Albian to Cenomanian Nanushuk Formation is defined by seismic topset reflections (Fig. 14; Houseknecht and Schenk, 2004). The Nanushuk Formation overlies and interfingers with mudstone and shale of the underlying Torok Formation and progrades eastward (Figs. 13,

14). The top of the formation is marked by a sharp flooding surface that is disconformably overlain by marine shale of the Seabee Formation (Mull et al., 2003; Houseknecht and Schenk, 2004). The Albian to Cenomanian Nanushuk Formation represents a thick deltaic unit that is more than 20,000 feet in maximum thickness and thins to approximately 775 feet in the northeast (Chapman and Sable, 1960; Moore et al., 1994; Mull et al., 2003).

The Nanushuk Formation is divided into regionally mappable upper and lower stratigraphic units (Houseknecht and Schenk, 2004; LePain et al., 2009). The lower Nanushuk (informal Lower Grandstand) consists of thick sequences of shallow-marine sandstone intertonguing with neritic shale and siltstone and is interpreted to have been deposited in a shorefront, delta front, and pro-delta environment (Fig. 14; Mull et al., 2003; Finzel, 2004; Houseknecht and Schenk, 2004; LePain et al., 2009). The middle Nanushuk Formation (informal Upper Grandstand) contains a second major reservoir interval and represents a dominantly deltaic facies. The upper part of the Nanushuk Formation (informal Upper Grandstand) consists of dominantly nonmarine facies, including interbedded resistant fluvial sandstone, conglomerate, mudstone, siltstone, and coal beds and is interpreted to represent upper shoreface and delta front sandstones that prograded from the southwest to the northeast (Figs. 11, 13, 14; Bird and Molenaar, 1992; Mull et al., 2003; Finzel, 2004; LePain et al., 2009).

3.2.4. Brookian Sequence, Seabee Formation

The Cenomanian to Coniacian Seabee Formation unconformably overlies the nonmarine facies of the upper Nanushuk Formation (Fig. 13). It is less than 500 feet thick in the western Colville basin and thickens to approximately 2,000 to 3,000 feet in the eastern part of the basin (Figs. 11, 14; Mull et al., 2003; Shimer et al., 2014). The Seabee Formation is composed of

bentonitic mudstone, silty mudstone, and medium-to-dark gray, organic-rich shale interbedded with bentonite and thick silicified tuff beds. It is interpreted to have been deposited in a marine slope, offshore marine shelf, and basin environment (Figs. 11, 13, 14; Mull et al., 2003; Houseknecht and Schenk, 2004).

3.2.5 Brookian Sequence, Tuluvak Formation

The Turonian to Coniacian Tuluvak Formation is defined by seismic topset reflections and overlies the Seabee Formation (Figs. 13, 14; Houseknecht and Schenk, 2004). The Tuluvak Formation is approximately 1,200 feet thick in the Colville basin and is composed of a thickening and coarsening upward unit of fine-grained sandstone, siltstone, and interbedded shale that is overlain by sandstone and conglomerate (Mull et al., 2003). The top of the Tuluvak Formation interfingers upward with the overlying Schrader Bluff Formation (Fig. 14; Mull et al., 2003). The Tuluvak Formation was deposited in a marine to marginal marine depositional environment (Mull et al., 2003).

3.3 General structural style of the Brooks Range foothills

The Brooks Range foothills are a prominent topographic feature extending northward into the Colville basin from the mountain front in northern Alaska (Fig. 11). The structural geometry and evolution of the foothills of the Brooks Range have been substantially influenced by mechanical stratigraphy (Moore et al., 2004; Wallace, 2009; Wallace et al., 2011). The Brooks Range foothills consist of gently deformed Cretaceous rocks. Wide, flat-bottomed synclines separate low-amplitude cuspate anticlines in the Nanushuk Formation, with anticlines spaced ~5 to 10 km apart (Figs. 2, 15; Wallace, 2009; Wallace et al., 2011). The Nanushuk

Formation is a relatively thick, structurally competent unit that forms a folded roof above the incompetent Torok Formation. A gently south-dipping detachment in or below the lower Torok Formation is responsible for the deformation of Cretaceous rocks (Moore et al., 2004; Wallace, 2009; Wallace et al., 2011; Sanders and Wallace et al., 2011). The anticlines are commonly cut by small-displacement thrust faults that may dip either to the south or north (Fig. 15; Wallace, 2009; Wallace et al., 2011). Local surface exposures and seismic reflection data indicate that the Torok is thickened in the core of anticlines (Moore et al., 2004; Wallace, 2009; Wallace et al., 2011; Sanders and Wallace, 2011). The overlying Seabee Formation is very incompetent and allows the Nanushuk to be detached relative to overlying competent units (Sanders and Wallace, 2011).

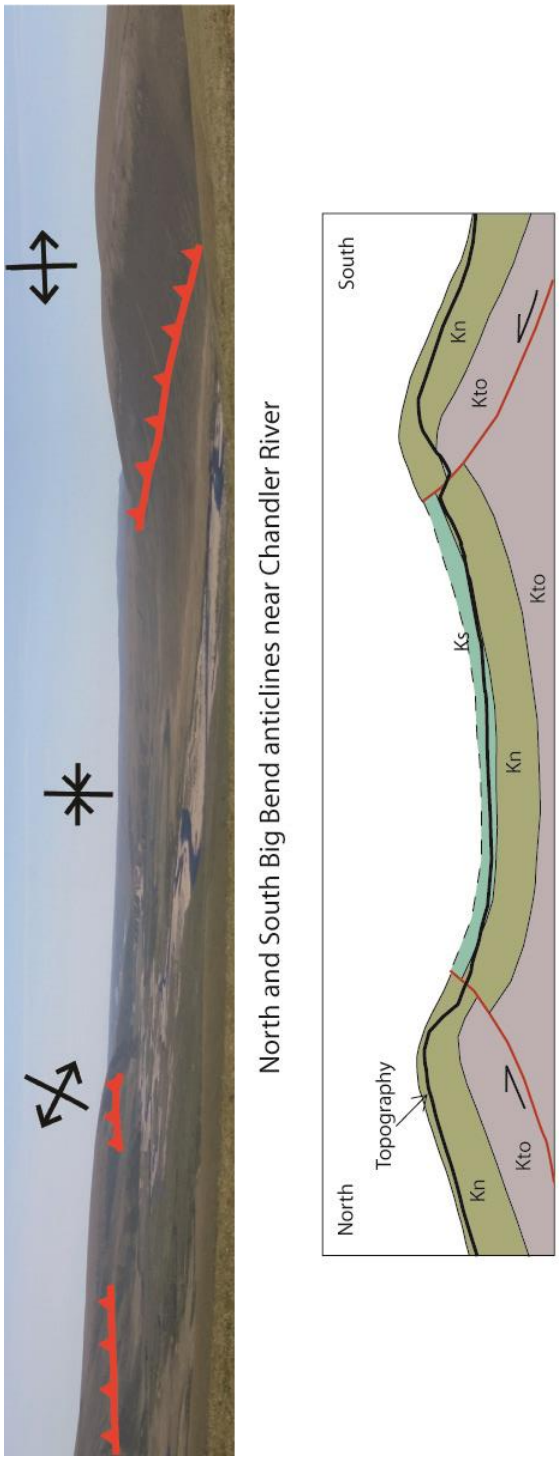

Figure 15: Panoramic photo view and schematic cross section showing thrust faults bounding the north and south branches of the Big Bend anticline. Photo is a view to the northeast. Photo and structural interpretation from Sanders and Wallace et al., 2011.

Collectively, these structures form a low-taper triangle zone (Jones, 1982; McMechan, 1985; Wallace et al., 2011; Sanders and Wallace, 2011). The gentle dip of the basal detachment and the low taper of the triangle zone are consistent with the variable vergence of the folds and thrust faults.

3.4 Previous fracture studies in northern Alaska

Previous fracture studies in the northeastern Brooks Range have focused on distinguishing fold-related fractures from regional and post-fold fractures and their relationship to mechanical stratigraphy (Hanks et al., 1997; Shackleton, 2003).

Four fracture sets have been recognized in northern Alaska and are interpreted to be pre-fold, syn-fold, and post-fold fractures. Where they have been studied in the northeastern Brooks Range, pre-fold fractures strike approximately north, normal to the advancing fold-and-thrust belt, and are interpreted to have formed under high fluid pressures with low differential effective *in situ* stress in flat-lying strata (Hanks et al., 2004; Hayes, 2004). Early pre-fold and syn-fold fractures are oriented parallel and perpendicular to the fold axis and are interpreted to have formed in the presence of fluids. Early pre-fold and syn-fold fracture sets are commonly filled with quartz or calcite cement (Shackleton et al., 2005; Hayes, 2004) and could have acted as conduits for fluid flow (Hanks et al., 2004).

Post-fold fractures strike north-northwest and are commonly unfilled, suggesting that they did not act as conduits for significant fluid flow (Hayes, 2004). Unfilled post-fold fractures are interpreted to form during late flexural slip folding and/or relief of stored elastic strain during unroofing (Engelder, 1985; Hancock and Engelder, 1989). Unfilled post-fold fractures parallel the filled pre-fold fractures and are potentially reactivated early pre-fold fractures (Engelder, 1985; Hanks et al., 2004; Hayes, 2004).

Hayes (2004) introduced a kinematic model that depicts the mechanical history of detachment folds and the character and relative timing of fracture sets that are associated with these folds. In the first stage of the model, the beds are flat-lying and lithified during regional burial. As pore fluid pressure increases ahead of an advancing deformation front and the differential stress ($\sigma 1 - \sigma 3$) remains low, regional extension fractures develop (Fig. 16; Hayes, 2004). Syn-fold fractures form as the result of outer-arc stretching during buckling and detachment folding and form in different orientations depending on the type of fold and the degree of folding (Fig. 16; Hayes, 2004; Hayes and Hanks, 2008). Regional uplift and erosional unroofing occur as folding stops in the last stage of this model (Fig. 16). Unloading fractures form after folding and normal to fold trend.

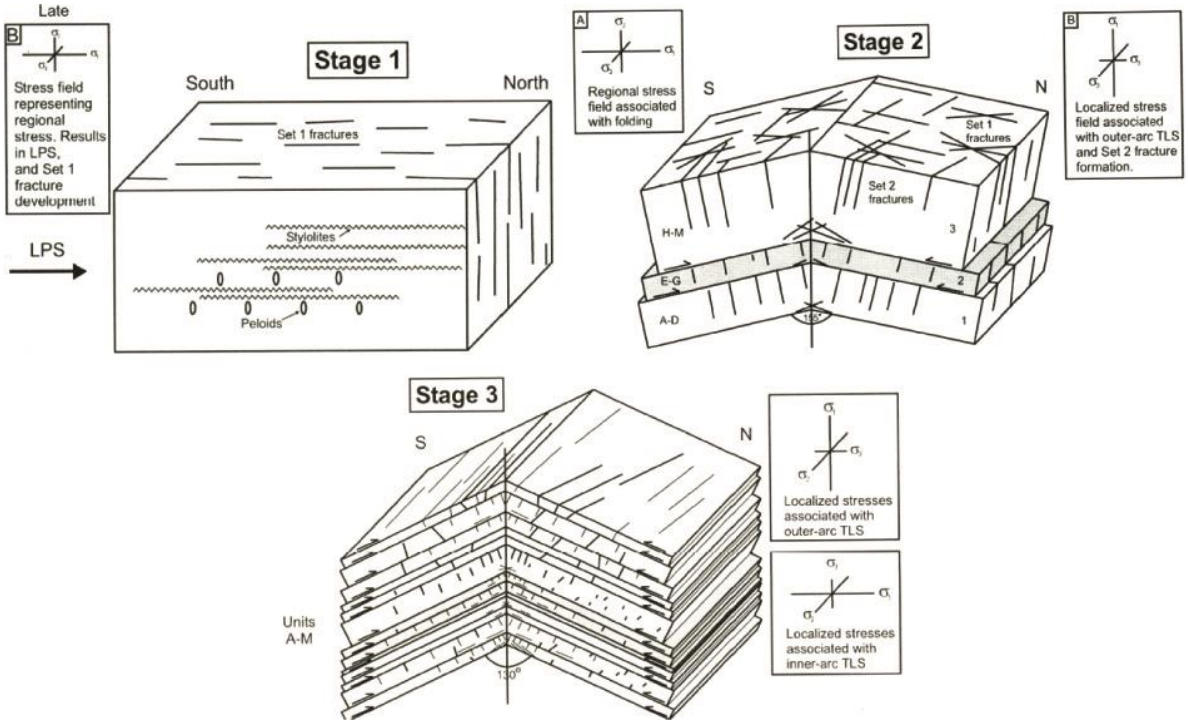

Figure 16a: Kinematic model proposed by Hayes (2004). Hayes defined fracture sets based on when they formed relative to the evolution of the fold. Consequently, a single set may include both extension and shear fractures and fractures formed with locally different orientations of principal stress axes. Stage 1: North-striking Set 1 extensional fractures develop after burial due to increased regional layer-parallel strain. Stage 2: Set 1 conjugate shear fractures form during early fold development due to increased differential regional stress; Set 2 fractures form under local stress conditions within mechanical units under inner and outer arc tangential longitudinal strain. Stage 3: Set 2 fractures continue to form by tangential longitudinal strain and cut through multiple mechanical units.

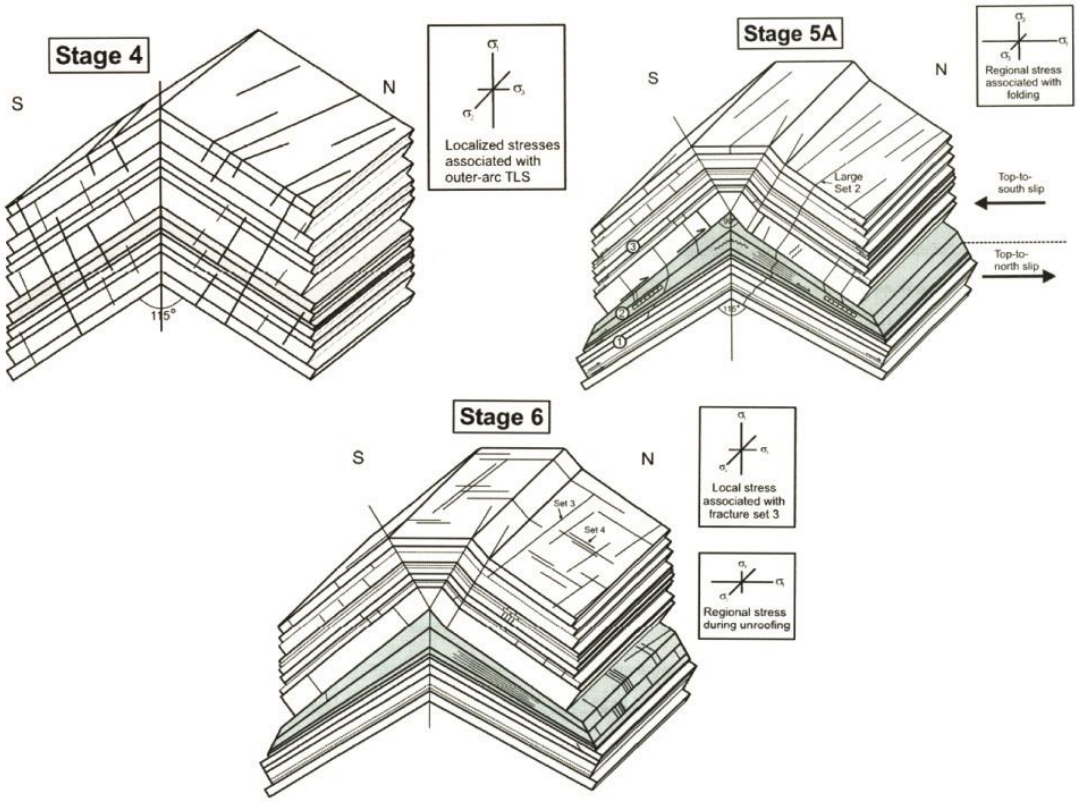

Figure 16b: Stages 4–5A: Set 2 fractures continue to form by tangential longitudinal strain and cut through multiple mechanical units. Stage 6: Set 3 fractures form as stored elastic strain related to folding is released after deformation. Set 4 north-striking unloading fractures form after folding.

3.5 Age of deformation of the central Brooks Range foothills in the southern Colville basin

Northern Alaska has undergone multiple deformational events since the Jurassic, with initial major shortening in the Late Jurassic to Early Cretaceous (Mull, 1982; Moore et al., 1994). Fission track data from the central Brooks Range and North Slope foreland basin indicate three later major episodes of rapid cooling during Cretaceous and Tertiary time (Fig. 17; O'Sullivan, 1996; O'Sullivan et al., 1997). The first episode of rapid cooling due to denudation occurred at ~100 Ma within the range, followed by episodes at ~60 Ma and at ~25 Ma in the range and the foothills (Fig. 17; O'Sullivan, 1996; O'Sullivan et al., 1997).

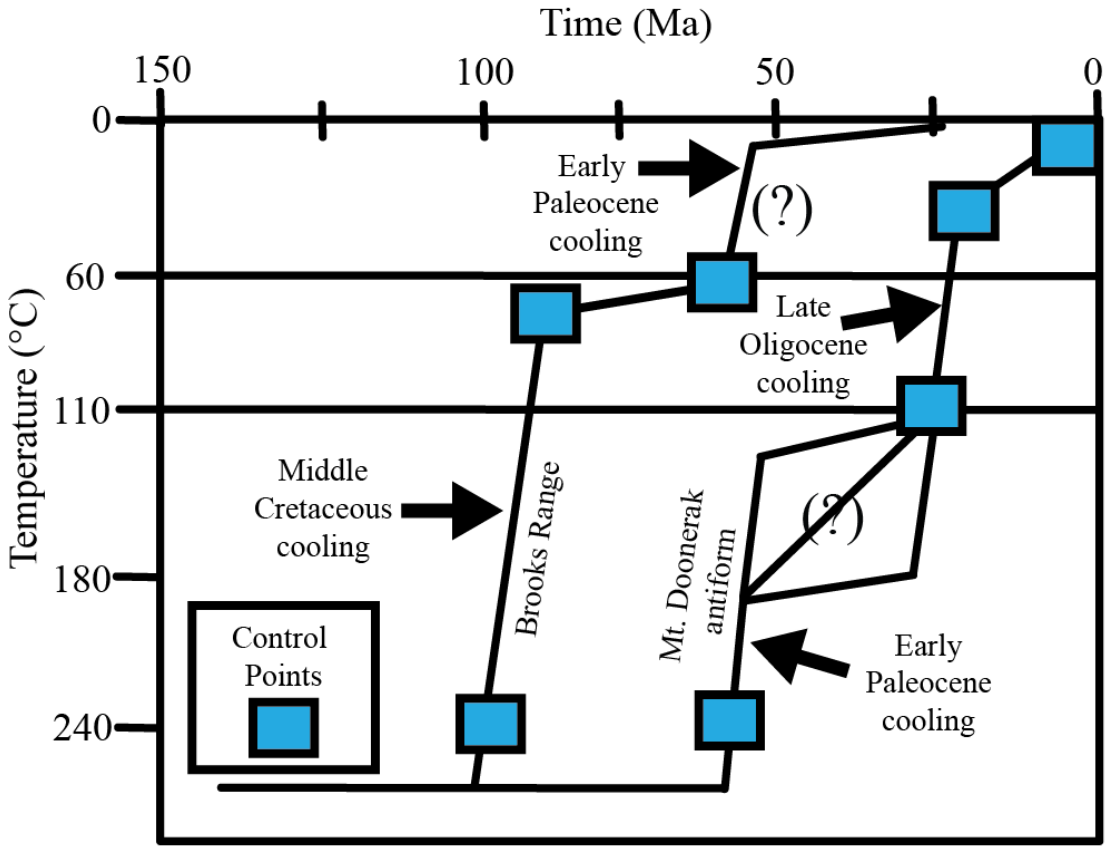

Figure 17: Schematic time-temperature history curve proposed by O'Sullivan et al. (1997) for the central Brooks Range, inferred from apatite and zircon fission track data. Three major cooling episodes are recorded, during the middle Cretaceous, early Paleocene, and late Oligocene. Control points are from apatite and zircon fission track data. Dashed lines with question marks represent cooling paths below ~ 240°C, which are not constrained by the data.

The oldest cooling event is interpreted as cooling related to uplift of the core of the Brooks Range orogen following earlier major shortening (O'Sullivan et al., 1997; O'Sullivan et al., 1998; Duncan et al., 2006). The second cooling event at ~60 Ma is regionally recorded from the core of the Brooks Range north into the Colville basin and is interpreted to be cooling associated with uplift during fold-and-thrust deformation that occurred from ~70 to 60 Ma (Fig. 17; O'Sullivan et al., 1997; Mull et al., 2003; Moore et al., 2004; Duncan et al., 2006). This is the main deformational event in the foothills. Cooling ages of ~25 Ma are observed in the distal

Colville basin and are interpreted to represent progressive denudation within the advancing deformation front during the late Oligocene (O'Sullivan et al., 1997; Houseknecht et al., 2011).

3.6 Umiat anticline and oil field

The Umiat anticline is a detachment fold in Cretaceous rocks located in the northern foothills region of the Brooks Range that formed as a result of north-south compression (Fig. 2; Molenaar, 1982). The anticline is a broad, low-amplitude fold with north-vergent reverse faults in its axial zone (Fig. 18). Different interpretations show the faults differently, but most show more than one. The reservoir is approximately 770 to 1,055 feet below ground surface in the Nanushuk Formation.

Between 1945 and 1952, eleven wells were drilled on the anticline to determine production possibilities (Fig. 18; Collins, 1958; Molenaar, 1982). These wells were extensively cored. Additional Umiat cores were collected during a second phase of exploration by the U.S. Navy and the U.S. Geological Survey between 1975 and 1981 (Baptist, 1960; Molenaar, 1982). Cores from both exploration phases are well preserved and available for study at the Alaska Division of Geological and Geophysical Surveys Geologic Materials Center in Eagle River.

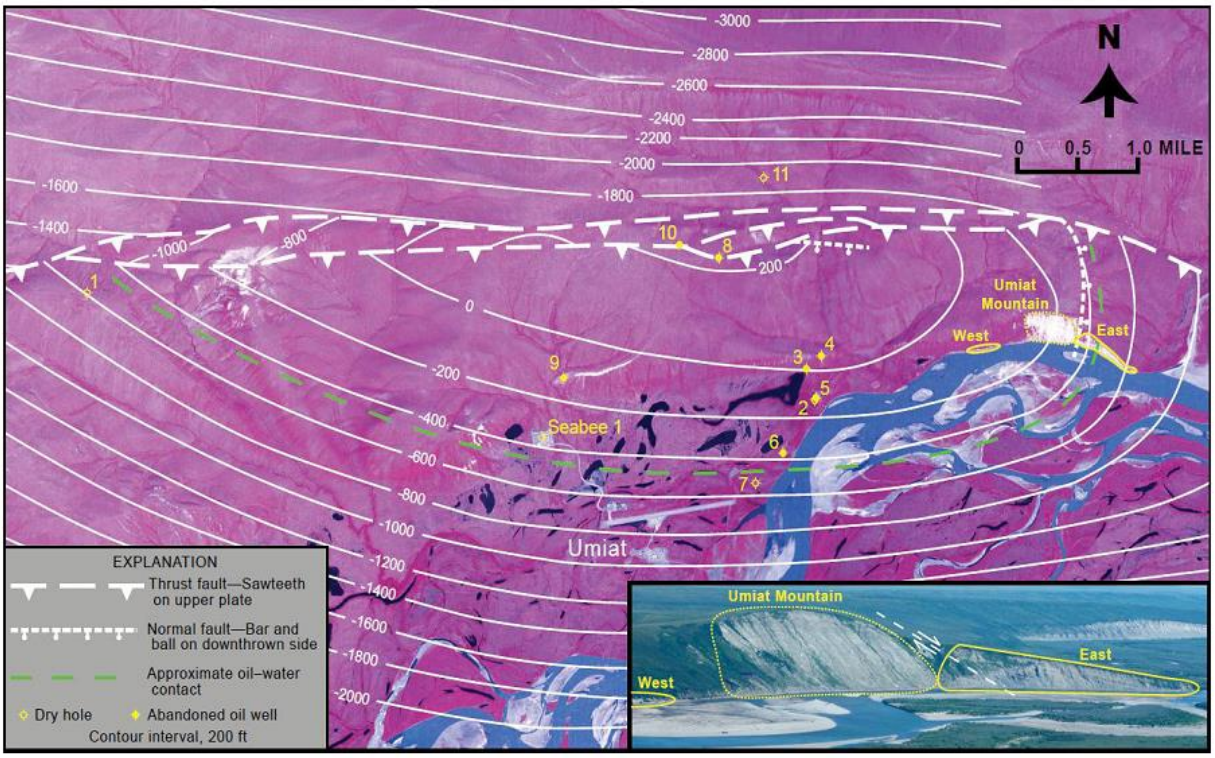

Figure 18: False-color infrared aerial photomosaic of Umiat area, northern Alaska, with superimposed structure contour map showing the locations of test wells in yellow. From Houseknecht and Schenk (2004).

Initial estimates of primary recoverable reserves at Umiat ranged from 30 to over 100 million barrels (bbl), with an average of about 70 million bbl (Baptist, 1960; Molenaar, 1982). Umiat oil is a light oil that has a specific gravity of 36.0° to 37.2° API (American Petroleum Institute), and it contains less than 0.1 wt. percent sulfur (Brosge and Whittington, 1966; Molenaar, 1982). The average vitrinite reflectance value for Umiat oil is 0.53 from a depth of 3,303 feet, making it light oil (Brosge and Whittington, 1966; Molenaar, 1982). This VR value indicates that the rocks are immature to marginally mature for oil generation.

Umiat oil field was never developed because the estimated recoverable reserves (~70 million bbl) were not economical to produce due to the shallow nature of the field, the remoteness of the area, and the harsh environment. The primary producible reservoir at Umiat

field is located within the permafrost zone in delta-front and shoreface sandstones (Molenaar, 1982). Permafrost complicates the production of the reservoir by freezing the oil migration pathways within the reservoir (Molenaar, 1982). Other complications that hinder production are borehole collapse, ice bridging (Collins, 1958), and pore-clogging ice (Baptist, 1960; Hanks et al., 2014) that significantly reduces the relative permeability of the oil (Hanks et al., 2014).

Magoon et al. (2003) identified three Lower Cretaceous organic-rich units as the source rocks for the Umiat oil field: the pebble shale unit (Pebble), gamma-ray zone (GRZ), and the lower Torok Formation (Fig. 13). A previous study by Claypool and Magoon (1985) suggested that this conformable package of Lower Cretaceous strata has a similar kerogen composition (Magoon and Bird, 1985) and should be considered one single source rock unit. According to the interpretation of Magoon et al. (2003), petroleum from the pebble shale unit, GRZ, and the lower part of the Torok Formation migrated up through foreset beds of the Torok to the updip Cretaceous Nanushuk reservoir rocks during the Early Cretaceous.

Shimer et al. (2014) have recently reevaluated existing cores from Umiat wells and defined three major Nanushuk Formation reservoir intervals at Umiat Field: Lower Grandstand A and B (Lower Nanushuk), and the Upper Grandstand (Upper Nanushuk) (Fig. 13). In the subsurface, these three intervals are laterally continuous across the entire Umiat field, although the Upper Grandstand is internally heterolithic (Shimer et al., 2014).

While horizontal permeability increases toward the top of each of these three reservoir units, the high-permeability zone is limited to the top of upward-coarsening successions where the sandstone is well sorted and fine- to medium-grained (Shimer et al., 2014). Vertical permeability will differ in the Lower and Upper Grandstand because the Upper Grandstand has more flow barriers as a result of micaceous and carbonaceous laminae (Shimer et al., 2014). The

Lower Grandstand sandstone is considered to be the best reservoir target for initial development because it is the deepest part of the reservoir interval and would be the least affected by permafrost (Shimer et al., 2014; Hanks et al., 2014). The intervening Shale Barrier was determined by Shimer et al. (2014) to be impermeable and would therefore act as a flow barrier (Hanks et al., 2014).

These new interpretations, suggest that the accumulation may be considerably larger than originally thought. The latest reservoir modeling incorporated a reservoir property model (Levi-Johnson, 2010) and the refined facies-controlled horizontal and vertical permeability characteristics and reservoir geometries proposed by Shimer et al. (2014). The final estimates of oil are 1.2 billion barrels in place, or 180 to 225 million barrels of recoverable oil (Kohshour et al., 2013; Shimer et al., 2014).

With the advancement in modern horizontal drilling techniques, the Lower and Upper Grandstand reservoir units are ideal targets, and production could be more efficient than in the past (Hanks et al., 2014). The most efficient means of accessing the target reservoir interval would be to use a wagon-wheel pattern (Hanks et al., 2014). This pattern will allow the maximum amount of reservoir to be stimulated while minimizing the surface footprint (Hanks et al., 2014).

3.7 Geology of the study area

This study focuses on developing a model of fracture distribution at Umiat anticline using Umiat core and surface fracture patterns at three nearby exposed anticlines: the Big Bend anticline, Fossil Creek, and the Colville incision (Figs. 2, 19). The structural geometry of these anticlines is comparable to that of Umiat anticline, and Wallace (2009) and Wallace et al. (2011)

interpreted them to be detachment folds in the competent Nanushuk above thickened Torok Formation. The surface outcrops expose different structural levels and different stratigraphy, providing an opportunity to evaluate fracture distribution and character with structural level and stratigraphy. This information can then be used to refine the Umiat fracture model.

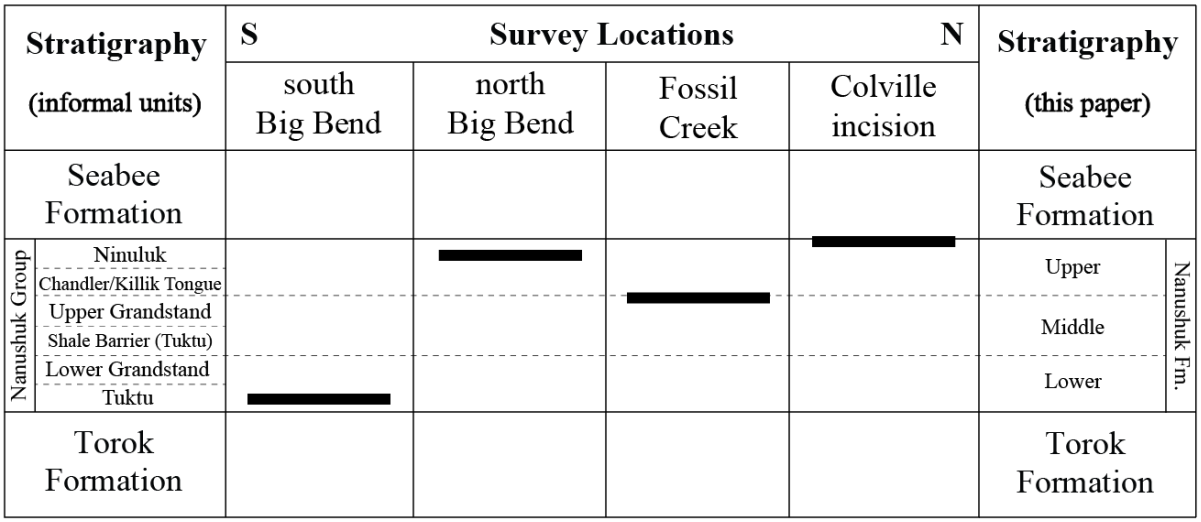

Figure 19: Schematic diagram showing approximate stratigraphic level at each fracture survey location.

The Big Bend anticline is located approximately 30 km south-southeast of the Umiat anticline. The Big Bend anticline is an east-west trending symmetric anticline in the Nanushuk Formation with a core of thickened Torok Formation (Figs. 2, 19) and exposes rocks equivalent to deeper structural levels of the Umiat anticline (Fig. 19) at south Big Bend. At north Big Bend, a level near the top of the Nanushuk is exposed (Sanders and Wallace, 2011) (Fig. 19). Big Bend anticline branches westward into two anticlines that are each cut by relatively steep and low-displacement thrust faults (Sanders and Wallace, 2011). The north limb of the south anticline is cut by a south-dipping thrust fault, and the south limb of the north anticline is cut by

a north-dipping thrust fault (Fig. 16). Sites suitable for fracture surveys were located in the south limb of the south branch and the south limb of the north branch.

The Fossil Creek site is located in the south limb of the Fossil Creek anticline, approximately 24 km southwest of Umiat anticline (Figs. 2, 19). The Fossil Creek anticline is an east-west trending cuspate anticline with a similar size and shape to the Big Bend anticline. The middle Nanushuk is exposed at this site (Figs. 2, 19).

The Colville incision is in the upper Nanushuk Formation in the north limb of an anticline that branches to the west-northwest from the east-west trending Fossil Creek anticline approximately 22 km west-southwest of Umiat anticline. This site is only 8 km from the Fossil Creek site but is separated from it by an inferred left lateral fault along the Colville River (Fig. 2). This site is equivalent to the upper part of the Umiat anticline (Fig. 19).

Chapter 4

METHODS

4.1 Introduction

The characterization of fractures at Umiat anticline uses two important components: subsurface analysis of cores and surface analysis of outcrop through fieldwork. Cores provide significant information about vertical changes within the Umiat reservoir but provide limited information about fracture characteristics and distribution. Outcrop observations supplement analysis of cores by documenting spatial variability of fracture density at the reservoir scale and provide a bridge across gaps in data from core and well logs.

4.2 Identification of fractures in cores

Fractures are spatial phenomena and as such are best characterized based on both exposed rock and in well data. During June and early July of 2009, cores taken from Umiat wells #1, #2, #8, #9, #10 and #11 were examined for natural fractures.

In examination of cores, it is important to distinguish between natural fractures and those that are induced by coring. Natural fractures in cores can provide statistical information such as spacing, width, and orientation, provided that (1) natural fractures are distinguished from those artificially induced by coring and (2) the orientation of the core is known (Stearns and Friedman, 1972). Natural fractures have a tendency to occur at a high angle to bedding in both deformed and undeformed rocks. In cores, natural fractures are planar structures that show no genetic geometric relationship to the core barrel. If open, natural fractures may have surface staining and/or surface ornamentation such as plumose structures or slickensides; healed fractures are

cemented (most commonly) by calcite or quartz. In contrast, coring-induced fractures are all open, commonly are non-planar and/or curved, and show a clear genetic geometric relationship to the core and/or core boundaries.

All cores were inspected for fractures. Once identified, geometric characteristics with respect to the core were used to determine if the fracture was natural or coring-induced. The following information was also recorded:

- the angle of the fracture with respect to bedding observed in the core,
- the depth of occurrence,
- the host lithology,
- any surface staining on fracture, and
- the presence of cement.

Because the orientation of the core with respect to north is unknown, the strike of fractures in the core could not be determined. Observing more than one fracture with different strike and dip orientations with respect to bedding in a single core may help identify different fracture sets. However, because the core is not oriented, this information gives no orientation of fracture sets with respect to north.

A classification scheme was used to distinguish between coring-induced and natural fractures (Table 1). Because it was not always possible to determine unambiguously if a fracture was natural or coring-induced, all fractures were classified on a scale from 1 to 5 according the criteria shown in Table 1. All fractures were measured relative to bedding. Bedding is perpendicular to the core axis, and all wells were drilled as vertical wells. Fractures considered to be coring induced were assigned a classification of 1 or 2 and fractures considered to be natural were assigned a classification of 3 to 5. All fractures with angles about 0 to 22° with

respect to bedding were designated 1. A classification of 2 was given to all fractures that exhibited an angle from 23 to 44° with respect to bedding and no surface staining or apparent cementation. All fractures with an angle of 45 to 68° with respect to bedding and no surface staining or cementation were classified as 3. A classification of 4 was given to all open fractures with angles ranging from 69 to 90° with apparent surface staining. Near-vertical fractures (~69 to 90°) that were calcite cemented were designated 5.

Table 1: Fracture classification scheme using the angle between the fracture and the normal to the core (bedding).

Class	Fracture Characteristics	Classification
1	Open, curved fractures with a clear geometric relationship to the core barrel, approximately 0 to 22° with respect to core barrel	Coring induced
2	Open planar fractures at an angle from 23 to 44° with respect to bedding, no surface staining or apparent cementation	Coring induced
3	Open planar fractures at an angle of 45 to 68° with respect to bedding, apparent surface staining and/or cementation	Natural
4	Planar open fractures with an angle from 69 to 90° with respect to bedding; may have no surface staining to apparent surface stain	Natural
5	Planar open fractures with an angle from 69 to 90° with respect to bedding, calcite cemented	Natural

4.3 Surface fracture mapping

During June and early July 2010, eight fracture surveys were conducted at four sites on anticlines similar to the Umiat anticline (Fig. 2). Fracture data were collected using the straight scan-line fracture survey method used by Priest (1993), Shackleton (2003), Hanks et al. (2006), Duncan (2007), and Hayes and Hanks (2008). A flexible tape measure was laid along an exposed fracture face or bedding surface, and every fracture that intersected the tape line was recorded. The length of each fracture transect varied from location to location, with the shortest transect (~24 feet) taken at Fossil Creek and the longest transect (~212 feet) taken at the Colville

incision. The following information was recorded: orientation of fractures, spacing between adjacent fractures, height of fracture (perpendicular to bedding), length of fractures (parallel to bedding), fracture aperture (width of opening normal to fracture wall), fracture fill and composition (quartz or calcite), nature of fracture terminations, and the fracture type (shear or extension).

Classification of fractures as mode 1 extension fractures or mode II conjugate shear fractures was based on observations consistent with previous fracture morphology research and modes of fracture formation (Sterns, 1968; Engelder, 1985; Ramsay and Huber, 1987; Hancock and Engelder, 1989; Lorenz et al., 1991; Hanks et al., 2004; Duncan et al., 2006; Hayes and Hanks, 2008). If the movement on either side of the fracture plane is normal to the fracture, the fracture is classified as an extension fracture. If the movement on either side of the plane is parallel to the fracture, it is classified as a shear fracture. Slickenlines on fracture surfaces indicate this type of shear movement.

Fracture orientations, presence or absence of fill, morphology, and relative age relationships between fractures were used to define fracture sets and their characteristics.

Chapter 5

OBSERVATIONS

5.1 Fracture distribution and characteristics in Umiat core

Cores taken from Umiat wells number 1, 2, 8, 9, 10, and 11 were examined for natural fractures (Fig. 18). Umiat wells 1, 2, and 9 are located near the Colville River at a lower elevation on the limbs of the fold (Fig. 18). Umiat wells 8, 10, and 11 are located at higher elevations near the fold hinge and near several thrust faults identified by Houseknecht and Schenk (2004) (Fig. 18). All wells were drilled as vertical wells, and bedding is perpendicular to the core axis. No natural fractures were identified in cores from wells 8, 9, and 10.

Natural fractures were identified in Umiat wells 1, 2, and 11 and classified using the scheme illustrated in Table 1 (Fig. 18, Tables 1, 2). All the natural fractures observed in the cores included steep dips that range from 46° to 90° with respect to bedding, calcite cementation, and apparent surface iron oxide staining.

Umiat well 1 was drilled to approximately 6,005 feet deep. The amount of cored section that was recovered and examined was approximately 1,294 feet (Table 3). Two natural fractures were identified in core from Umiat well 1 at interval depths of 2,337 to 2,347 feet and 2,347 to 2,357 feet (Figs. 18, 20; Table 2). Both fractures are natural fractures with very steep dips with respect to bedding and calcite cementation (Table 2). These fractures were assigned a classification of 5 based on observed fracture characteristics according to Table 1.

Umiat well 2 was drilled to approximately 6,212 feet deep with 592.75 feet of recovered core. Approximately 500 feet of core was examined and three natural fractures were identified in interval depths of 544 to 554 feet, 562 to 572 feet, and 1,429 to 1,439 feet (Fig. 21, Table 2).

The first fracture identified was near vertical (88°) with no surface staining or cementation and was classified as a 4 (Table 2). The second natural fracture had a dip of approximately 79° with respect to bedding and was open with no cementation or surface staining, so it was classified as a 4 (Fig. 21, Table 2). The third fracture observed in Umiat well 2 core was open with no surface staining and had a dip of 76° with respect to bedding and was classified, based on observed characteristics, as a 4 (Table 2).

Natural fractures were most abundant in Umiat well 11 (Figs. 18, 22; Table 2). Approximately 740 feet of core was recovered from 3,303 feet of drilled section in Umiat well 11. Approximately 740 feet of core was examined and six natural fractures were identified (Table 2). The three fractures that were each classified as a 3 have dips of 80°, 82°, and 85° and have no apparent surface staining or cementation (Table 2). Fractures identified at 452 to 469 feet and 1,354 to 1,356 feet have a dip of 83° with respect to bedding and each is classified as a 5 because it is calcite cemented (Table 2). Figure 23 shows a significantly gentler dipping fracture (~45°) with extensive surface staining that was identified in Umiat well 11 Core box 1 at a depth of 126-129'. This fracture was classified as a 3 based on the surface staining and the lack of calcite cementation.

Table 2: Characteristics and classification of the natural fractures identified in Umiat well 1, 2, and 11 cores. All angles of fractures were measured with respect to bedding. Bedding is horizontal and perpendicular to the core axis.

Well	Core	Depth	Host Lithology	Classification	Characteristics
1	144	2,347–2,357 ft	Microfossils abundant. 2 ft, medium to light gray, very fine sandstone with vertical veinlets. 7 in., medium to dark gray, slightly to very silty claystone.	5	88° with respect to bedding, strike unknown, no staining, calcite cemented.
1	143	2,337–2,347 ft	Microfossils very rare. 3 ft 6 in., massive sandstone. 5 ft 6 in., medium to light gray, very fine-grained sandstone.	5	89° with respect to bedding, strike unknown, no staining, calcite cemented.
2	73	1,429–1,439 ft	Medium to dark gray, slightly to very silty claystone, micaceous, non-calcareous. Microfossils abundant.	4	88° with respect to bedding, strike unknown, no staining, not cemented.
2	38	562–572 ft	Very lightly silty claystone.	4	79° with respect to bedding, strike unknown, no staining, not cemented.
2	5	544–554 ft	6 in., sandstone grading to siltstone to claystone. Abundant laminae of dark gray clay shale. 8 ft 10 in., medium-dark gray, very silty claystone	4	76° with respect to bedding, strike unknown, no staining, not cemented.
11	27	452–469 ft	Interbedded clay-shale, fine-grained sandstone and siltstone.	5	83° with respect to bedding, strike unknown, no staining, calcite cemented.
11	25	1,357–1,377 ft	Medium-gray clay shale.	3	85° with respect to bedding, strike unknown, no staining, not cemented.
11	24	1,354–1,356 ft	Very fine grained, slightly silty, olive-gray sandstone.	5	83° with respect to bedding, strike unknown, no staining, calcite cemented.
11	14	709–729 ft	Medium-gray clay shale, slightly bentonitic.	3	82° with respect to bedding, strike unknown, no staining, not cemented.
11	3	222–242 ft	Medium-gray claystone, bentonitic, micaceous, slightly silty.	3	80° with respect to bedding, strike unknown, no staining, not cemented.
11	1	0–136 ft	Light-gray, fine-grained sandstone.	3	45° with respect to bedding, open, stained

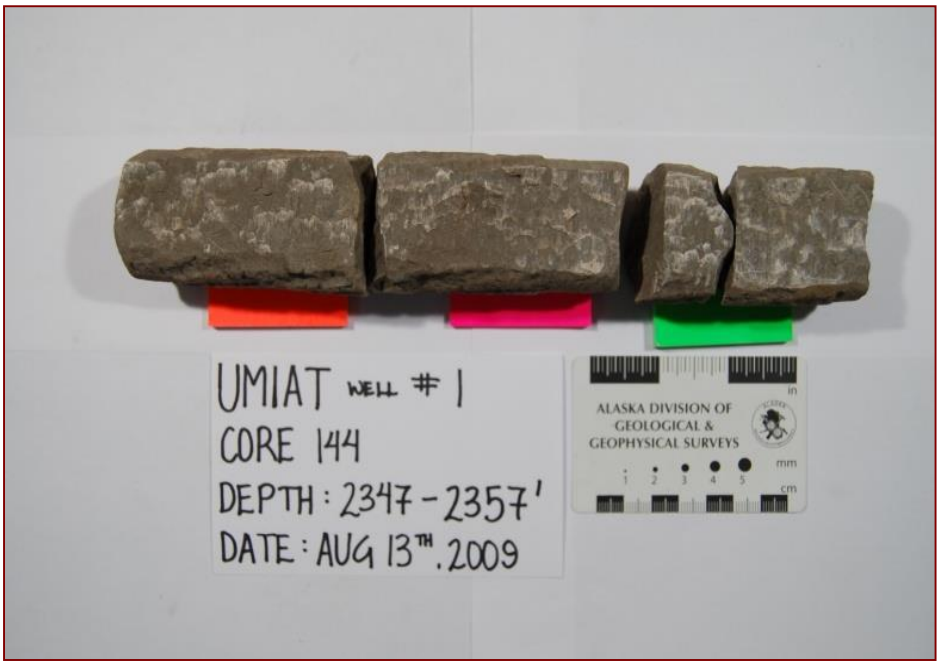

Figure 20: Near-vertical natural fracture identified in core 144 of Umiat well 1, showing calcite cementation.

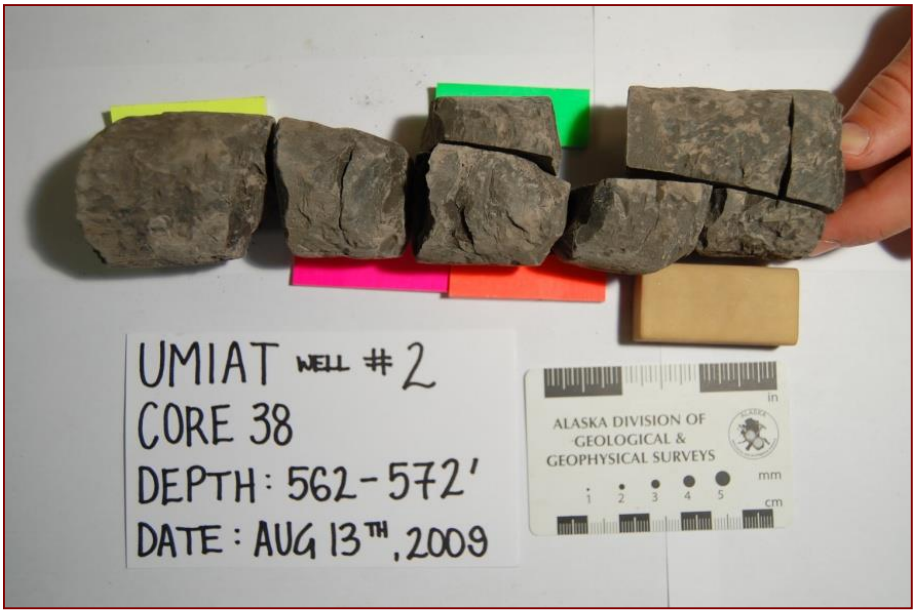

Figure 21: Fracture with a 79° dip in Umiat well 2, core 38, depth of 562 to 572 feet.

Figure 22: Fracture with an 82° dip in Umiat well 11, core 14, depth of 709 to 729 feet.

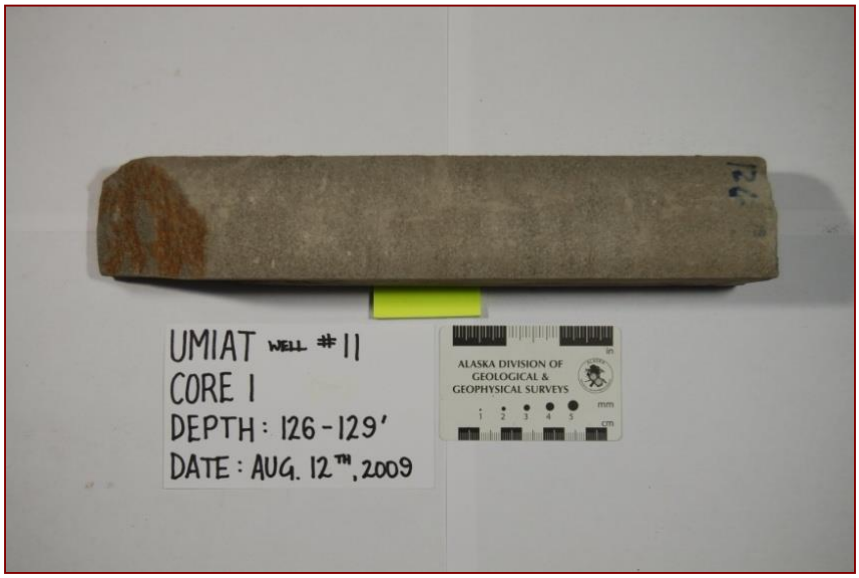

Figure 23: Significantly gentler dipping fracture (~45°) with surface staining in Umiat well 11, core 1.

Table 3: Well depth, amount of recovered and examined core, and number of natural fractures identified in Umiat wells 1, 2, and 11.

Well number	Well depth (ft)	Amount of recovered core (ft)	Amount of core examined (ft)	Number of natural fractures identified (ft)
1	6,005	1,294	1,294	2
2	6,212	592.75	500	3
11	3,303	740.45	740	6

5.2 Fracture character and distribution in the field

Fracture characteristics were observed at four locations in Cretaceous rocks near the Umiat anticline in the Colville basin. Figure 24 shows the location of each of the fracture transects. The orientations of each transect, with respect to north, is shown with a red line.

One east-west transect was taken at the Colville incision, one north-south transect was taken at Fossil Creek, and two transects (both oriented northwest-southeast and treated as a composite transect) were taken on the south limb of the south branch of Big Bend anticline (Big Bend south) (Fig. 24). Four transects were taken on the south limb of the north branch of Big Bend anticline (Big Bend north). Transect 4 is oriented northwest-southeast and transects 6, 3, and 5 (from northeast to southwest) are oriented northeast-southwest and treated as a composite transect. All transects were measured parallel to bedding so fracture spacing is relative to bedding.

I identified three sets of fractures (A–C) interpreted from measurements I obtained on eight scan line transects (Figs. 24, 25). I assigned each fracture to a fracture set based on my analysis of fracture orientation and definition of fracture sets using orientation, relative age, apparent sense of shear, presence of cement, standard rose diagrams, and stereonets. Fracture set A includes both open (Ao) and filled (Af) fractures that strike north-northwest to north-northeast.

Set B fractures are defined by an east-west orientation and are open fractures. Set C fractures are open conjugate shear fractures and are oriented northwest-southeast (Cnw) and northeast-southwest (Cne). Slickenlines are present on set C fracture faces, indicating that these are shear fractures. The letters assigned to the fracture sets reflect the interpreted order of their formation. Not all fracture sets were present in a single location, and there is no strong and direct observational evidence of relative timing of two sets at any location.

I used the following criteria to assess and determine relative ages of fractures: the presence or absence of surface staining or fracture infilling material, interaction of fractures of different sets, the morphology of the fractures, fracture spacing, and bed thickness. Typically, when more than one set of joints has developed, the younger joints will terminate against the older joints because the younger fracture cannot propagate across the open surface of another fracture. The termination of younger fractures is typically at high angles, often forming a T-shaped intersection, or it may curve toward an older fracture.

Fractures that cross-cut other fractures or geologic structures postdate the formation of that structure. If fractures maintain a constant orientation across folded layers of rock, the fractures must have formed after folding, while fractures that are affected by a geologic structure are older than the structure. A fracture set that changes orientations over a fold but maintains a constant angular relationship with bedding could either predate folding or be synchronous with it.

Another indication of relative age between fracture sets is mineralization. If a fracture set is consistently mineralized, then it must be older than the mineralizing event. Likewise, if there is a second fracture set existing in the same area as filled fractures and that is not mineralized, then this set probably formed after the mineralizing event. Observations of fractures are summarized by transect in Tables A9–A16 in Appendix A.

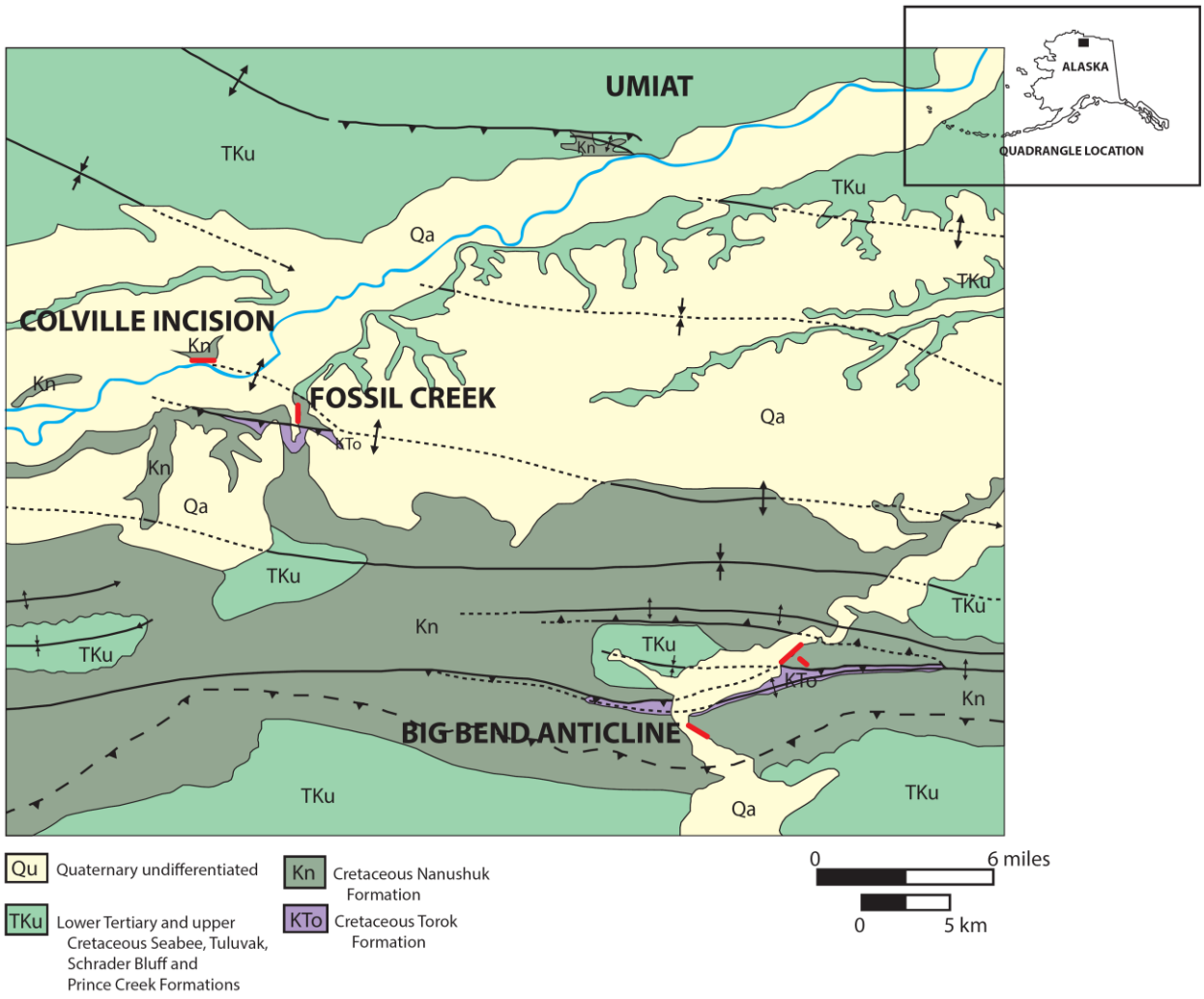

Figure 24: Map showing the Colville incision, Fossil Creek, and the Big Bend anticline with the location and relative orientations of each fracture transect shown with red lines. Two fracture transects taken on the south limb of the south branch of Big Bend anticline share the same orientation of northwest-southeast and have been combined to form one transect. Four transects were taken on the south limb of the north branch of the Big Bend anticline. These transects have been combined into two transects with orientations of northwest-southeast and northeast-southwest. The GPS locations of each transect, transect orientations, and bedding dip(s) are recorded for each transect in Table A17. Modified from Mull et al. (2004).

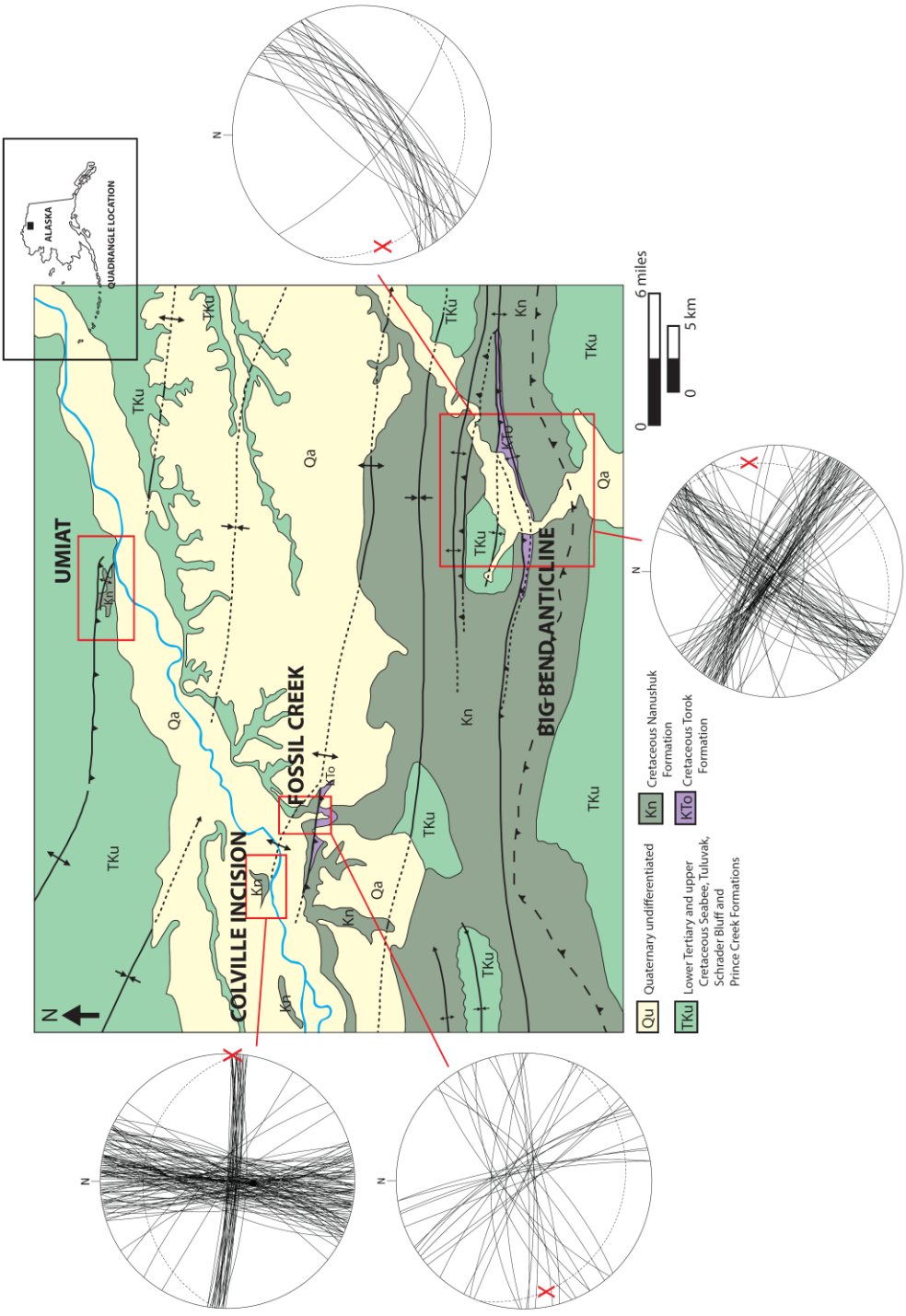

Figure 25: Map showing the Colville incision, Fossil Creek, and the Big Bend anticline with fracture stereonets from each location. The bedding planes for each location are marked with a dashed black line; red X marks the fold axis. Map modified from Mull et al. (2004).

5.2.1 Structural data

I identified three fracture sets using the rose diagrams, contoured stereonets, fracture fill, relative age, and sense of shear data. All fracture data were compiled in Microsoft Excel for easy data transfer and sorting. I combined transects 1 and 2 from the south limb of the south branch of the east-west-trending Big Bend anticline because each transect had the same orientation with respect to north and both had similar bedding orientations. I also combined transects 3, 5, and 6 from the south limb of the north branch of Big Bend anticline for the same reasons. For each transect, I generated a raw stereonet for fracture orientation and bedding in their present orientation (Figs. 26a, 26b). A red X marks the orientation of the local fold axis. I determined the fold axis using the strike and dip of the fold limb I measured at each location combined with fold trend and other strikes and dips from the geologic map of Mull et al. (2003). I also generated rose diagrams for each transect using the strike of each fracture (Figs. 26a, 26b). The final projection that I produced using Rockworks15 was a stereonet of orientation data for each transect (Figs. 26a, 26b). For each location, I restored the fractures to their orientation when bedding was horizontal using Stereo32 (Fig. 27). I identified three fracture sets using the rose diagrams, contoured stereonets, fracture fill, relative age, and sense of shear data. Sense of shear data for all fractures was recorded and is presented in Tables A11 through A18 in Appendix A.

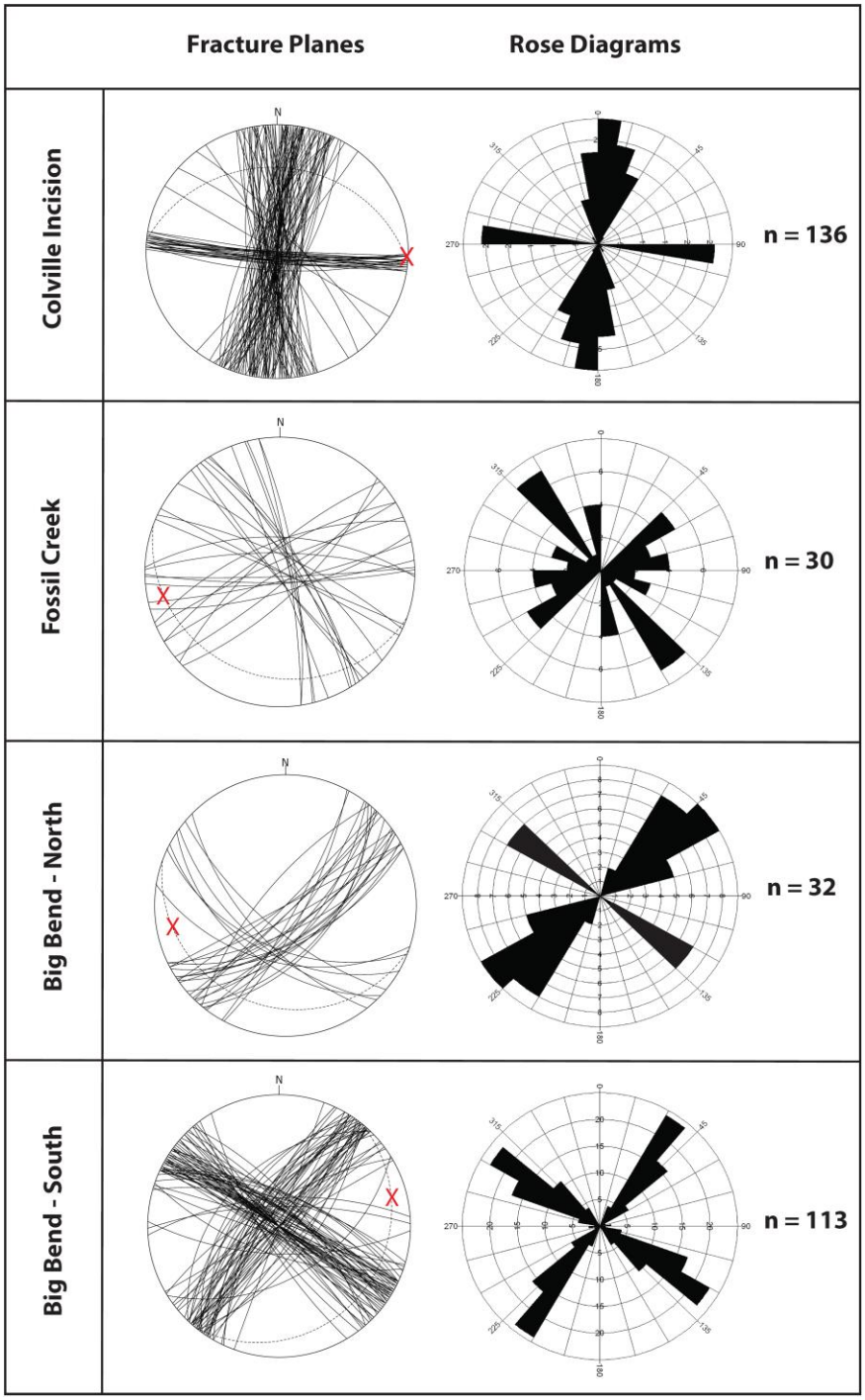

Figure 26a: Raw data stereonets and rose diagrams for four scan-line fracture surveys at Big Bend anticline, Fossil Creek anticline, and the Colville incision. Only data from transect 4 is presented in this figure for Big Bend north because it is the best representative plot for that location. Big Bend north transects 3, 5, and 6 have a slightly anomalous dip and are presented in Figure 26b. The bedding planes for each location are marked with a dashed black line on the stereonet diagrams; a red X marks the fold axis.

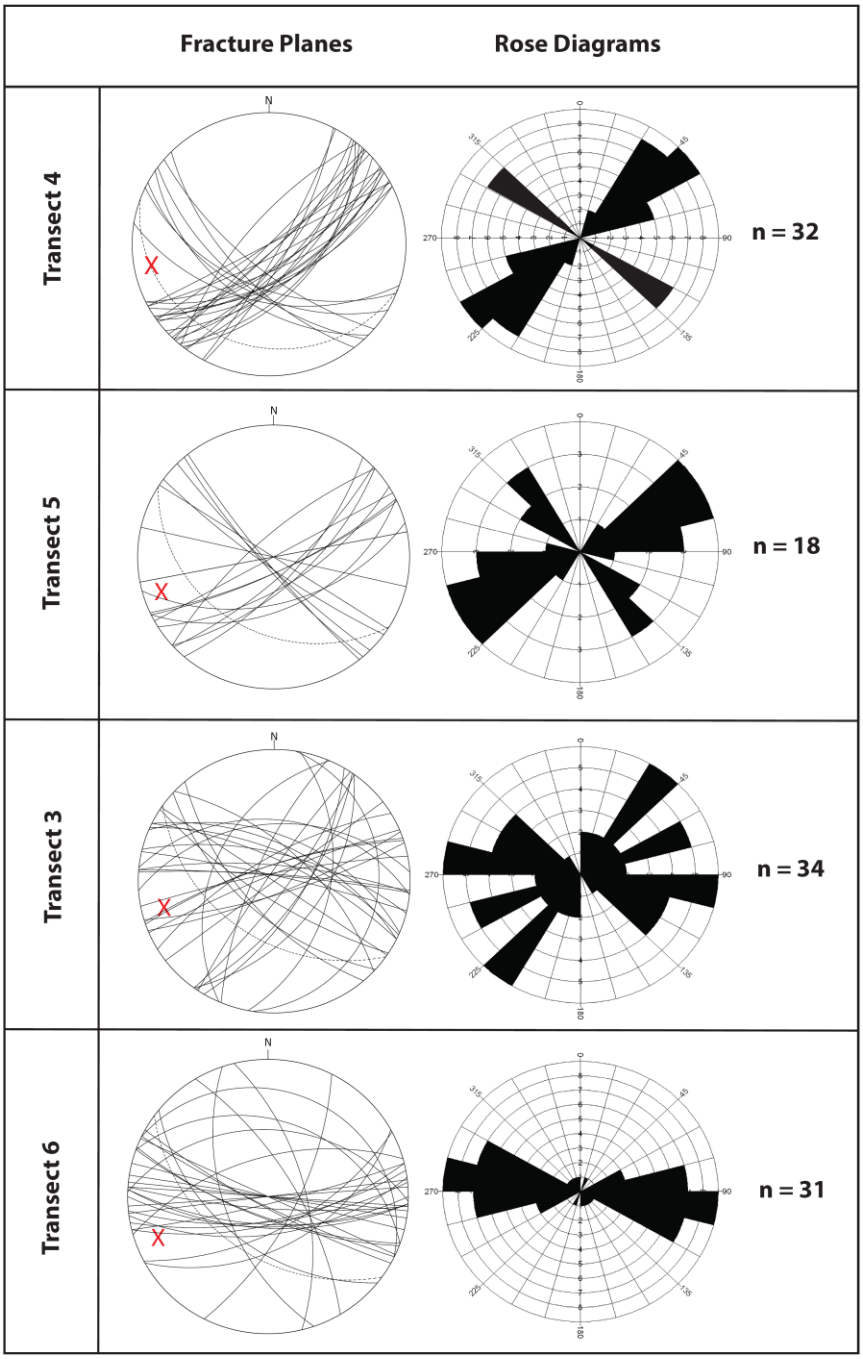

Figure 26b: Raw data stereonets and rose diagrams for fracture surveys taken at Big Bend north anticline. The bedding planes for each location are marked with a dashed black line on the stereonet diagrams; a red X marks the fold axis.

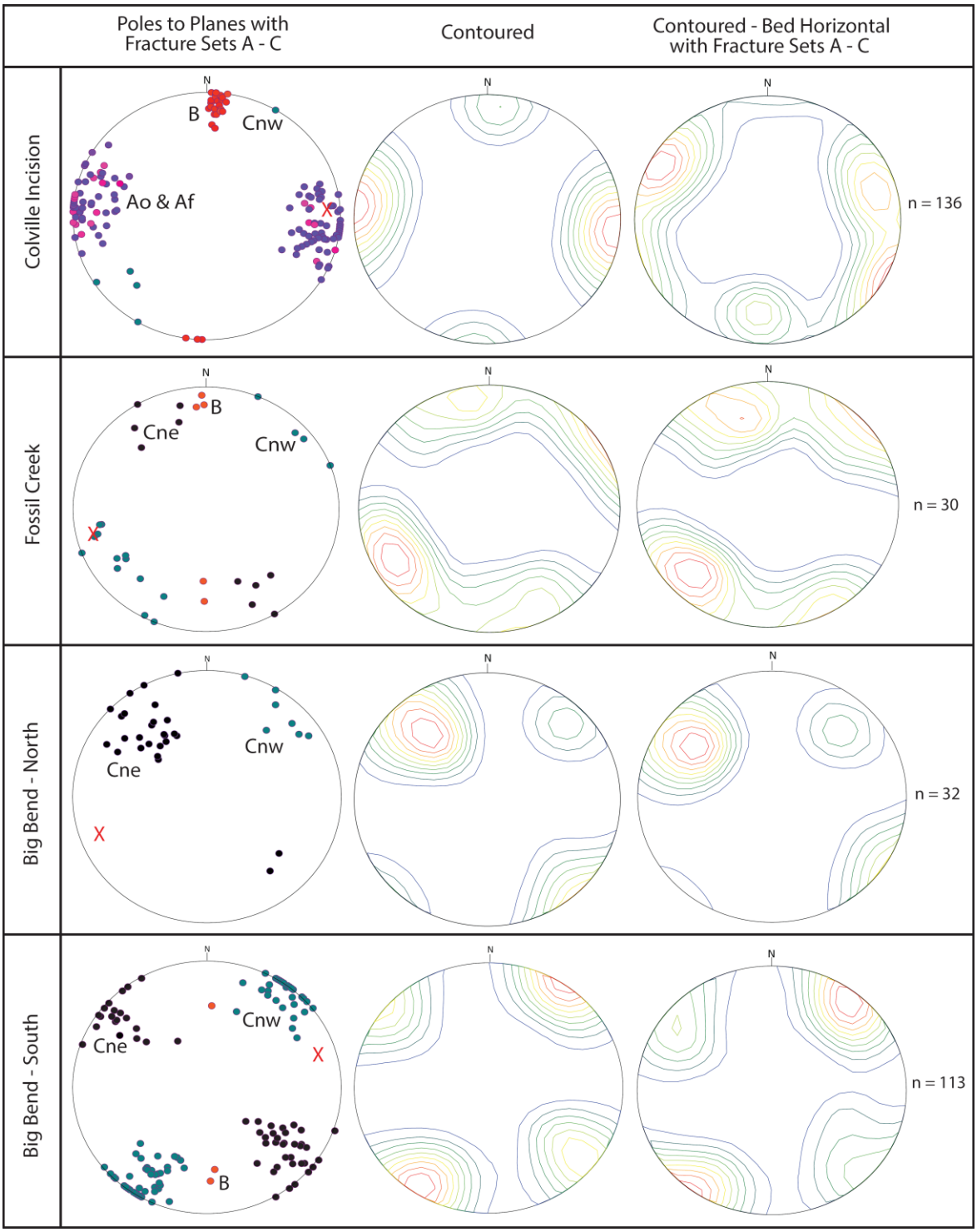

Figure 27: Poles to planes, contoured, and contoured-bed horizontal stereonets for fracture surveys at Big Bend anticline, Fossil Creek anticline, and the Colville incision. Only data from Big Bend north transect 4 is presented in this figure because it is the best representative plot for the Big Bend north location.

5.2.2 Colville incision observations

Intertonguing sandstone and neritic shale and siltstone of the upper Nanushuk Formation and mudstone to organic-rich shale of the Seabee Formation are exposed on the south limb of an open east-west trending anticline near the Colville incision (Fig. 25) (Houseknecht et al., 2011; Shimer et al., 2014). The dip of beds in the south limb of the anticline is approximately 23° (Table A9). The Upper Grandstand and Lower Grandstand intervals of the Nanushuk Formation are not exposed at the surface (Shimer et al., 2014). This location represents the upper part of the structural/stratigraphic section encountered in the Umiat anticline (Fig. 19).

One east-west fracture transect was taken at the Colville incision in the upper Nanushuk Formation (Ninuluk) (Figs. 2, 28). The stratigraphic position of the east-west transect was determined using geologic maps from Detterman et al. (1963), Mull et al. (2003), and Shimer et al. (2014).

Fracture sets A, B, and C are documented within the resistant upper Nanushuk Formation at the Colville incision (Figs. 2, 24, 26a, 28, Table 4). Ao fractures strike north to north-northeast and are unfilled (Fig. 26a, Table 4). Ao fractures are open fractures, perpendicular to bedding, and range from 6 to 200 cm in height and 0.2 to 300 cm in length (Table 4). Ao fractures have apertures from 0.1 to 4 cm and are evenly spaced. Ao fractures are interpreted as extension fractures because they are normal to the fold axis and lack evidence of shearing.

Af fractures strike north to north-northeast and are distinguished from fracture set Ao because they are partially or completely filled with calcite (Fig. 32, Table 4). Af fractures are perpendicular to bedding and range from 28 to 200 cm in height and 0.3 to 50 cm in length (Table 4). Af fractures have apertures from 0.05 to 1 cm and are evenly spaced. Af fractures are classified as extension fractures because the movement of rock on either side of the fracture

plane is normal to the plane. The movement of rock on either side of the fracture plane was determined to be normal by examining nearby fracture surfaces for evidence of shearing.

Set B fractures strike east-west and are parallel to the east-west striking fracture transect (Fig. 28). Set B fractures are perpendicular to bedding and are unfilled (Fig. 26a, Table 4). These fractures are vertically extensive and range in height and length from 2.0 cm to 5–10 m (Table 4). Apertures for set B range from 0.1 to 5 cm. Plumose structures are evident on east-west fracture faces at Colville incision and indicate that fractures in set B are extensional fractures (Fig. 29).

Set Cnw fractures at Colville incision are typically perpendicular to bedding; they commonly terminate at bed boundaries and range from 6 to 34 cm in height and from 2 to 4 cm in length (Figs. 26a, 30, Table 4). Set Cnw fractures strike northwest and are open fractures (Fig. 30). Set Cnw apertures are 0.05 to 0.1 cm. Set Cnw are classified as shear fractures based on evidence of shearing.

The Colville incision is the only single location where all three fracture sets are present. This location provides an opportunity to observe evidence of relative timing and relative age of the three fracture sets. Fracture set Af is consistently mineralized and clearly must be older than the mineralizing event filling the fractures (Fig 31). Fracture set Ao shares the same characteristics and orientation as Af but is not mineralized (Fig. 31). This suggests that set Ao formed after the mineralizing event and is younger than set Af. Because set Af fractures are cemented by calcite, the fracture is no longer a free space. Fracture set B cross-cuts fracture set Af, indicating that set B is a later fracture cutting the older fracture set Af. Set B fractures do not change orientations over the fold and also maintain a constant angular relationship with bedding throughout the fold. This relationship indicates that set B formed synchronous with folding. No

clear evidence of timing for set C is apparent so the relative age for this fracture set is ambiguous.

Figure 28: Photo of the eastern Colville incision. The base of the outcrop is upper Nanushuk Formation and the location of transect 7 is shown with a red dashed line. Fracture sets A, B, and C are present at the Colville incision. Photo courtesy of Grant Shimer.

Table 4: Characteristics, orientations, and relative ages of fracture sets observed at the Big Bend anticline, Colville incision, and Fossil Creek. Solid black line indicates a known whereas the dashed black line indicates an approximation.

Fracture Set	Orientation & Type	Fracture Characteristics	Fracture Distribution				Relative Age with Respect to Folding			
			south Big Bend	north Big Bend	Fossil Creek	Colville Incision				
			Stratigraphy							
			lower Nanushuk (Lower Grandstand/Tuktu)	upper Nanushuk (Ninuluk/Chandler/ Killik Tongue)	middle Nanushuk (Killik Tongue/Upper Grandstand)	upper Nanushuk (Ninuluk/Chandler/ Killik Tongue)	Pre-Folding	Early-Folding	Late-Folding	Post-Folding
Af NNW-NNE Filled	*Perpendicular to sub-perpendicular to fold axis *Perpendicular to bedding *Extension	Extension fractures: small apertures, calcite filled; terminate at bedding planes; evenly distributed				▬	▬			
Ao NNW-NNE Open	*Perpendicular to sub-perpendicular fold axis *Perpendicular to bedding *Extension	Extension fractures; open, small apertures, vertically extensive; evenly distributed			▬	▬	▪ ▪ ▪	▪ ▪ ▪ ▪	▪ ▪ ▪ ▪	▪ ▪ ▪ ▪
B East-West Open	*Parallel to fold axis *Perpendicular to bedding *Extensional	Apparent extension fracture: open, vertically extensive	▬		▬	▬			▬	
Cnw Northwest-Southeast Open	*Acute bisectors perpendicular to fold axis *Perpendicular to bedding *Shear	Unfilled shear fractures with conjugate geometry, small apertures; vertically extensive	▬	▬	▬	▬	▪ ▪ ▪	▪ ▪ ▪ ▪	▪ ▪ ▪ ▪	▪ ▪ ▪ ▪
Cne Northeast-Southwest Open	*Acute bisectors perpendicular to fold axis *Perpendicular to bedding *Shear	Unfilled shear fractures with conjugate geometry, small apertures; vertically extensive	▬	▬	▬		▪ ▪ ▪	▪ ▪ ▪ ▪	▪ ▪ ▪ ▪	▪ ▪ ▪ ▪

Figure 29: Photo of plumose structures on east-west-striking set B fracture faces at Colville incision.

Figure 30: Photo of northwest striking set Cnw fractures at the Colville incision. Fractures indicated by blue dashed lines. Horizontal bedding surface indicated by green dashed line. Rock hammer for scale.

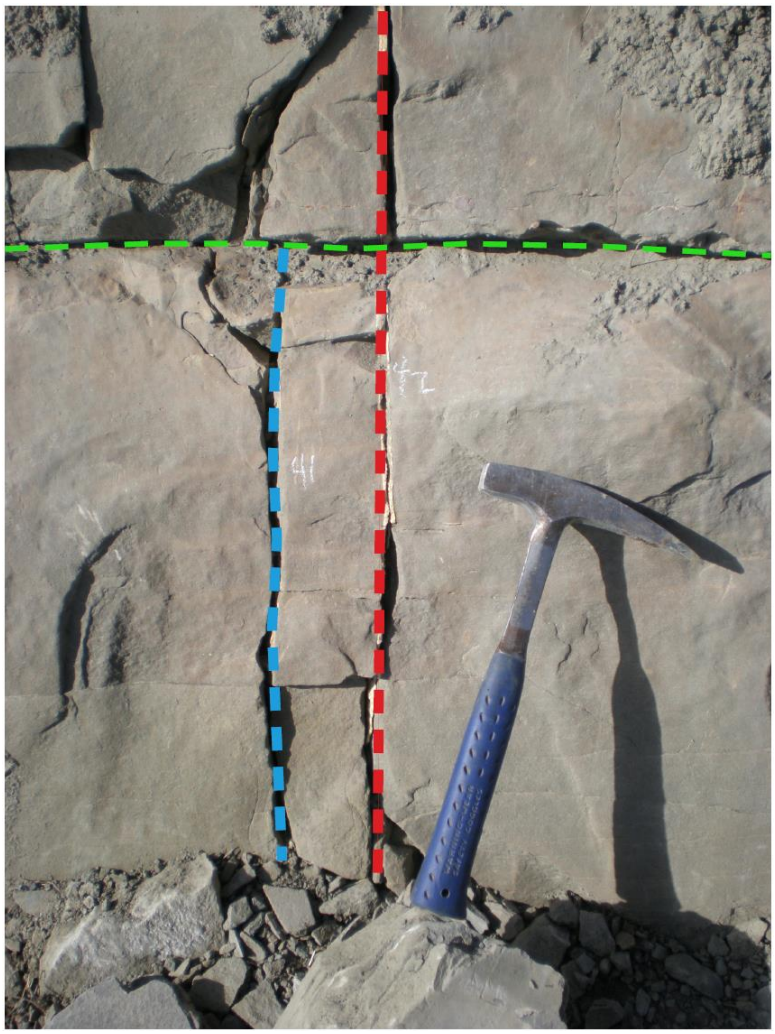

Figure 31: Photo of north to north-northwest striking Ao fractures (dashed blue line) and Af partially filled fractures (dashed red line) at the Colville incision. Horizontal bedding surface indicated by green dashed line. Rock hammer for scale.

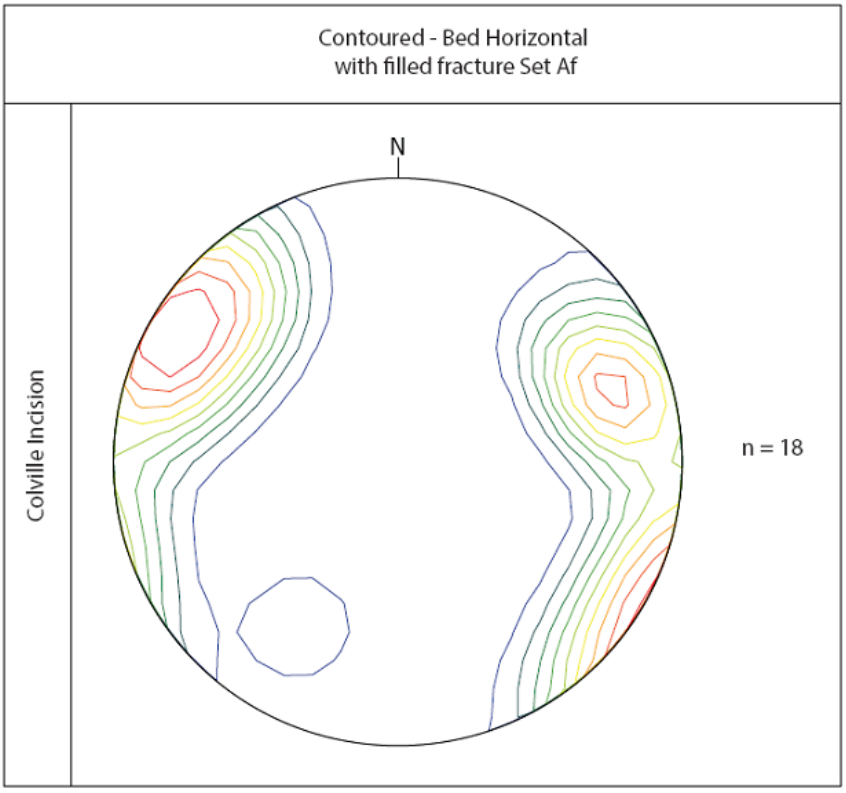

Figure 32: Bed horizontal stereonet for partially filled to completely filled fracture set Af at the Colville incision.

5.2.3 Fossil Creek anticline: south limb observations

The lower Nanushuk Formation is exposed on the south limb of an east-west trending anticline at Fossil Creek (Figs. 2, 24) (Shimer et al., 2014). The dip of beds in the south limb of the anticline is approximately 12° (Figs. 33). The Fossil Creek transect was taken between a fault to the south and the north anticline hinge of the Fossil Creek anticline and is shown in Fig. 24. Shimer et al. (2014) place the stratigraphic location of the transect site in the Upper Grandstand, which is the top of the upper Nanushuk Formation in the old stratigraphic nomenclature. Fracture sets observed at this location are summarized in Table 4.

At Fossil Creek, Ao fractures range in height from 40 to 100 cm and in length from approximately 30 to 85 cm and have apertures from 0.05 to 0.1 cm. Ao fractures are perpendicular to bedding, vertically extensive, and are classified as extension fractures based on the movement of rock on either side of the fracture plane and lack of evidence of shearing.

Unfilled fractures (set B) strike east-west and are roughly parallel to the Fossil Creek anticline (Fig. 26a, Table 4). Set B fractures are vertically extensive and range in height and length from 2 cm to 5–10 m (Figs. 24, 26a). Apertures for set B range from 0.2 to 0.3 cm.

Set B fractures are mode 1 extension fractures that strike east-west (Fig. 26a, Table 4). Fractures of set B are classified as extensional fractures based on the movement of rock on either side of the fracture plane and lack of evidence of shearing.

Fracture sets Cnw and Cne at Fossil Creek are well-defined conjugate sets of shear fractures that consistently strike northeast-southwest and northwest-southeast (Figs. 24, 26a). The acute bisector of the conjugate set is oriented roughly north-south, perpendicular to the trend of the fold axis (Fig. 26a). Fractures of set C strike northwest (Cnw) and northeast (Cne), range in height from 13 to 100 cm, and have measured lengths of 6 to 140 cm with apertures of 0.1 to 2.5 cm (Figs. 26a, 34, Table 4). Pervasive slickenlines are apparent on Cnw and Cne fracture surfaces.

Set Cnw and Cne fractures are defined as conjugate shear fractures based on the pervasive slickenlines and on a model assumption that the contraction direction is where the dihedral angle between the two sets is significantly less than 90° (~60°).

Figure 33: Photo of the south limb of the Fossil Creek anticline and the location of transect 8. The hinge of the anticline is to the north (left side of photo) and the transect is parallel to bedding. A red star marks the location of Figure 35.

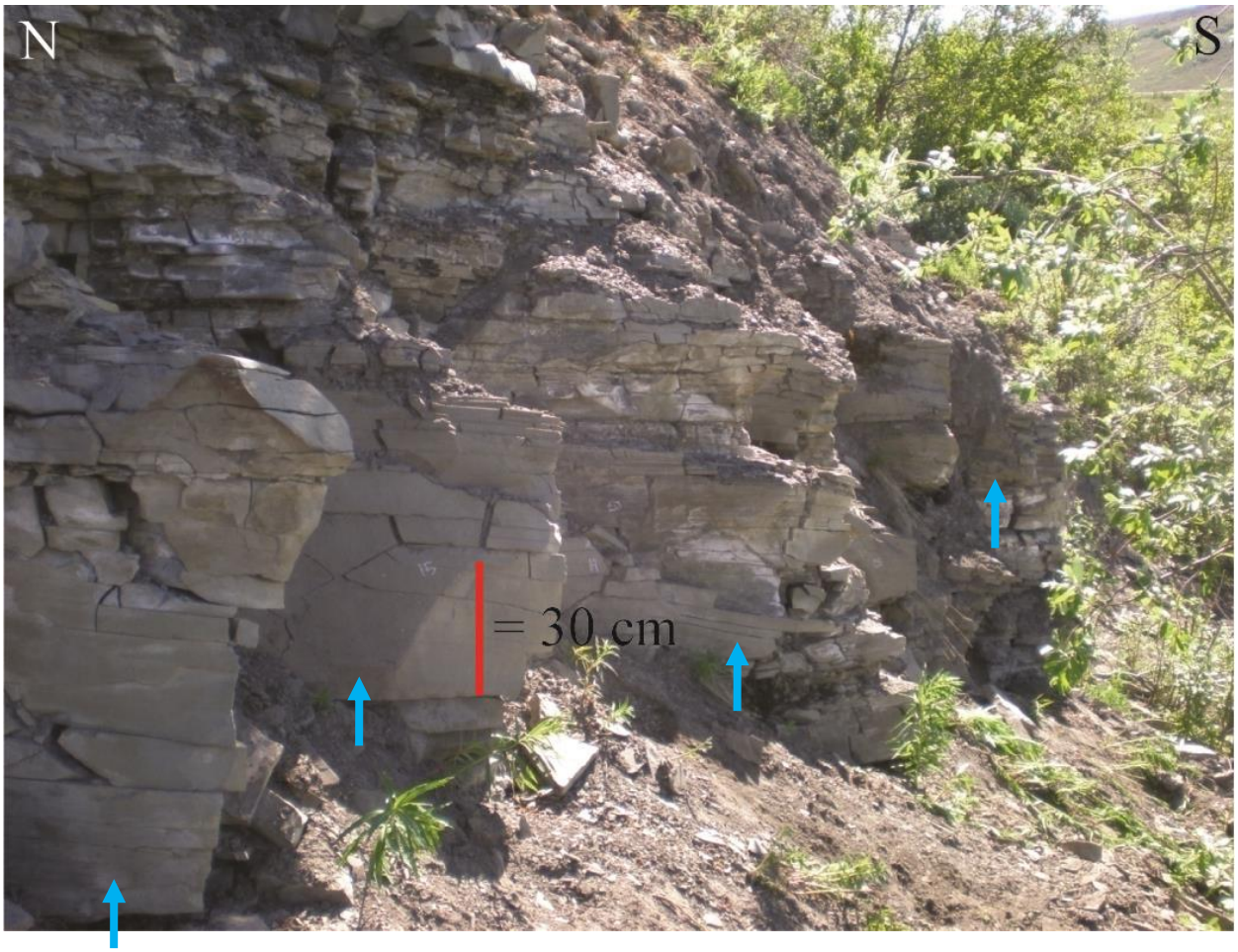

Figure 34: Photo of fracture set Cnw at Fossil Creek. These fractures are characteristically unfilled with systematic northwest-southeast strike. Blue arrows indicate Cnw fracture surfaces.

Figure 35: Photo of Fossil Creek set Cne fractures that are vertically extensive. The hinge of the anticline is to the north (left side of photo). The location of this photo is marked by a star in Figure 33. Red arrows indicate Cne fractures.

5.2.4 Big Bend South anticline observations

Outcrops along the Chandler River expose the Big Bend anticline, which changes geometry along strike and is cut by thrust faults in both its south and north branches (Wallace, 2009; Sanders and Wallace, 2011).

Two fracture transects were taken near the base of the lower Nanushuk Formation on the south limb of the south branch of the east-west-trending Big Bend anticline (Figs. 2, 24, 36). Previous work done by Detterman et al. (1963) and more recent studies done by Sanders and Wallace (2011) identify the south Big Bend transect in the lower Nanushuk Formation (informally Tuktu). The dip of beds in the south limb of the anticline is approximately 12° to the south (Fig. 36). Fracture sets B and C are documented here (Figs. 2, 26a, Table 4).

Set B fractures strike east-west and are unfilled. These fractures are vertical and are roughly parallel to the axis of the Big Bend anticline (Fig. 26a, Table 4). Set B fractures range in height from 9 to 10 cm and in length from 1.0 to 27 cm (Fig. 36). Apertures for set B range from 0.1 to 5 cm. Set B fractures are classified as extensional based on the normal movement of rock relative to the fracture plane. This was determined by the absence of slickenlines indicating shear movement.

Fracture sets Cnw and Cne together constitute a well-defined conjugate set of shear fractures that consistently strike northeast-southwest and northwest-southeast and dip steeply (Figs. 26a, 33, 34). The dihedral angle between the two sets is approximately 60°, and the acute bisector between Cnw and Cne is oriented roughly north-south (Fig. 26a). Fractures of set Cnw strike northwest, range in height from 1 to 300 cm, and have measured lengths of 0.5 to 200 cm with apertures of 0.1 to 2.5 cm (Figs. 26a, 37, 38, Table 4). Moderate to pervasive slickenlines are evident on fracture faces, indicating shearing. The northwest-striking set Cnw fractures share

the same strike as right-lateral faults mapped in the Big Bend anticline area (Fig. 6; Sanders and Wallace, 2011). Fractures from set Cnw are 4 to 300 cm in height and range in length from 1 to 182 cm (Figs. 26a, 37, 38, Table 4).

Set Cne fractures strike northeast and have measured heights that range from 4.5 to 300 cm, lengths ranging from 0.5 to 123 cm, and apertures of 0.1 to 5 cm (Figs. 26a, 37, 40, Table 4). Moderate to pervasive slickenlines are apparent on fracture surfaces.

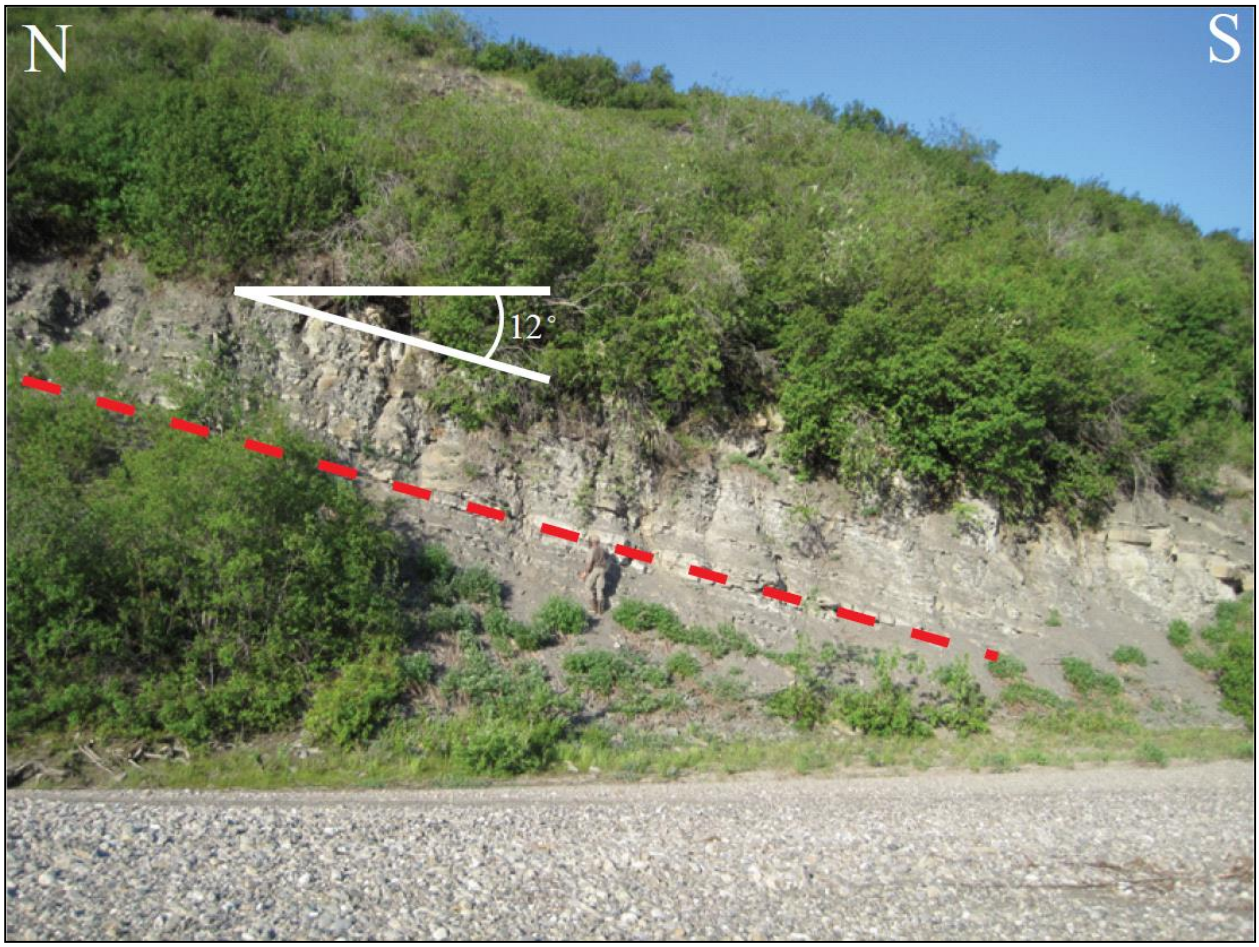

Figure 36: Photo of the south limb of the south branch of Big Bend anticline and the location of transect 2 (red dashed line). Geologist for scale. Photo courtesy of Cheryl Sanders.

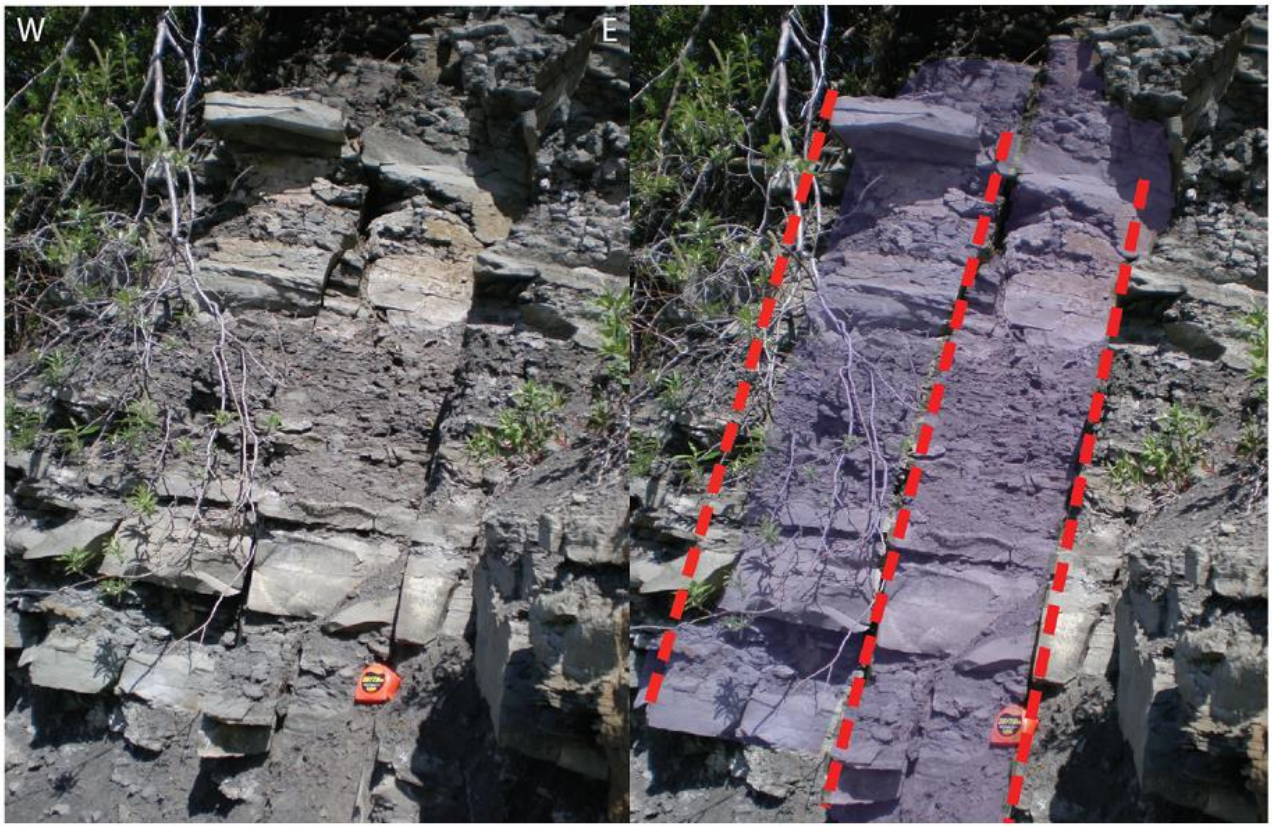

Figure 37: Photo of fracture sets Cnw and Cne in the south limb of the south branch of Big Bend anticline. The Cnw fracture surface is represented by a dashed red line and Cne is shaded purple. Tape measure for scale.

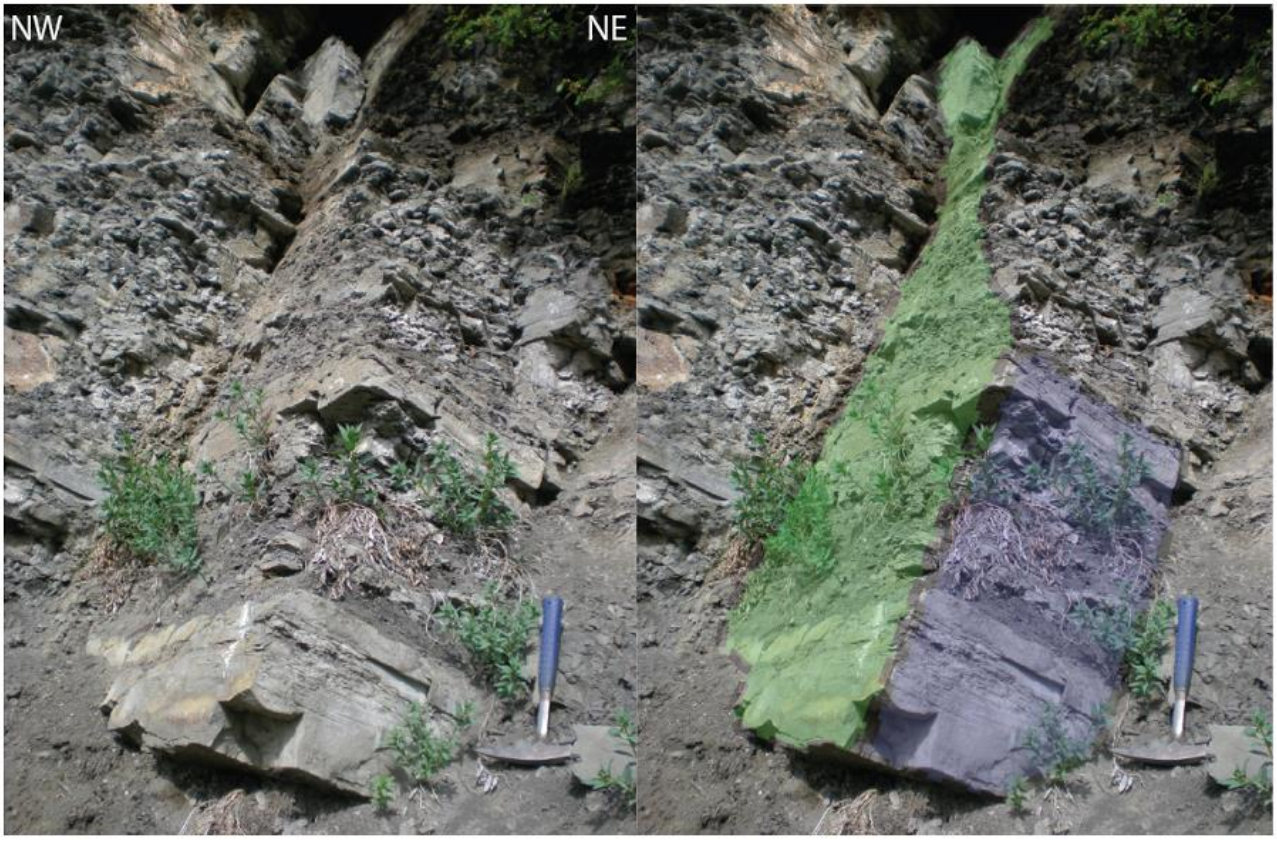

Figure 38: Photo of fracture set Cnw (fracture surface shaded green) and Cne (fracture surface shaded purple) in the south limb of the south branch of Big Bend anticline. Rock hammer for scale.

5.2.5 Big Bend north anticline observations

Sandstone intertonguing with shale in the middle to upper part of the Nanushuk Formation is exposed on the south limb of the north branch of the east-west trending and open Big Bend anticline (Figs. 2, 19). Four fracture transects were taken here (Figs. 2, 24, 39, Table 4). Detterman et al. (1963) and Sanders and Wallace (2011) place the stratigraphic position of the north Big Bend transect site in the upper Nanushuk Formation (informally Ninuluk). Transects 3, 5, and 6 were taken on an outcrop slightly downhill from transect 4, near the river and farther from the anticline hinge (Fig. 39). The dip of beds near the river where transects 3, 5,

and 6 were taken is approximately 39° degrees to the southwest (Figs. 24, 26b, 39). Transect 4 was taken on an outcrop slightly uphill and closer to the anticline hinge than the other transects (Fig. 39). The beds here dip approximately 16° to the south-southwest (Figs. 24, 26b, 39).

Ao fractures are only present in transect 6 and are approximately 500 cm in height (Fig. 26b, Table 4). Ao fractures range from 5 to 14 cm in length and have an average aperture of 1 cm (Table 4).

Set B fractures strike east-west, are unfilled, and are roughly parallel to the regional trend of the anticlinal axis (Fig. 26b). Set B fractures are extensional fractures based on the normal movement of rock relative to the fracture. This was determined by the lack of slickenlines indicating shear movement. Set B fractures are vertically extensive and range in height from 2 to 100 cm and length from 0.1 to 76 cm (Table 4). Apertures for set B range from 0.1 to 2 cm (Table 4). In transects 3, 5, and 6, the dips of set B fractures are shallower than set B fractures from other locations (Figs. 26a, 26b).

Fracture set C (Cnw and Cne) constitutes a well-defined conjugate set of shear fractures with slickenlines on fracture surfaces. The two orientations of fractures have an acute bisector oriented roughly north-south. These fractures systematically strike northeast-southwest and northwest-southeast in transect 4 of north Big Bend anticline (Fig. 28). Contoured stereonets for transects 3, 5, and 6 show shallow dips for set Cnw and set Cne but still show the conjugate orientations of these sets (Fig. 26b).

Set Cnw fractures in north Big Bend anticline are unfilled and strike northwest. Fractures of set Cnw range in height from 5.4 to 100 cm and have measured lengths parallel to bedding of 0.2 to 100 cm with apertures of 0.1 to 11 cm (Figs. 26b, 36, 40, Table 4). Slickenlines were

identified on exposed set C fracture faces (Fig. 41) and indicate parallel movement of rock on either side of the fracture plane. The slickenlines are sub-horizontal (Fig. 41).

Set Cne fractures strike northeast-southwest and are unfilled (Fig. 40). They have measured heights that range from 7.5 to 143 cm, lengths parallel to bedding ranging from 0.3 to 113 cm, and apertures of 0.2 to 1 cm. The northwest-striking set Cnw fractures share the same strike as right-lateral faults mapped in the Big Bend anticline area (Fig. 5; Mull et al., 2003; Sanders and Wallace, 2011).

Figure 39: Photo of the north Big Bend anticline and the location of four fracture transects. Transect 3: green line; transect 4: pink line, transect 5: blue line; transect 6: purple line. Geologist circled in red for scale. All transects are parallel to bedding.

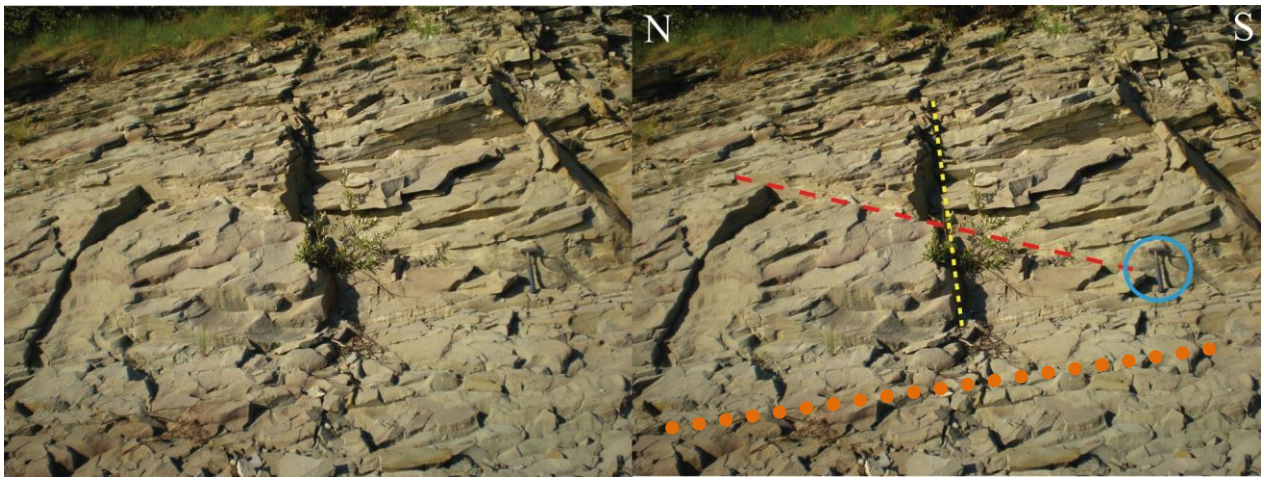

Figure 40: Photo of fracture sets Cnw (red long-dashed line) and Cne (yellow short-dashed line) in transect 6 on the north Big Bend anticline. Transect was taken parallel to bedding (orange dotted line). Rock hammer (circled in blue) for scale.

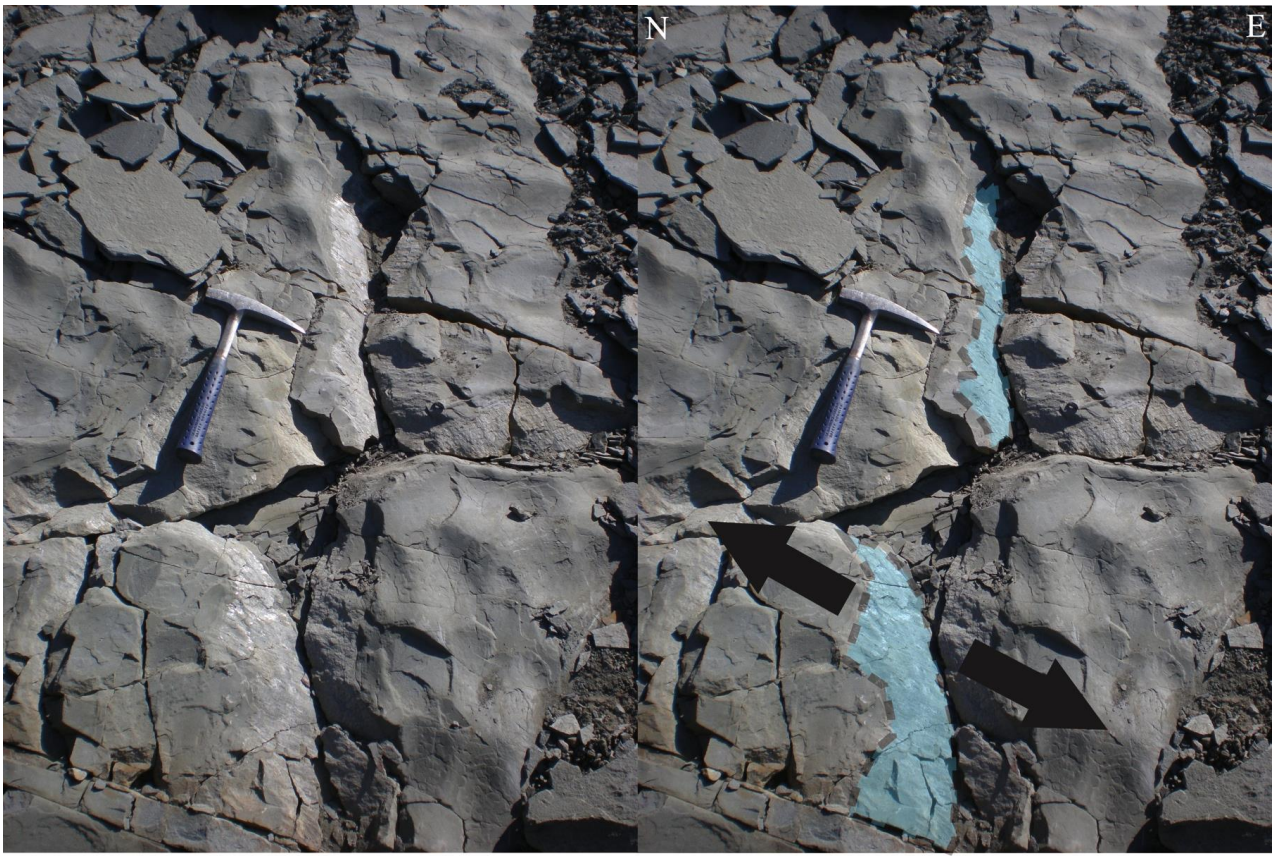

Figure 41: Photo of bedding surface with slickenlines (surface shaded blue) on exposed set Cne fracture faces in north Big Bend anticline. Arrows indicate the direction of bed movement.

Chapter 6

STATISTICAL ANALYSIS OF FRACTURE SPACING DATA

6.1 Statistical analysis of fracture spacing data

Performing a statistical analysis on the fracture spacing data collected allows overall trends of fractures to be identified. Box and whisker plots were generated to assess the distribution of fracture spacing (Fig. 42). Histograms (Fig. 43), one-sample Kolmogorov-Smirnov (K-S) tests (Table B2), and quantile-quantile (Q-Q) plots were used to assess data distribution normalcy (Figs. 44, 45, 46). Log transforms were applied to normalize distributions before higher-level data analysis using a one-way parametric analysis of variance (ANOVA) test (Davis, 2002). A homogeneity of variance test further confirmed the suitability of the log-transformed datasets for a simple ANOVA to determine whether the average fracture spacing values for each of the three fracture sets are statistically different at the 95% confidence level (Davis, 2002). Subsequent post-hoc analyses were then used to calculate which of the fracture set pairs could be statistically distinguished at this same certainty level.

6.2 Fracture sets observed in field

Box and whisker plots have been generated to graphically depict the distribution of fracture spacing by fracture sets for north and south Big Bend anticline, the south limb of the Fossil Creek anticline, and the north limb of an anticline located near the Colville incision (Fig. 42). The box plots are non-parametric and display the populations with no assumptions of statistical distribution. The plots indicate that the median fracture spacing for fracture sets A, B,

and C are comparable; however, the degree of variability for fracture set A is greater than fracture sets B and C (Fig. 42).

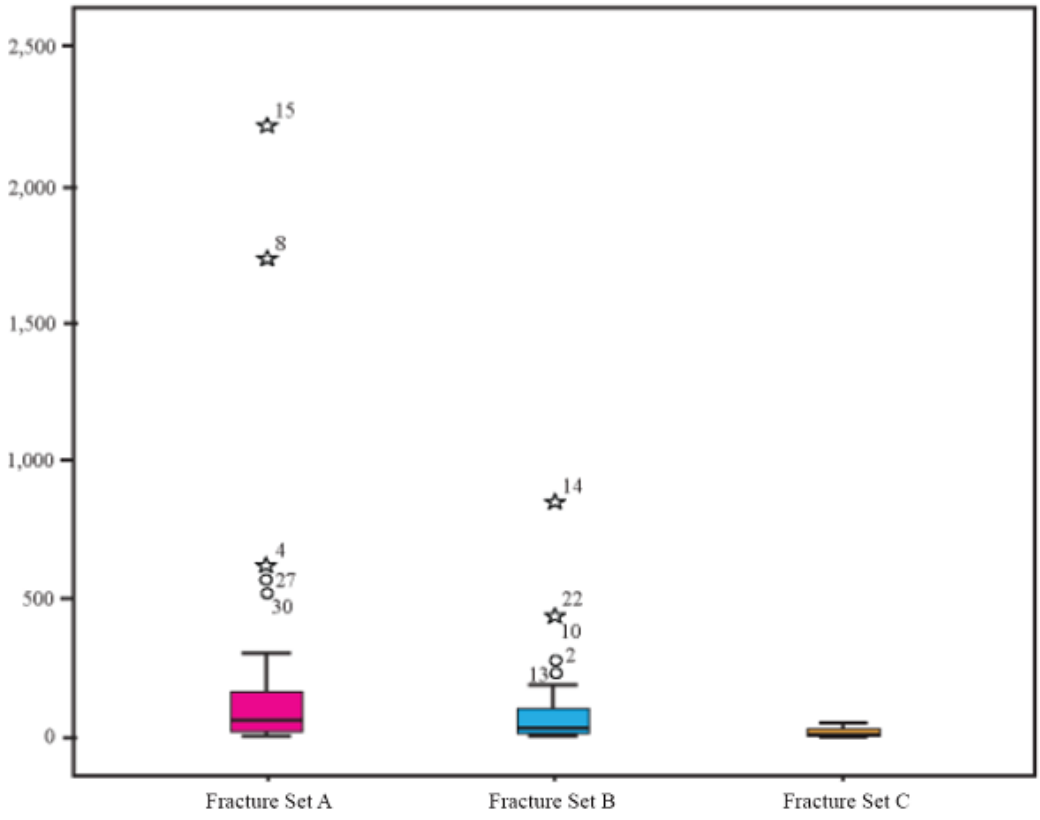

Figure 42: Boxplots of fracture spacing of sets A, B, and C. Median spacing is represented by solid lines in the middle of the boxplot. The vertical lines extending from each box indicate variability outside the upper and lower quartiles and indicate the degree of dispersion in the data. Whiskers represent the ends of the minimum and maximum of the observed data, excluding the farthest outliers. The outliers for each fracture set have been plotted with an open circle or a star.

Fracture set A (Ao and Af combined) (Fig. 43) was surveyed predominately at the Colville incision in the middle to upper Nanushuk Formation (Table 4). Ao and Af were combined because there was no significant difference between the fractures other than partial calcite filling and they would be indistinguishable by the statistical tests performed. These

fractures (Ao and Af) measure 15 to 200 cm in height, 0.3 to 300 cm in length, have apertures 0.05 to 1.0 cm wide, and their range of spacing follows a log-normal distribution (Fig. 43, Tables B1, B2). A one-way ANOVA and one of the two subsequent post-hoc tests applied (the LSD test; Davis, 2002; Tables B3, B4) indicate that the average spacing is statistically distinguishable from that of sets B and C (Cnw and Cne combined). However, the Bonferroni post-hoc test (Davis, 2002), which uses an alternate set of thresholds in identifying statistical similarities/differences, suggests that the average spacing of fracture set A is not different from set B at the 95% confidence level, although it is distinguishable from set C (Table B4). However, the total range of values for sets A and B differs (set A = 2,210.6, set B = 848) due to a small sub-population of larger-than-average spacing values noted in the distribution of fracture set A. Fractures from set A are also three times less abundant in the measured transects (n = 30) than those of set B (n = 91) (Fig. 42). These considerations, coupled with the observed differences in morphology and orientation, suggest that the average spacing between sets A and B should be treated as statistically different in reservoir modeling**.** This information is also useful when designing well trajectories.

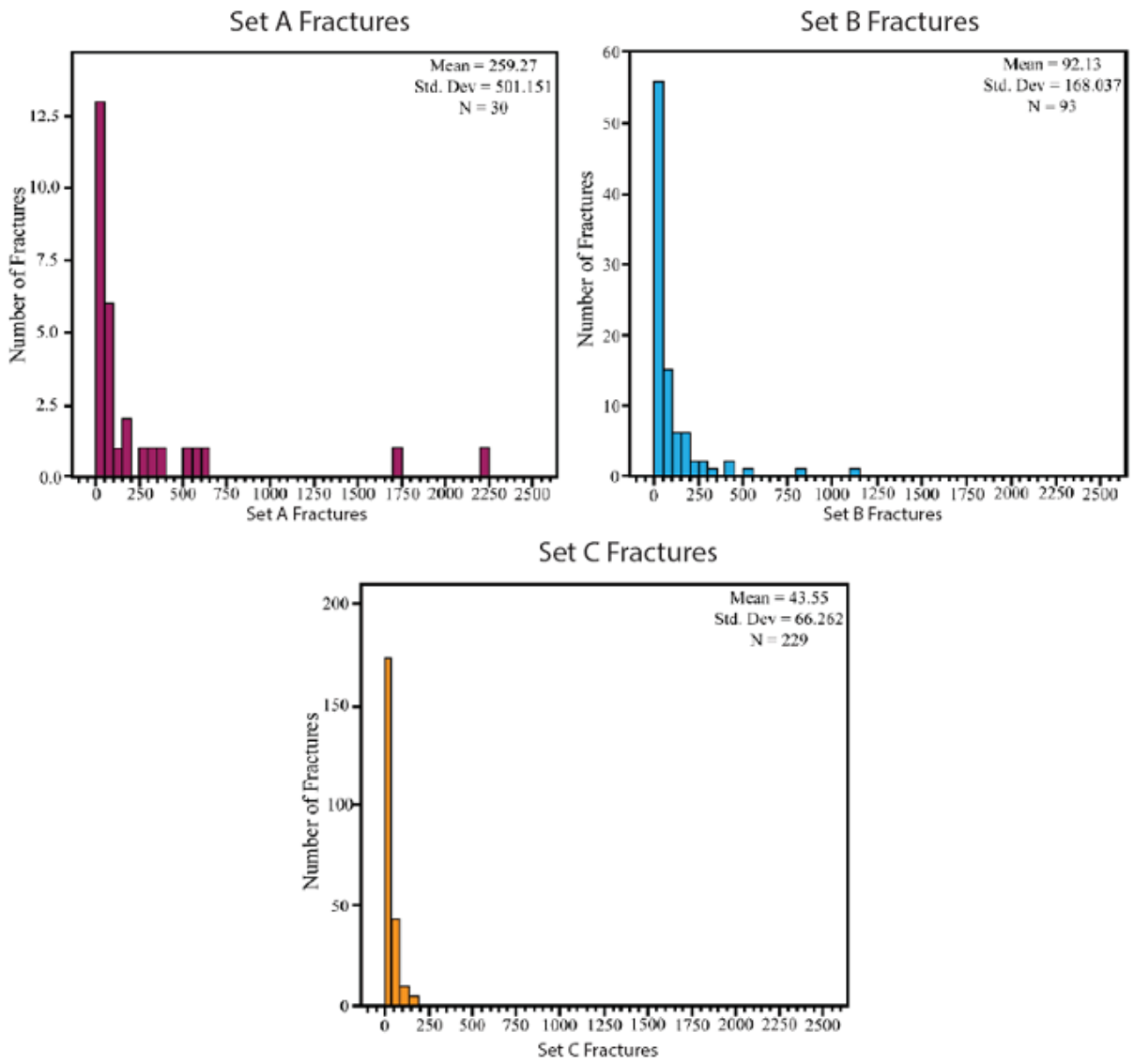

Figure 43: Histogram plots of set A (Ao and Af), set B, and set C (Cnw and Cne) fracture spacing distribution. The distribution of each data set is log normal and clearly skewed toward the lower spacing values.

Fracture set B (Fig. 42) was recorded at the Colville incision, Fossil Creek, and in the south limb of the south branch of the Big Bend anticline in the lower, middle, and upper Nanushuk Formation (Table 4). These fractures are vertically extensive and range from 15 to

200 cm in height and from 2 cm to many meters in length, have apertures 0.1 to 5 cm wide, and their range of spacing follows a log-normal distribution (Fig. 44, Tables B1, B2).

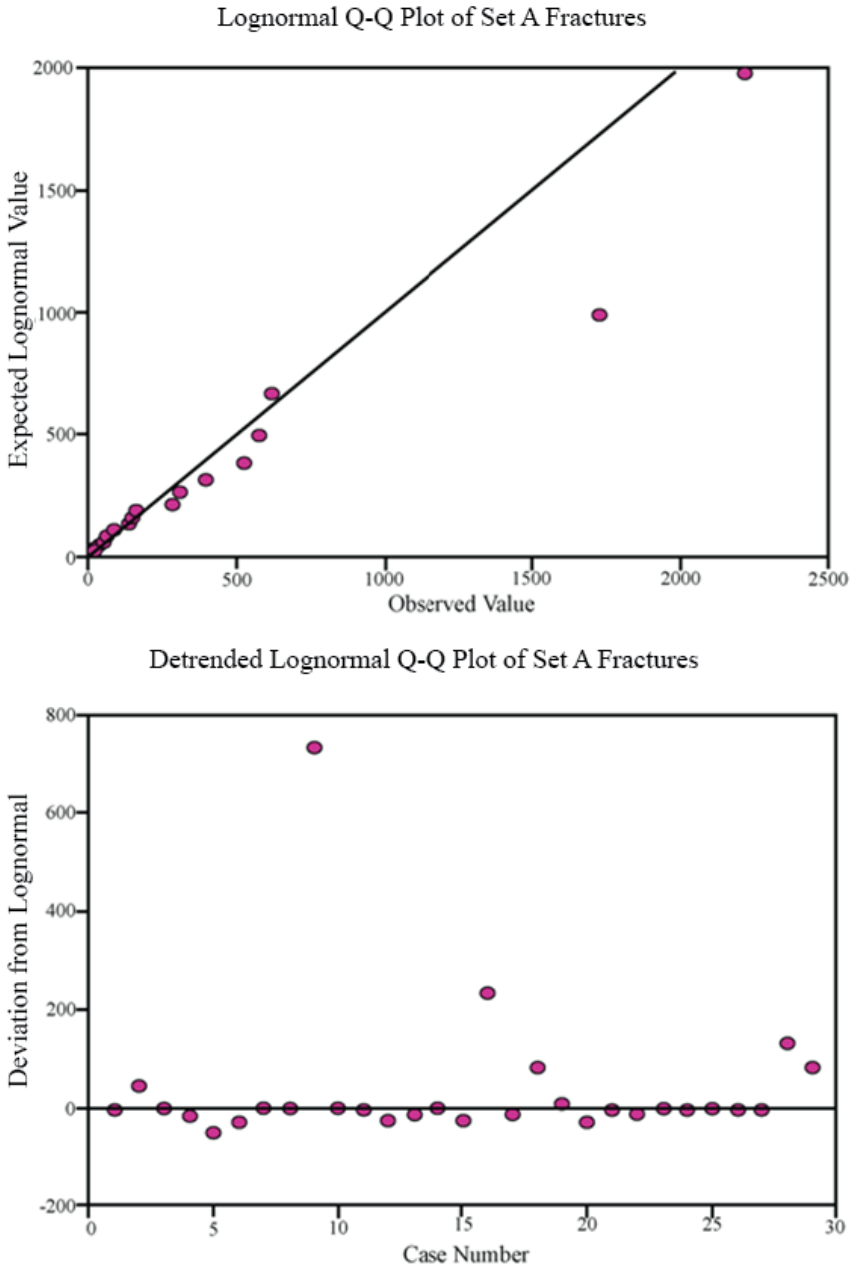

Figure 44: Log normal and detrended log normal Q-Q plots for fracture set A.

Fracture set C (Fig. 42) was surveyed predominately in the lower, middle, and upper Nanushuk Formation at Fossil Creek and the Big Bend anticline (Table 4). These fractures measure 5 to 500 cm in height, 0.1 to 200 cm in length, have apertures 0.1 to 5 cm wide, and their spacing displays a log-normal distribution (Fig. 45, Tables B1, B2). A one-way ANOVA and both of the two subsequent post-hoc tests applied (the LSD test; Davis, 2002; Tables B3, B4) indicate that the average spacing is statistically distinguishable from that of sets A and B at the 95% confidence level.

Fracture sets Ao and Af are statistically indistinguishable by the statistical tests performed and may be treated as one set. The one-way ANOVA and one of the two subsequent post-hoc tests applied to fracture set A (Ao and Af combined), set B and set C (Cnw & Cne) indicate that the average spacing offsets for A, B and C are statistically different and should be treated as separate fracture sets during reservoir modeling**.**

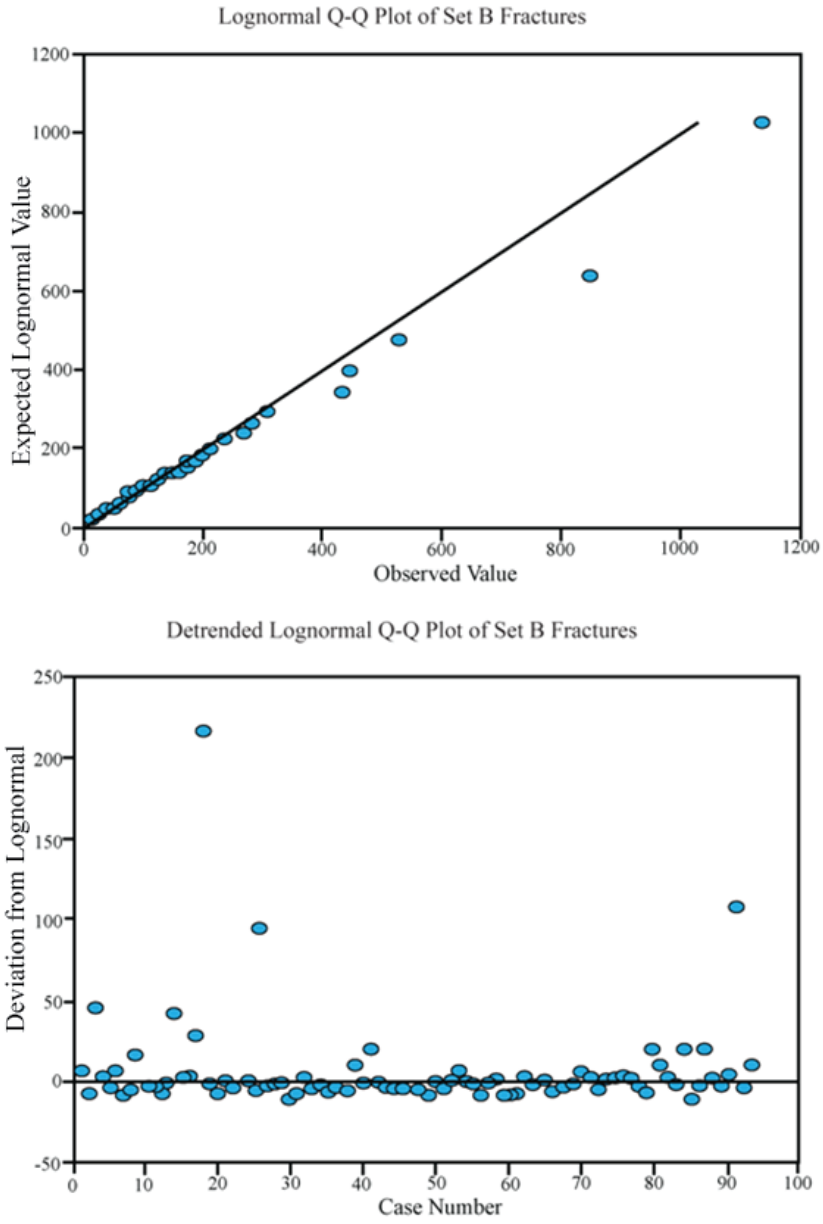

Figure 45: Log normal and detrended log normal Q-Q plots for fracture set B.

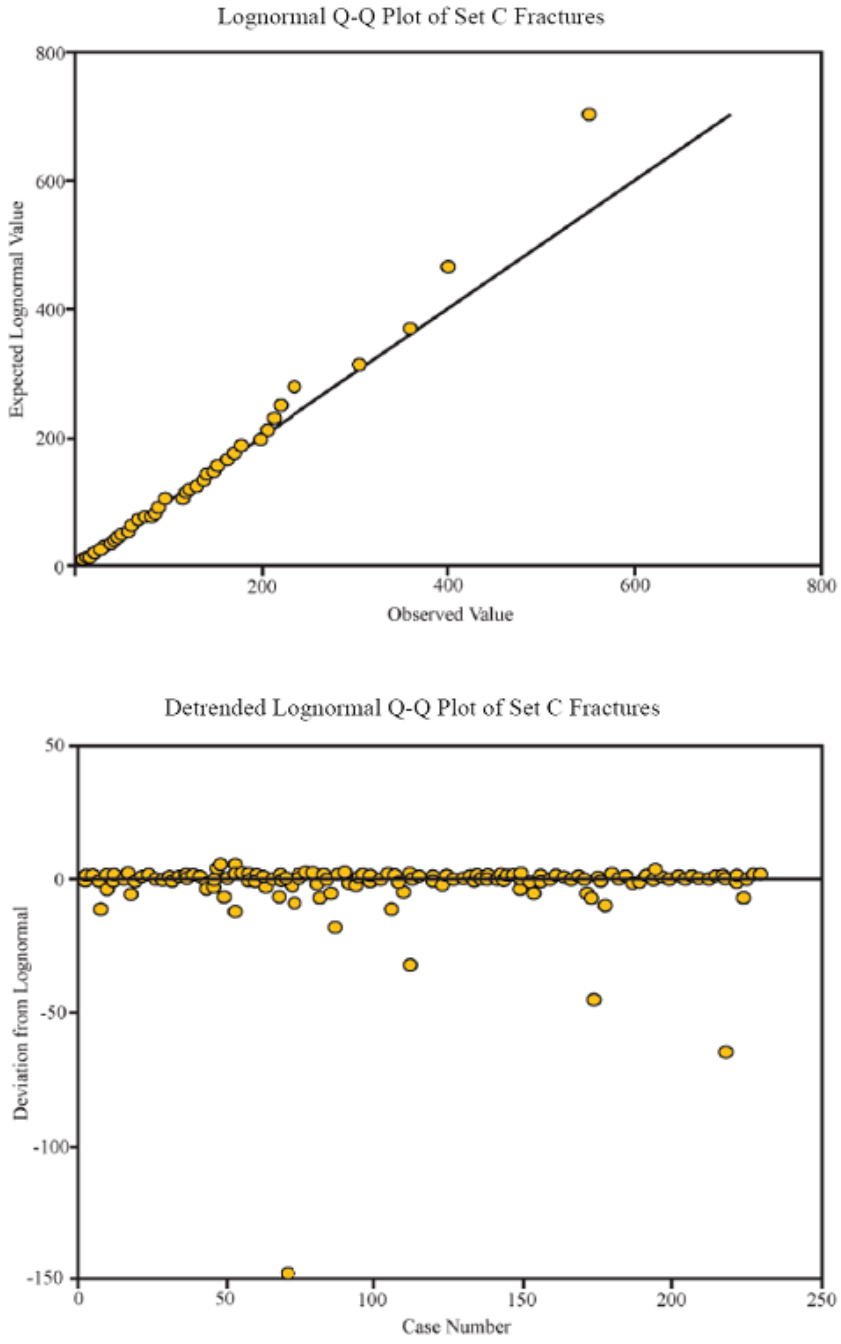

Figure 46: Log normal and detrended log normal Q-Q plots for fracture set C.

6.3 Predicting fracture spacing in the subsurface

Modern drilling and production techniques can be more efficient if the behavior of fluid flow within the reservoir is understood and the structural controls on the character of the reservoir can be determined. Analyzing fractures in surface exposures and in Umiat cores will allow fluid migration pathways to be modeled and better understood. The density of fractures observed in surface exposures can be used by drilling engineers to predict fracture spacing in vertical cores as well as determining directional permeability and permeability anisotropy in the reservoir.

The relatively small number of natural fractures in Umiat cores (Tables 2–4) is most probably related to the fact that these fractures are spaced, near-vertical phenomena; shallow, vertical, small-diameter wells are not likely to encounter many vertical or near-vertical fractures.

The following discussion attempts to determine what the fracture spacing would be in a vertical hole through the Umiat anticline and surrounding areas. The calculations are based entirely on the surface transects and include no core data. All fractures encountered at the Colville incision, Fossil Creek, and Big Bend anticlines are mostly at a high angle to bedding; the greater the departure from perpendicular to bedding (assuming gently dipping bedding), the greater the chance of hitting a fracture. The measured fracture dips were used to determine what their spacing would be in a vertical hole. Transect orientation makes a significant difference in fracture spacing if big differences in abundance occur according to orientation (e.g., Colville incision). The orientations of the fracture transects can be seen in Fig. 24.

The fracture transect at the Colville incision was measured approximately normal to set Ao and Af. In this case, the average spacing would be representative for fracture-normal spacing of set Ao and Af (but not of set B). Orthogonal sets with roughly equal abundance are present at

the other locations. Consequently, the spacing for each set would depend on how close to orthogonal the transect is to that set. Because they're orthogonal sets with roughly equal abundance, the average spacing for both sets (assuming similar distributions for each set) probably wouldn't vary much according to orientation. In other words, a well drilled normal to one set will encounter a closest spacing for that set but would not hit many of the other set; if drilled along a bisector of the two sets, an equal number of each would be encountered.

Fig. 47 is a schematic representation of a vertical well bore penetrating formations and fractures as seen at the surface. The average dip of bedding from Big Bend anticline, Fossil Creek, and the Colville incision is approximately 12°; α is the average dip of fractures measured at the surface and projected into the subsurface. Fractures are assumed, on average, to be at a very high angle relative to bedding. Y represents the fracture spacing parallel to bedding calculated for fractures measured in surface exposures. X represents the calculated fracture spacing that would be observed in a vertical section through the fractured rocks and is calculated using the following formula:

$$X = Y/\cos(\alpha)$$

Calculated values of fracture spacing for the survey locations are summarized in Table 5. Based on this analysis, if the distribution and spacing of fractures in the subsurface is the same as that observed in surface exposures in the upper Nanushuk Formation at Colville incision, set A fractures (Ao and Af) would be encountered on average every 398.0 cm in a vertical well (Table 5). Fractures (all sets combined) would be encountered on average every 175.7 cm in middle stratigraphic levels and would be encountered on average every 149.0 cm in the lower Nanushuk Formation (Table 5). However, as well trajectories approach the dip of bedding, the possibility

of encountering fractures would approach the fracture spacing measured parallel to bedding (Y; Fig. 47, Table 5).

Fig. 48 is a graph showing the relationship of the observed fracture spacing in a borehole with respect to the dip of the well trajectory. Tables 6, 7, and 8 were used to determine how many fractures will be encountered as the well goes from being vertical (or perpendicular to bedding) to horizontal (parallel to bedding). To encounter the most north-south striking fractures, as are dominant at the Colville incision, the well trajectory should be oriented east-west, perpendicular to the strike of the north-south fractures. Assuming this geometry, as the well's trajectory becomes parallel to bedding, true fracture spacing for north-south fractures will be encountered: approximately 58 cm at Umiat. Similarly, conjugate fractures that have near-orthogonal populations with similar numbers (and presumably similar spacing) as observed at Fossil Creek and Big Bend anticline will have an average spacing that will be about the same in any direction. As wells approach the dip of bedding, fractures with orientations similar to those observed at Fossil Creek will be encountered at a true fracture spacing of approximately 25 cm (Tables, 5, 6, 7, 8). Fractures documented at the Big Bend anticline will be encountered approximately every 43 cm as a well trajectory approaches the dip of bedding (Tables 5, 6, 7, 8).

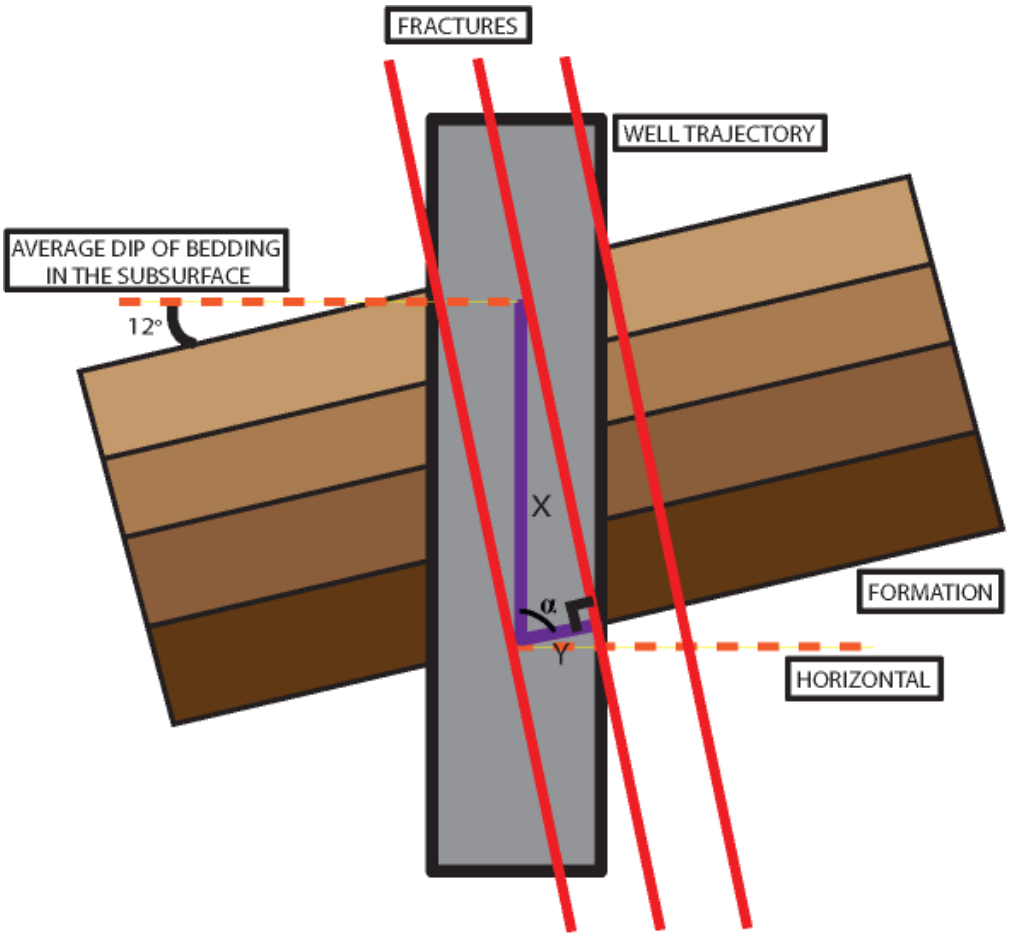

Figure 47: Y is the fracture spacing parallel to bedding calculated from fractures in surface exposures, X is the calculated fracture spacing that would be observed in a vertical core using outcrop data, and α is the average dip of fractures.

Table 5: Average fracture spacing parallel to bedding and vertical distance between fractures calculated for the subsurface. Y is the fracture spacing in outcrop by transect; α is the dip of fractures measured in outcrop for each transect; and X is the calculated vertical distance between fractures in a borehole.

Location	Transect	Y (average fracture spacing parallel to bedding)(cm)	α (average dip of fractures in outcrop)	Cos(α)	X (distance between fractures in vertical wellbore)(cm)	Fracture Set	Stratigraphic Section
Colville incision	7	58.5	81.53	0.147	398.0	set Ao and Af	upper Nanushuk
Fossil Creek	8	25.0	78.53	0.199	125.7	set B	middle Nanushuk
Big Bend	1–6	43.0	73.28	0.288	149.0	set C	upper-lower Nanushuk

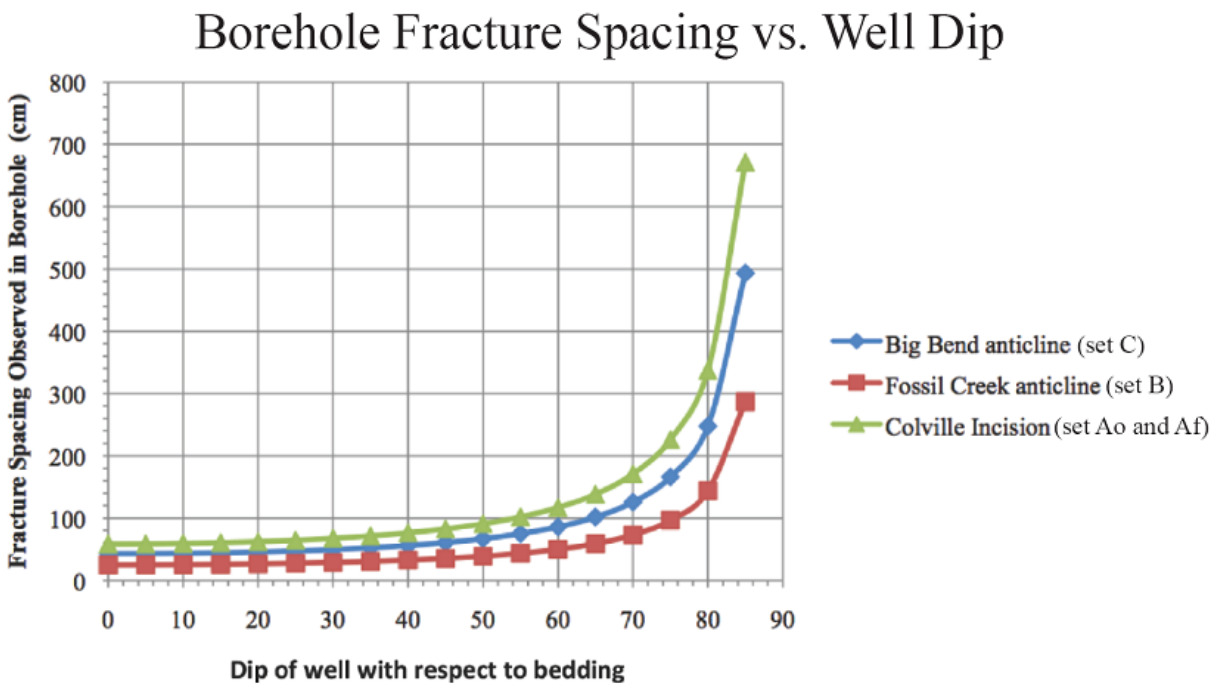

Figure 48: Relationship of observed fracture spacing in a borehole with respect to change in dip of the well trajectory, assuming the well trajectory is perpendicular to the strike of the fractures observed at the Colville incision.

Table 6: The Colville incision showing the predicted fracture spacing for set Ao and Af in a borehole (X) as the trajectory of a well (β) approaches dip of bedding, assuming the well is drilled perpendicular to the strike of fractures.

Colville Incision set Ao and Af				
Y (bed-parallel fracture spacing) (cm)	**β (degrees) (dip of well trajectory)**	**β (radians) (dip of well trajectory)**	**Cos(α)**	**X (predicted fracture spacing observed in borehole)**
58.5	0	0	1	58.5
58.5	5	0.087	0.996	58.7
58.5	10	0.174	0.984	59
58.5	15	0.261	0.965	60
58.5	20	0.349	0.939	62
58.5	25	0.436	0.906	64
58.5	30	0.523	0.866	67
58.5	35	0.610	0.819	71
58.5	40	0.698	0.766	76
58.5	45	0.785	0.707	82
58.5	50	0.872	0.642	91
58.5	55	0.959	0.573	101
58.5	60	1.047	0.500	117
58.5	65	1.134	0.422	138
58.5	70	1.221	0.342	171
58.5	75	1.308	0.258	226
58.5	80	1.396	0.173	336
58.5	85	1.483	0.087	671

Table 7: Fossil Creek anticline showing the predicted fracture spacing for set B in a borehole (X) as the trajectory of a well (β) approaches dip of bedding.

Fossil Creek set B				
Y (bed-parallel fracture spacing) (cm)	**β (degrees) (dip of well trajectory)**	**β (radians) (dip of well trajectory)**	**Cos(β)**	**X (predicted fracture spacing observed in borehole)**
25	0	0	1	25
25	5	0.087	0.996	25
25	10	0.174	0.984	25
25	15	0.261	0.965	25
25	20	0.349	0.939	26
25	25	0.436	0.906	27
25	30	0.523	0.866	28
25	35	0.610	0.819	30
25	40	0.698	0.766	32
25	45	0.785	0.707	35
25	50	0.872	0.642	38
25	55	0.959	0.573	43
25	60	1.047	0.500	50
25	65	1.134	0.422	59
25	70	1.221	0.342	73
25	75	1.308	0.258	96
25	80	1.396	0.173	143
25	85	1.483	0.078	286

Table 8: Big Bend anticline showing the predicted fracture spacing for set C in a borehole (X) as the trajectory of a well (β) approaches dip of bedding.

Big Bend set C				
Y (bed-parallel fracture spacing) (cm)	**β (degrees) (dip of well trajectory)**	**β (radians) (dip of well trajectory)**	**Cos(β)**	**X (predicted fracture spacing observed in borehole) (cm)**
43	0	0	1	43
43	5	0.087	0.996	43
43	10	0.174	0.984	44
43	15	0.261	0.965	45
43	20	0.349	0.939	46
43	25	0.436	0.906	47
43	30	0.523	0.866	50
43	35	0.610	0.819	52
43	40	0.698	0.766	56
43	45	0.785	0.707	61
43	50	0.872	0.642	67
43	55	0.959	0.573	75
43	60	1.047	0.5	86
43	65	1.134	0.422	102
43	70	1.221	0.342	126
43	75	1.308	0.258	166
43	80	1.396	0.173	248
43	85	1.483	0.087	493

Chapter 7

DISCUSSION

7.1 Summary of observations and preliminary interpretation

Open fractures will aid in fluid flow while filled fractures will impede fluid flow. Naturally occurring fractures are present in Umiat cores and may have a significant effect on the mobility of fluids in the subsurface. Natural fractures in cores from Umiat field characteristically are steeply dipping and can vary in spacing from a few centimeters to many meters, but fractures in cores are sporadic and uncommon. Relatively few steep fractures would be intersected in a vertical core because of the small size of the core (27 to 85 mm diameter) and the steeply dipping fractures with varying spacing.

Three fracture sets were identified in surface exposures near Umiat anticline. Fracture sets were distinguished based on orientation and presence or absence of fracture cement and sense of shear data at the Big Bend anticline, Fossil Creek, and Colville incision survey locations (Fig. 2, Table 4). Some fractures (set Af) contain calcite cement. I presume that the parallel to sub-parallel open fractures of set Ao are younger than the calcite-filled veins of set Af. If the set Ao was the same age or older than set Af, they would also be cemented with calcite.

Fracture set Af is present in coherent resistant sandstone beds of the upper Nanushuk Formation at the Colville incision (Figs. 2, 19, 26a, Table 4). Set Af fractures are calcite-filled extension fractures that are oriented orthogonal to the fold axes. I suggest that fractures of set Af formed prior to folding under low-magnitude differential stress ($\sigma 1$ to $\sigma 3$) and high pore fluid pressures in the upper Nanushuk Formation (Table 4). The calcite filling in these fractures and the orientation of stress needed to produce these fractures suggest that they are the earliest

fracture set formed under north-south compression. Price (1966) presented observations of fracture patterns in flat-lying sediments of the Cotswold Hills, England. In that study, Price determined that fractures similar to set Af are common ahead of evolving fold-and-thrust belts, and the qualitatively low differential stress indicated by the extension fractures is consistent with folding not having begun.

Fracture set B is observed in the upper Nanushuk at Colville incision but is also recorded in the middle Nanushuk at Fossil Creek and lower Nanushuk at south Big Bend anticline (Figs. 2, 26a, Table 4). I suggest that the east-west-striking extension fractures formed as a result of a minimum principal stress ($\sigma 3$) oriented north-south (Figs. 5, 6). The appropriate orientation of the minimum principal stress ($\sigma 3$) is easiest to explain where outer-arc tangential longitudinal strain in the hinge zone occurred with a vertical maximum principal stress ($\sigma 1$) (Stearns, 1968, set 3) (Fig. 5, 6). A possible vertical intermediate principal stress ($\sigma 2$) during folding (Stearns, 1968, set 2) is harder to explain but could be a local stress orientation that resulted from curvature changes along the trend of the fold. Fractures of set B are more pronounced and vertically extensive than any fractures of the other sets. These characteristics suggest that they developed over a significant amount of time and probably initiated during early stages of folding. I interpret fractures of set B to have formed during early stages of folding.

Alternatively, fracture set B may have formed within the thickening orogenic wedge at shallow depths as previously folded sections of the orogenic wedge were uplifted and unroofed, resulting in the release of accumulated stress and tensile fracturing. This would require the unusual stress orientations of Stearns (1968) sets 2 or 3 (Fig. 5) to occur at a regional scale; this interpretation is not supported because set B is weakly developed to absent at most of my survey locations.

Fracture sets Cnw and Cne are present in the lower, middle, and upper Nanushuk Formation at north Big Bend anticline and Fossil Creek (Figs. 2, 26a, Table 4). Northeast- and northwest-striking fractures of sets Cnw and Cne are characterized as open conjugate shear fractures whose acute bisector is oriented perpendicular to fold axes. This set of fractures can be interpreted as resulting from local stresses on the fold. This would require a maximum principal compressive stress ($\sigma 1$) parallel to the north or south dip of bedding, a minimum principal stress ($\sigma 3$) parallel to the east-west-trending fold axis, and a vertical intermediate ($\sigma 2$) stress (Figs. 5, 6; Stearns, 1968; Bergbauer and Pollard, 2004). This local stress orientation (Stearns, 1968, set 1) and resulting conjugate fracture pattern is not compatible with the stress orientation required to form east-west striking thrust faults (Stearns, 1968, set 4) on the Big Bend anticline and the Umiat anticline. Thrust faults may develop late during folding but would still require a local stress orientation like Stearns set 4, not set 1. Another, more plausible, interpretation is that sets Cnw and Cne formed as a result of regional stresses before folding, at higher mean and differential stress than set A. I interpret fracture sets Cnw and Cne to have formed prior to the main stages of fold-and-thrust deformation at a higher mean and differential stress than set A (Table 4).

Fractures of set Ao are oriented like set Af, perpendicular to the fold axes and perpendicular to bedding, but they are uncemented extension fractures. Fracture sets Af and Ao formed as a result of a minimum principal stress ($\sigma 3$) oriented east-west and horizontal, normal to the fractures (Stearns, 1968, set 1; Figs. 5, 6). The orientation of the fractures is consistent with the interpretation that the fractures formed during north-south compression in the foothills, when regional $\sigma 1$ remained horizontal. However, stress could have been locally reoriented during folding or could have changed during periods between north-south compression.

Alternatively, these fractures may be interpreted as reactivated fractures that formed as the result of erosional unroofing and the release of residual stress after fold-and-thrust related uplift.

7.2 Relations between fractures and structural/stratigraphic position

Three fracture sets have been identified based on orientation, presence or absence of fracture cement, presence or absence of evidence of shear, and relative age at the Big Bend anticline, Fossil Creek, and Colville incision survey locations (Figs. 2, 19, 24, Table 4). Unfortunately, exposures in the Nanushuk Formation were not extensive enough to evaluate the relationship between fracture character and mechanical stratigraphy.

Set Af fractures were observed in stratigraphically higher levels than many fractures of set B and conjugate set Cnw and Cne and can be interpreted as extension fractures that were formed during north-south compression in the foothills (Figs. 8, 9, 19). Set B fractures were observed in stratigraphically higher levels than set Cnw and Cne except in the upper Nanushuk at north Big Bend, where set B is absent, and where they are present with set C in lower Nanushuk at south Big Bend. Set B fractures are extension fractures that could represent outer-arc tangential longitudinal strain in fold hinge zones as mechanically competent formations folded (Fig. 9, 19). The fact that set C fractures are present and set A fractures are absent high in Nanushuk at north Big Bend argues against control by stratigraphic position.

Although the transects were taken in limbs, the curvature in these folds is probably distributed over very wide zones. Fractures with similar orientations as set Cnw and Cne would form in the lower stratigraphic levels where confining pressure and differential stress likely were the greatest. Set Cnw fractures were observed in the middle Nanushuk at Fossil Creek and the upper Nanushuk at the Colville incision (Fig. 9, 19, Table 4). Set Cnw and Cne fractures were

observed in the upper Nanushuk Formation at north Big Bend and in the lower Nanushuk at south Big Bend. The presence of set C fractures in the upper Nanushuk at north Big Bend and the Colville incision argues against set C fractures resulting from inner arc shortening (Fig. 9).

The distribution of the different fracture sets varies between survey locations, but whether the occurrence of fracture sets correlates only with stratigraphic position, with distance from the deformation front, or with both cannot be determined from currently available information.

Chapter 8

FRACTURE MODEL FOR THE UMIAT ANTICLINE

8.1 Model introduction

Three models have been constructed that incorporate the fracture observations from cores and surface observations from south and north Big Bend anticline, the south limb of the Fossil Creek anticline, and the Colville incision to predict fracture distribution at the Umiat anticline (Figs. 2, 24, 49, 50, 51, 52). The proposed fracture models are schematic structural models that do not incorporate spacing data from this study. Fracture spacing data will be incorporated into a reservoir model by petroleum engineers.

8.2 Primary elements of all Umiat fracture models

The essential starting assumptions of the three Umiat models are that all fractures are assumed to be bed-normal, vertically extensive, and may have similar distributions and orientations to those seen at the Colville incision, Fossil Creek, and the Big Bend anticline. Fractures related to faults are not considered in this thesis, and no assumptions or statements are being made regarding them.

The proposed models for the fracture distribution at the Umiat anticline incorporate fracture orientation data from three different surface locations that represent different structural levels (Figs. 5, 20, 24, 49, 50, 51, 52, Table 4). Fracture set Af is present in the upper Nanushuk Formation at the Colville incision (Figs. 2, 26a, Table 4). Fracture set Cnw is present in the upper Nanushuk Formation at the Colville incision, in the upper and lower Nanushuk Formation at Big Bend anticline, and the middle Nanushuk Formation at Fossil Creek (Figs. 2, 26a, Table

4). Fracture set Cne is present in the upper and lower Nanushuk Formation at Big Bend anticline, and the middle Nanushuk Formation at Fossil Creek but is absent in the upper Nanushuk Formation at the Colville incision (Figs. 2, 26a, Table 4). Fracture set B is best developed in the upper Nanushuk at Colville incision but is also recorded in the middle Nanushuk at Fossil Creek and in the lower Nanushuk at the south limb of the south branch of the Big Bend anticline (Figs. 2, 26a, Table 4). Set B fractures are oriented parallel to the fold hinges of the Colville incision, Fossil Creek, and the Big Bend anticline.

8.3 Model 1: All fractures are associated with regional stresses

This model relates the observed fracture sets to the regional stress field associated with the advance of a fold-and-thrust belt into a foreland basin (Price and Cosgrove, 1990). In this model, it is assumed that fracture sets A and C formed before folding and thrusting and set B formed during folding, not thrusting. It is also assumed in this model that the intermediate principal stress ($\sigma 2$) is perpendicular to bedding, the maximum principal stress ($\sigma 1$) is orthogonal to the thrust front, and the minimum principal stress ($\sigma 3$) parallels the east-west-trending fold axis (Fig. 49).

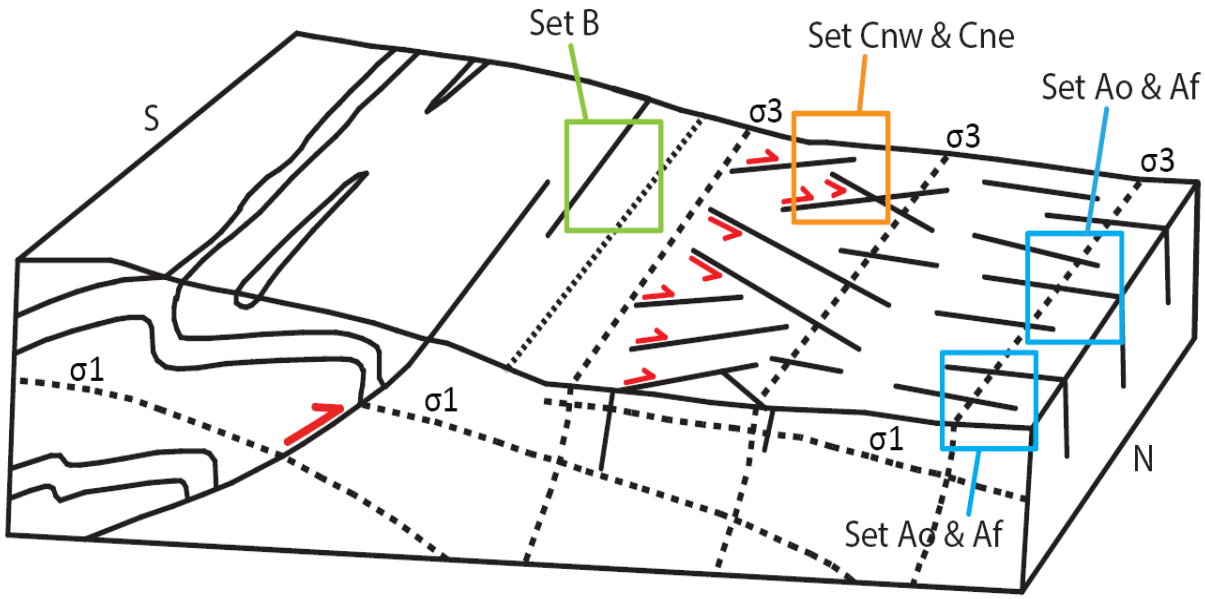

Figure 49: Regional schematic model of the distribution and orientations of fractures associated with regional stress states at Umiat field. Set B fractures are outlined in a green box, set Cnw and Cne are boxed in orange, and set Ao and Af are outlined in blue. Modified from Price and Cosgrove, 1990.

Figure 49 is a conceptual model of the distribution and orientations of three fracture sets associated with regional stress states that may occur at Umiat field. In this stress system, the rocks of the foreland basin that are closer to the fold belt will have a higher differential stress than the same rocks farther from the fold belt (Fig. 49). Vertical conjugate shear fractures will more likely develop in rocks near the fold belt where the differential stress is the greatest (fractures outlined in orange in Fig. 49). The magnitude of the differential stress will decrease steadily ahead of the thrust front into the foreland basin (Figs. 6, 49). North-south extension fractures (outlined with a blue box in Fig. 49) would likely develop in the foreland ahead of the advancing fold belt. East-west extension fractures (outlined in green) would develop as the orogenic wedge continues to thicken.

In this stress system, the vertical conjugate shear fractures that form closer to the fold belt under the highest differential stress correspond to sets Cnw and Cne (Fig. 49). Set Cnw and Cne are uncemented fractures with pervasive slickenlines on fracture surfaces. In this model, these fractures are interpreted as developing prior to folding during north-south compression in the foothills near the fold belt where the differential stress is the greatest. These fractures are outlined in orange in Fig. 49.

In this model, the vertical extension fractures that form normal to and at a greater distance from the thrust front correspond to sets Ao and Af (Fig. 49). Set Af and set Ao extension fractures similar to those seen at the Colville incision and at Fossil Creek are part of a regional fracture pattern that has been interpreted as being controlled by the development of north-south compression in the foothills. Sets Af and Ao are hinge-perpendicular fractures that are both calcite filled and uncemented and are interpreted to be the oldest fracture sets formed under low-magnitude differential stress ($\sigma 1$ to $\sigma 3$) (Figs. 6, 49, Table 4). As north-south compression progressed throughout the foothills, the regional stress ($\sigma 1$) remained horizontal, allowing open extension fractures (set Ao) oriented parallel to the principal ($\sigma 1$) stress direction. Alternatively, the Ao set of fractures may be interpreted as late unloading fractures that formed as the result of erosional unroofing and the release of residual stress after fold-and-thrust related uplift.

As compression decreased in the foreland basin or in the fold belt, north-south became the direction of least principal stress ($\sigma 3$) instead of maximum principal stress ($\sigma 1$). This change in stress direction may have resulted in the formation of east-west-striking vertical extension fractures in the basin (set B) (Fig. 49). Alternatively, fracture set B may have formed later, within the thickening orogenic wedge at shallow depths as previously folded sections of the

orogenic wedge were uplifted and unroofed, resulting in the release of accumulated stress by tensile fracturing (Fig. 49). This would require the stress orientations of Stearns (1968) sets 2 or 3 (Fig. 5) to occur regionally throughout the orogenic wedge.

8.3.1 Model 1: Implications for fracture distribution at Umiat

This model implies that fracture sets Ao, Af, and set B would occur in the subsurface at Umiat. The north-south extension fractures (Ao and Af) will be in the subsurface ahead of the thrust front in the foreland basin where the differential stress is the least. North-south extension fractures will be vertically extensive and widely spaced. East-west extension fractures (set B) will also be present in the subsurface in the foreland basin and on the crest of the anticline. These fractures will be vertically extensive. Set Ao and B fractures are open and will be potentially filled with ice in the upper portion of the reservoir where it is in permafrost. Af fractures that are calcite filled will hinder fluid flow.

According to this model, the widely spaced and vertically extensive conjugate shear fractures (set Cnw and Cne) would not be present at Umiat. This fracture set develops near the fold belt where the differential stress is the greatest, and Umiat is not close enough to the thrust front to form these fractures. Fracture set C is present in Big Bend and Fossil Creek but is poorly developed at the Colville incision, which is closer in proximity to Umiat anticline (Figs. 28, 49).

The most effective and efficient drilling model will target the reservoir zone with the highest permeability and porosity while avoiding the frozen permafrost zone. The orientation of fracture sets A, B, and C in the subsurface will have little effect on the overall porosity of the reservoir. However, Umiat model 1 suggests that calcite cemented fracture set Af will decrease fluid flow by acting as permeability barriers while partially filled fractures may still improve

fluid flow. Production in horizontal legs will be significantly reduced, depending on the azimuth of the borehole, due to set Af filled fractures. The potential to hit a north-south filled fracture will increase if the azimuth of the well is east-west. Likewise, model 1 suggests that if the horizontal leg of a drill hole is oriented north-south, it is more likely to encounter an east-west fracture set. Umiat model 1 suggests the drilling orientation of the horizontal legs should be dominantly north-south or east-west.

8.3.2 Model 1 deficiency

Set B fractures are difficult to explain in this regional model. The stress orientations needed to produce set B fractures would be the stress orientations of Stearns (1968) sets 2 and 3 (Fig. 5) and would need to occur regionally. Set B fractures are only present at Fossil Creek and the Colville incision, which is farther from the thickening orogenic wedge. Set B is most likely related to the development of the fold and thus a result of local stress states.

8.4 Model 2: All fractures are associated with local fold-related stresses

In this model, observed fracture sets are assumed to be related to local stresses that changed during folding (Stearns, 1968). Throughout the evolution of a fold, rock stresses and fluid pressures are continuously changing, along with the behavior of the rock units. The magnitude of the differential stress, fluid pressure, position of the fracture with respect to the neutral surface, and occurrence on limb vs. hinge controls whether extension or shear fractures develop (Fig. 6; Stearns, 1968).

Figure 50 is a schematic model of a fold with the distribution and orientations of three fracture sets that may occur at Umiat field associated with local stress states during folding.

North-south extension fractures (outlined in blue) would likely develop at low differential stress as folding-initiated and vertical conjugate shear fractures (outlined in orange) would form later at greater magnitude of differential stress. East-west open extension fractures (outlined in a green box) would develop parallel to the fold hinge as a result of tangential longitudinal strain in the outer arc of the fold.

In this model, set Af is assumed to have formed early during folding under low-magnitude differential stress ($\sigma 1$ to $\sigma 3$) and high pore fluid pressures on the limbs of the anticline (Figs. 50, 51, Table 4). The calcite filling these fractures and the orientations of stress axes needed to produce these fractures indicate that they are the earliest formed fractures formed as folding initiated under north-south compression. Set Ao could form at any time during or after folding when differential stress is low and vein-forming fluids are absent. Alternatively, they could be related to extensional tangential longitudinal strain related to curvature along the trend of the fold hinge.

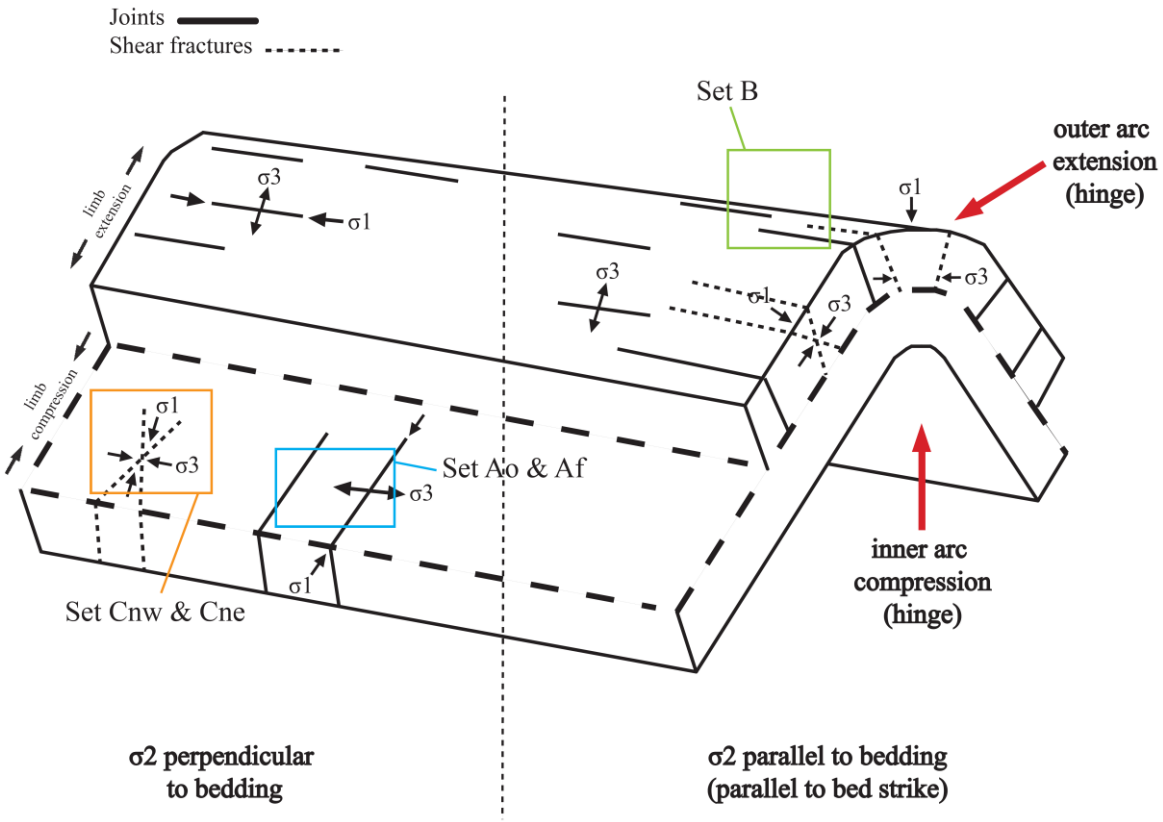

Figure 50: Local schematic model of the distribution and orientations of fractures associated with folding, as may be expected at Umiat field. Set B fractures are outlined in a green box, set Cnw and Cne are boxed in orange, and set Ao and Af are outlined in blue. Modified from Hayes (2004).

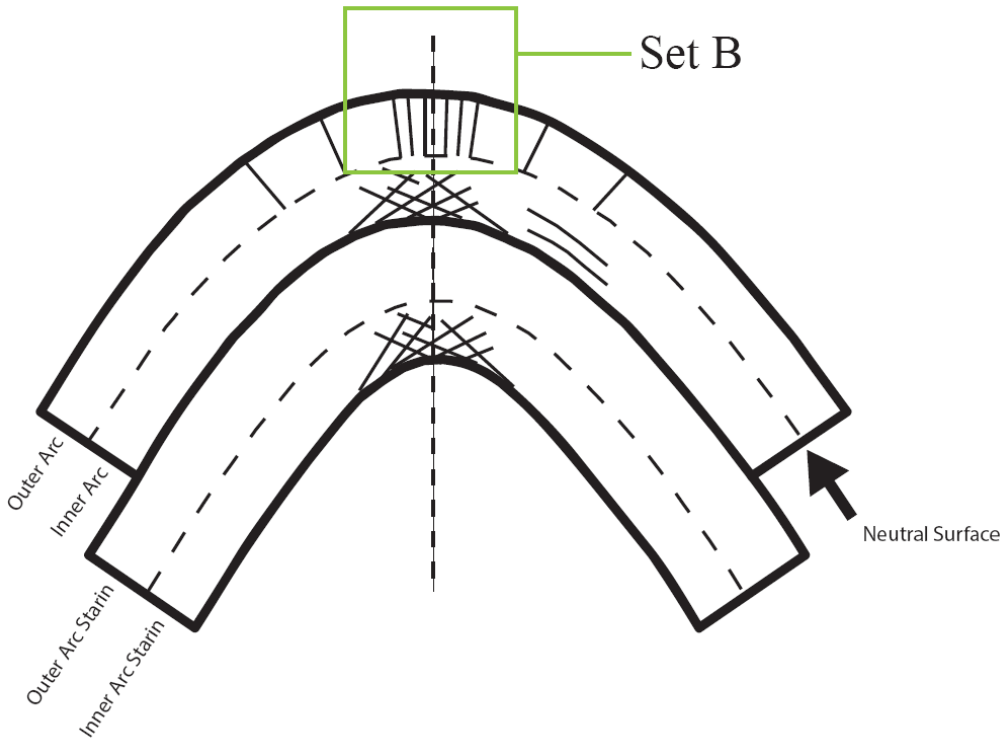

Figure 51: Schematic model of the orientation of fracture set B oriented parallel to the fold axis. Fracture set B is outlined in a green box. Modified from Hayes (2004).

During folding, the principal stress axes tend to be oriented parallel or normal to bedding, and the orientation of these axes controls the fracture patterns (Fig. 50). If the least principal stress direction (σ3) is parallel to the fold axis, the maximum principal stress direction (σ1) is north-south, and the differential stress is sufficiently high, the result would be bed-normal conjugate shear fractures (set Cnw and Cne), especially in fold limbs (orange box, Fig. 50). As the fold develops and the curvature of the beds increases, especially in hinge zones, extensional tangential longitudinal strain increases in the outer arc of folds, and the least principal stress direction (σ3) will be normal to the fold axis (north-south) (Fig. 50). The resulting fractures

would be oriented normal to bedding and parallel to the fold axis (set B) (green box, Figs. 50, 51).

8.4.1 Model 2: Implications for fracture distribution at Umiat

At Umiat, the distribution and orientation of fractures will vary throughout the fold. More set B (east-west) fractures would be expected on the crest of the reservoir where there is higher outer arc extension, while set C fractures would be absent. Set Af and Ao (north-south) fractures along with set C (Cnw and Cne) conjugate fractures would be expected in the limbs of the folds where limb compression occurs. The north-south fractures would be both open and calcite filled, vertically extensive, and widely spaced in the limbs, while east-west fractures will be open and vertically extensive. Open fractures in the upper portion of the reservoir where it is in the permafrost zone will be filled with ice and will impede fluid movement while fractures in the lower reservoir below the permafrost will remain open and increase permeability. Open conjugate shear fractures will be found in the limbs of the fold and will be widely spaced and vertically extensive. These fractures will be open unless in the upper permafrost zone.

In Umiat model 2, maximum strain will occur in the fold hinge where parallel to the fold hinge extension fractures occur due to outer-arc tangential longitudinal strain, while maximum compression will occur in the limbs of the fold. Although the orientation of fracture sets A, B, and C in the subsurface will have little effect on the overall porosity of the reservoir, model 2 suggests that set Af fractures will decrease fluid flow by acting as permeability barriers. The production in horizontal legs will be significantly reduced, depending on the azimuth of the borehole, due to the Af fracture set. Model 2 predicts that fracture sets Af, Ao, and C will be encountered more on the limbs of the anticlines while set B will be encountered on the crest of

the fold. Although model 2 predicts fracture set C occurring on the limbs of Umiat anticline, the lack of set C fractures at Colville incision indicates that set C may not be present at Umiat. Umiat model 2 indicates that the well pattern will need to be adjusted based on the location of the borehole relative to the fold, and placement of well pads should be concentrated on the crest and upper limbs of the anticline. According to this model, horizontal legs on the crest of the field should be oriented north-south in order to intersect set B fractures. If drilling on the upper limbs of the anticline, drilling orientation of the borehole should be dominantly east-west to offset the permeability reduction caused by filled set A fractures.

8.4.2 Model 2 deficiency

The abundance of the conjugate fracture set C decreases at each location northward. The lack of set Cne altogether at the Colville incision is puzzling. If all fractures are a direct result of folding, then set C (both Cnw and Cne) fractures would be expected on the fold limbs. The stress orientations needed to produce set C fractures would be the stress orientations of Stearns (1968) set 1 (Fig. 5) and would need to occur locally throughout the fold. Set C fractures are only present at north and south Big Bend and Fossil Creek, which are farther south from the Colville incision and Umiat. This could imply that Set C is related to the regional stress states and formed prior to the main stages of fold-and-thrust deformation at a higher mean and differential stress than set A.

8.5 Model 3: Composite fracture model

This model relates the observed fracture sets to both regional and local stress fields during the advancement of a fold-and-thrust belt into a foreland basin (Stearns, 1968; Price and

Cosgrove, 1990). In this stress system, the regional stress axes are assumed to be oriented as follows: maximum principal compressive stress (σ1) perpendicular to the fold and thrust belt, minimum principal stress (σ3) parallels the thrust front and a vertical intermediate principal stress (σ2), or equivalent to the overburden in most cases. This model also assumes that stress states within the fold control whether extension or shear fractures develop. The local stress states are assumed to be oriented as follows: intermediate principal stress (σ2) is normal to bedding, the maximum principal compressive stress (σ1) parallels the north-south dip of bedding, and the minimum principal stress (σ3) parallels the east-west-trending fold axis (Fig. 52).

Figure 52 is a conceptual model combining elements from both the regional and local stress models into one model for the distribution and orientation of fractures sets that may occur at Umiat field. Regional vertical conjugate shear fractures developed closest to the thrust front where the differential stress was the greatest, while vertical extension fractures formed normal to and farther ahead of the thrust front (Fig. 52). As north-south compression continued and folding occurred, local stresses related to folding controlled fracture orientations within the fold (Fig. 52). Local stresses during folding may have reactivated the regional fracture sets and overprinted them with new fractures (Fig. 52).

In this model, fracture set Ao and Af corresponds with the vertical extension fractures that formed normal to and farther from the thrust front and on the folds (Fig. 52). Set Af are hinge-perpendicular fractures that are calcite filled and that are interpreted to be the oldest fracture sets that formed under low-magnitude differential stress (σ1 to σ3) (Figs. 6, 52, Table 4). These fractures are assumed to be part of a regional fracture pattern that was controlled by the

development of north-south compression in the foothills. Ao fractures are interpreted to be reactivated locally during fold evolution (Fig. 52).

As the fold develops and the curvature of the beds increases, especially in hinge zones, extensional tangential longitudinal strain increases in the outer arc of folds, and the least principal stress direction (σ3) will be normal to the fold axis (north-south) (Fig. 52). The resulting fractures would be oriented normal to bedding and parallel to the fold axis (set B). Vertical conjugate shear fractures will more likely develop on the fold limbs (Fig. 52).

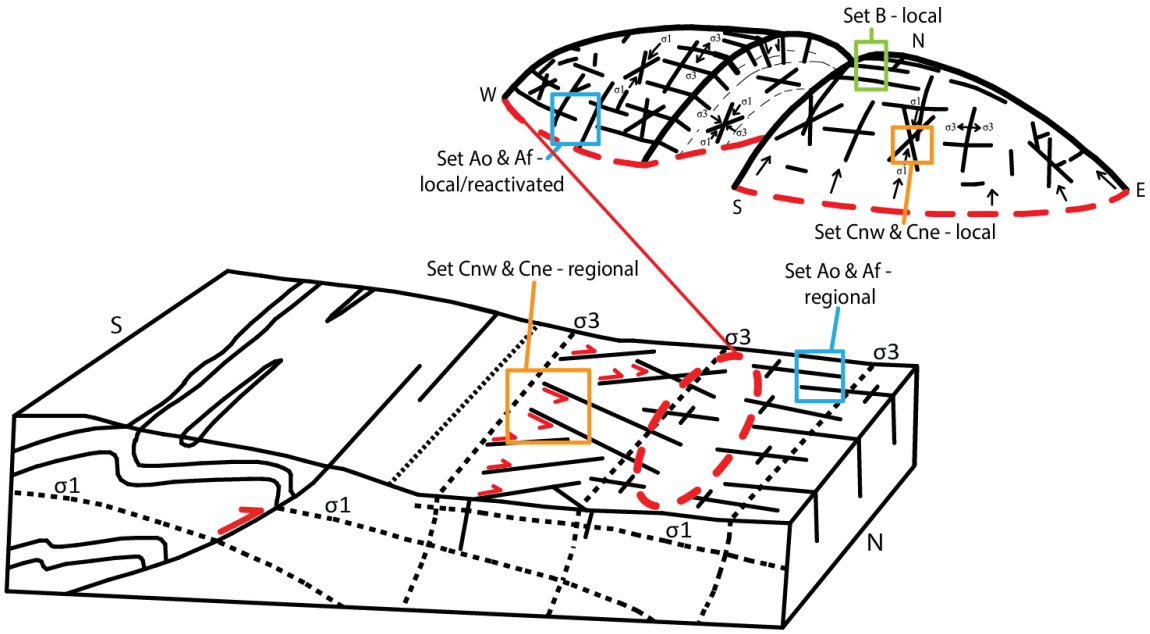

Figure 52: Schematic composite model of the Umiat field, showing the distribution and orientations of fractures associated with regional stress states and local folding. Set B (local) fractures are outlined in a green box, set Cnw and Cne (both local and regional) are boxed in orange, and set Ao and Af (both local and regional) are outlined in blue. The red dashed outline on the regional drawing corresponds to the bottom red line on the local fold. Modified from Price and Cosgrove (1990).

8.5.1 Model 3: Implications for fracture distribution at Umiat

This model implies that both regional and local sets of fractures would occur in the subsurface at Umiat. Regional north-south extension fractures that formed ahead of the thrust front in the foreland basin would predate the formation of Umiat anticline and will be vertically extensive and widely spaced. Observations from the Big Bend anticline, Fossil Creek, and the Colville incision indicate that these filled fractures will occur throughout the stratigraphic section at Umiat. As folding continued, more fractures would be expected associated with local stresses along the fold. North-south and east-west fracture sets would develop more on the crest of the anticline, while open conjugate shear fractures could develop in the limbs of the fold. The north-south fractures would be both open and calcite filled, vertically extensive and widely spaced. North-south and east-west open fractures in the upper portion of the reservoir could be filled with ice where the reservoir is in the permafrost zone and, if so, will impede fluid movement. Fractures in the lower reservoir not in permafrost will remain open and enhance permeability.

Umiat model 3 suggests that the placement and drilling orientation of the borehole could result in different productivity because of the wellbore encountering different fracture sets. Set Af fractures could decrease east-west fluid flow in the reservoir by acting as permeability barriers, so placing horizontal legs in an east-west direction would offset any permeability reduction caused by these fractures. In contrast, the open E-W and ~N-S conjugate fractures could result in early water breakthrough in legs oriented in the N-S and E-W directions. Based on model 3, the proposed drill plan (wagon wheel pattern on the crest and limbs of the Umiat field targeting the reservoir below the permafrost, Hanks et al., 2014) should expect varying recovery of the horizontal legs, depending upon the orientation.

8.5.2 Model 3 deficiency

Model 3 predicts that local conjugate shear fractures (Cnw and Cne) could develop on the fold limbs where limb compression is the greatest. However, the lack of observed set C fractures at the Colville incision and decreased number observed at Fossil Creek suggest that fracture set C could be absent from Umiat altogether because it's too far north of the thrust front. Although not all fractures may occur at Umiat, model 3 provides a comprehensive explanation for the different sets of fractures observed in the outcrop.

Chapter 9

DISCUSSION

The preferred model for the Umiat oil field is the third, the composite model, which combines elements from both regional and local stress models into one model. It is the preferred model because it takes into account the multiple stress states both regionally and locally that can occur at Umiat because fractures can form at any time during the history of the fold and more than one mechanism can produce fractures. The composite model will give reservoir engineers an all-encompassing history of fractures at Umiat field to incorporate into simulations of the Umiat reservoir.

Fracture characteristics were observed at four locations in Cretaceous rocks near the Umiat anticline in the Colville basin. Based on outcrop observations, open fractures in the subsurface may be oriented north-south, east-west, northeast-southwest, and northwest-southeast. Fractures of set Af were observed only in stratigraphically higher levels in the upper Nanushuk Formation at the Colville incision and measure 15 to 200 cm in height and are widely spaced (~58 cm). Set Ao fractures were predominately recorded in the middle Nanushuk Formation at Fossil Creek and the upper Nanushuk at the Colville incision. Set Af fractures are extension fractures that formed under north-south compression, prior to folding due to elevated pore pressures during burial. Set Ao fractures formed during north-south compression in the foothills. Fractures of set B occur in the lower, middle, and upper Nanushuk Formation at south Big Bend anticline, Fossil Creek, and the Colville incision. Set B fractures are absent at north Big Bend anticline. Fracture set B is widely spaced and vertically extensive (~15 to 200 cm in height). Set B fractures are extension fractures that represent outer arc tangential longitudinal strain in fold

hinges as mechanically competent formations folded. Fractures of set C range from 5 to 500 cm in height and are widely spaced (~149 cm). Fracture set Cnw was observed in the upper, middle, and lower Nanushuk at the Colville incision, Fossil Creek, north Big Bend anticline, and south Big Bend anticline. Fracture set Cne was observed in the upper, middle, and lower Nanushuk at Fossil Creek, north Big Bend anticline, and south Big Bend anticline but was absent in the upper Nanushuk at the Colville incision. Set Cnw and Cne are well-defined conjugate shear fractures that formed on the fold limbs as compression increased the differential stress in the rocks.

Natural fractures are observed in Umiat cores. Although no orientation data is available for the Umiat cores, the calcite-filled fractures identified in Umiat cores may correspond to set Af fractures observed in the outcrop. In the outcrop, calcite filling was only observed in the Af fracture set. Therefore, calcite infilling is a distinguishable characteristic of fracture set Af that neither set B nor C possesses. These filled fractures will impede fluid flow in the reservoir, while open fractures will be conducive to fluid flow in the subsurface. However, all open fractures that are within the permafrost zone will be filled with ice and will in turn decrease the permeability of the upper reservoir zone. Below the permafrost zone, the open to partially filled fractures for set A (Ao and Af), B, and C (Cnw and Cne) will allow fluid movement and permeability throughout the sandstone reservoir.

The most effective and efficient drilling model will target the reservoir zone with the highest permeability and porosity while avoiding the frozen permafrost zone. Stratigraphy of the Umiat reservoir indicates that the Lower Grandstand sandstone is the best reservoir target for initial development because it is the deepest part of the reservoir interval and would be the least affected by permafrost (Shimer et al., 2014). Surface and subsurface observations suggest that permeability within the reservoir will be affected by all fracture sets. Calcite cemented fractures

will decrease fluid flow by acting as permeability barriers, while partially filled fractures may still improve fluid flow.

The orientation of each fracture set in the subsurface will have little effect on the overall porosity of the reservoir. However, the potential to hit a north-south filled or partially filled fracture will increase if the azimuth of the well is east-west. Production could be enhanced if the fractures are partially open; if fractures are totally filled, the negative impact of these filled fractures could be offset. Likewise, if the horizontal leg of a drill hole is oriented north-south, it is more likely to encounter an open east-west fracture set. While open fractures increase permeability in a wellbore and aid in hydrocarbon migration, hitting open fractures may cause loss of drilling products to the surrounding formations through these open fracture networks and/or early water breakthrough.

Chapter 10

CONCLUSIONS

Fracture studies play an important role in determining potential migration pathways and the porosity and permeability in a reservoir. Fractures can form at any time during the history of the fold and more than one mechanism can produce fractures. This study focused on determining the characteristics and distribution of fractures in cores and in surface exposures to generate a fracture model for the Umiat anticline.

Several natural fractures were identified in Umiat wells 1, 2, and 11. Characteristics of these natural fractures include planar geometry, steep dip with respect to bedding, calcite cementation and/or open, with apparent surface staining. None of the wells examined had cores from the actual thrust faults, so fractures related to thrusting could not be evaluated.

The very limited subsurface information from Umiat cores requires reliance on surface observations from the Colville incision, Fossil Creek, and the Big Bend anticline. Three sets of fractures were identified in outcrops near the Umiat anticline and are interpreted to have formed due to regional and local differential stress distributions and orientation resulting from overburden, folding, and/or unroofing. Fracture sets Af and Ao are present in the middle and upper Nanushuk Formation at the Colville incision and at Fossil Creek. Set Af fractures are interpreted to be extension fractures that formed prior to folding under low-magnitude differential stress ($\sigma 1$ to $\sigma 3$) and high pore fluid pressures ahead of the advancing deformation front (Table 8). The calcite cement in these fractures and the orientation of stress axes needed to produce these fractures indicate that they are the earliest formed fracture sets.

Set Ao fractures are interpreted to have formed before the early stages of folding. These fractures are open fractures, which suggests that set Ao is younger than set Af because a

significant amount of time passed, allowing calcite to heal early fractures. Fracture set Ao also shares the same orientation as set Af, which indicates the same orientation of stress axes existed during the evolution of each fracture set. Set Ao fractures are likely the result of *in-situ* regional stress or reactivation of earlier set Af fractures with similar orientations. Set Ao would not have been reactivated as shear fractures because they are parallel to the principal ($\sigma 1$) stress and consequently would have no shear stress. However, they could be reactivated as extension fractures.

Fracture set B is recorded in the middle Nanushuk Formation at Fossil Creek and in the lower Nanushuk at the Big Bend anticline but is best documented in the upper Nanushuk at the Colville incision (Fig. 26a). Fractures in set B strike east-west and are more pronounced and vertically extensive than any fractures of the other sets. These characteristics suggest that they developed over a significant amount of time and probably initiated early during folding as a result of outer arc extension in the fold hinges where the maximum principal stress ($\sigma 1$) is normal to bedding.

Fractures of set Cnw and Cne are present in the upper and lower Nanushuk Formation at the Big Bend anticline and in the middle Nanushuk Formation at Fossil Creek and are open conjugate shear fractures. Fractures of set Cnw and Cne are interpreted to have developed prior to the main stages of fold-and-thrust deformation, closer to the deformation front than set Ao, where mean and differential stresses were higher. Alternatively, these conjugate shear fractures could have formed during folding and be equivalent to Stearns (1968) set 1 fractures that form due to compression in the fold limbs. Fracture sets Cnw and Cne are not likely to have formed during thrusting because a vertical intermediate principal stress ($\sigma 2$) is not consistent with thrusting.

Fractures observed in the Umiat core cannot be assigned directly to a fracture set observed in surface exposures because of the lack of orientation data. However, calcite cementation on fracture surfaces in Umiat core may suggest that these fractures belong to the north-south calcite-filled fracture set (Af) seen in nearby surface exposures.

Surface observations of fracture orientation and spacing can be incorporated into a model for the fracture distribution at the Umiat anticline. Regional vertical conjugate shear fractures equivalent to set C fractures developed closest to the thrust front where the differential stress was the greatest, while vertical extension fractures (set Af) formed normal to and farther ahead of the thrust front in more distal sediments. As north-south compression continued and folding occurred, local stresses controlled the orientations and character of new fractures that formed within the fold. The fractures controlled by local stresses during folding reactivated and overprinted the regional fracture sets. As the fold developed and the curvature of the beds increased, especially in hinge zones, extension increased in the outer arc of folds, with the least principal stress direction ($\sigma 3$) normal to the fold axis (north-south). The resulting fractures would be oriented normal to bedding and parallel to the fold axis (set B). Vertical conjugate shear fractures similar to Set C fractures could also form on the fold limbs due to limb compression increasing during folding.

Previous work from Shimer et al., 2014 suggests that horizontal drilling should target the Lower Grandstand below the permafrost. The orientations of fracture sets throughout the field should not affect the proposed wagon-wheel well design. However, production in horizontal legs could potentially be reduced depending on the azimuth of the borehole relative to the north-south striking calcite-filled fractures. Alternatively, encountering open fractures could enhance the potential of water break through or loss of circulation in the borehole. Within the reservoir,

recovery will be reduced in parts that are located in the permafrost zones due to the reduction of permeability and the presence of ice in open fractures.

10.1 Future work

This fracture study could be improved by constraining thermal conditions throughout the history of folding and fracturing as a proxy for burial depth. From field observations it has been interpreted that set Af fractures formed prior to set Ao, Cnw, Cne, or B fractures. The burial history of the area could be modeled if pressure and temperature constraints could be used from set Af fractures. A fluid inclusion analysis as well as a stable isotope analysis would be beneficial on calcite-filled fractures (set Af) and the surrounding rocks to determine the source of calcite in the fractures.

Multiple fracture transects taken on anticlines similar to and in close proximity to Umiat may give a more accurate representation of fracture geometry and patterns in the Brooks Range foothills. Additional fracture transects taken in stratigraphically higher and lower formations, preferably within the same fold, would also provide a better understanding of how fractures form during folding and give a better understanding of the influence of mechanical stratigraphy on fracture distribution and evolution.

Chapter 11

REFERENCES

Adabi, M.H., Sadeghi, A.D., Hosseini, M., Moalemi, A., Lotfpour, A., Khatibi Mehr, M., Salehi, A., Zohdi, A., and Jafarzadeh, M., 2009, Reservoir characterization and tectonic setting of Ahwaz Sandstone member of the Asmari formation in the Zagros Mountains, southwest of Iran: European Geosciences Union General Assembly 2009, 19-24 April 2009, in Vienna, Austria, p. 365.

Allen, P.A., and Allen, J.R., 2005, Basin analysis, principles and applications: Oxford, UK, Blackwell Publishing Ltd., 317 p.

Atkinson, B.K., 1987, Fracture mechanics of rock: Academic Press, London, 534 p.

Bachu, S., 1995, Synthesis and model of formation-water flow, Alberta Basin, Canada: American Association of Petroleum Geologists Bulletin, v. 79, p. 1159-1178.

Baptist, O.C., 1960, Oil recovery and formation damage in permafrost, Umiat field, Alaska: Report of investigation 5642, U.S. Dept. of Interior, Bureau of Mines, 19 p.

Bergbauer, S., and Pollard, D. D., 2004, A new conceptual fold-fracture model including prefolding joints, based on the Emigrant Gap anticline, Wyoming: Geological Society of America Bulletin, v. 116, no. 3-4, p. 294-307.

Bird, K.J., 1988, The geologic basis for appraising undiscovered hydrocarbon resources in the National Petroleum Reserve in Alaska by the play-appraisal method, *in* Gryc, George, ed., Geology and exploration of the National Petroleum Reserve in Alaska, 1974 to 1982: U.S. Geological Survey Professional Paper 1399, p. 81-116.

Bird, K.J., 1999, Geographic and geological setting in the oil and gas resource potential of the 1002 Area, Arctic National Wildlife Refuge, Alaska, by ANWR Assessment Team: U.S. Geological Survey Open-File Report 98-34

Bird, K.J., and Bader, J.W., 1987, Regional geologic setting and history of petroleum exploration, *in* Bird, K.J., and Magoon, L.B., eds., Petroleum geology of the northern part of the Arctic National Wildlife Refuge, northeastern Alaska: U.S. Geological Survey Bulletin 1778, p. 17-25.

Bird, K.J., and Molenaar, C.M., 1992, The North Slope foreland basin, Alaska, *in* Macqueen, R.W., and Leckie, D.A., eds., Foreland basins and fold belts: American Association of Petroleum Geologists Memoir 55, p. 363-393.

Bons, P.D., Elburg, M.A., and Gomez-Rivas, E., 2012, A review of the formation of tectonic veins and their microstructures: Journal of Structural Geology, v. 43, p. 33-62.

Brosge, W.P., and Whittington, C.L., 1966, Geology of the Umiat-Maybe Creek region, Alaska: U.S. Geological Survey Professional Paper 303-H, p. 501-638.

Chapman, R.M., and Sable, E.G., 1960, Geology of the Utukok-Corwin region, northwestern Alaska: U.S. Geological Survey Professional Paper 303–C, p. 47–167.

Claypool, G.E., and Magoon, L.B., 1985, Comparison of oil-source rock correlation data for Alaskan North Slope: Techniques, results, and conclusions, *in* Magoon, L.B., and Claypool, G.E., eds., Alaska North Slope oil-rock correlation study: Tulsa, Oklahoma, American Association of Petroleum Geologists Studies in Geology 20, p. 49–81.

Coakley, B.J., and Watts, A.B., 1991, Tectonic controls on the development of unconformities: The North Slope, Alaska: Tectonics, v. 10, p. 101-130.

Collins, F.R., 1958, Test wells, Umiat area, Alaska: U.S. Geological Survey Professional Paper 305-B, 175 p.

Cooper, M., 1992, The analysis of fracture systems in subsurface thrust structures from the foothills of the Canadian Rockies, *in* McClay, K., ed., Thrust tectonics: London, Chapman & Hall, p. 391-405.

Cuong, T.X., and Warren, J.K., 2009, Bach Ho field, a fractured granitic basement reservoir, Cuu Long Basin, offshore southeast Vietnam: a "buried-hill" play: Journal of Petroleum Geology, v. 32, no. 2, p.129-156.

Davis, J.C., 2002, Statistics and data analysis in geology, 3rd edition: New York, John Wiley & Sons, Inc., 646 p.

Davis, G.H., and Reynolds, S.J., 1996, Structural geology of rocks and regions: New York, John Wiley & Sons, Inc., 776 p.

Decker, P.L., 2007, Brookian sequence stratigraphic correlations, Umiat Field to Milne Point Field, west-central North Slope, Alaska: Alaska Division of Geological and Geophysical Surveys Preliminary Interpretive Report 2007-2, 19 p., 1 sheet.

Detterman, R. L., Bickel, R. S., and Gryc, G, 1963, Geology of the Chandler River Region, Alaska: U.S. Geological Survey Professional Paper 303-E, 223-324 p.

Duncan, A.S., 2006, Evolution of fractures and Tertiary fold-and-thrust deformation in the central Brooks Range foothills, Alaska [M.S. thesis]: Fairbanks, University of Alaska Fairbanks, 122 p.

Duncan, A.S., Hanks, C.L., Wallace, W.K., O'Sullivan, P.B., and Parris, T.M., 2007, Fracture distribution, thermal history and structural evolution of the central Brooks Range Foothills, Alaska [abs.]: Geological Society of America Abstracts with Programs, v. 38, no. 5, p. 89.

Engelder, T., 1985, Loading paths to joint propagation during a tectonic cycle: An example from the Appalachian Plateau, U.S.A.: Journal of Structural Geology, v. 7, p. 459-476.

Engelder, T., and Fischer, M.P., 1996, Loading configurations and driving mechanisms for joints based on the Griffith energy-balance concept: Tectonophysics, v. 256, p. 253-277.

Engelder, T., Gross, M.R., and Pinkerton, P., 1997, Joint development in clastic rocks of the Elk Basin anticline, Montana-Wyoming, *in* Hoak, T., Klawitter, A., and Blomquist, P., eds., An analysis of fracture spacing versus bed thickness in a basement-involved Laramide structure: Rocky Mountain Association of Geologists 1997 Guidebook, Denver, Colorado, p. 1-18.

Engelder, T., and Lacazette, A., 1990, Natural hydraulic fracturing, *in* Barton, N., and Stephansson, O., eds., Rock joints: Rotterdam, A.A. Balkema, p. 35-44.

Finzel, E.S., 2004, Architectural analysis and fold geometry of syntectonic fluvial conglomerate in the Nanushuk Formation, Brooks Range foothills, Alaska [M.S. thesis]: Fairbanks, University of Alaska Fairbanks, 125 p.

Fischer, M.P., and Wilkerson, M.S., 2000, Predicting the orientation of joints from fold shape: Results of pseudo-three-dimensional modeling and curvature analysis: Geology, v. 28, p. 15-18.

Flaig, P.P., McCarthy, P.J., and Fiorillo, A.R., 2009, A tidally-influenced, high-latitude alluvial/coastal plain: the Late Cretaceous (Maastrichtian) Prince Creek Formation, North Slope, Alaska: SEPM Special Publication, Tulsa, Oklahoma, v. 97, p. 233-264.

Griggs, D.T., and Handin, J., 1960, Observations on fracture and a hypothesis of earthquakes, *in* Griggs, D.T., and Handin, J., eds., Rock deformation: Boulder, Colorado, Geological Society of America Memoir 79, p. 347-364.

Hancock, P.J., and Engelder, T., 1989, Neotectonic joints: Geological Society of America Bulletin, v. 101, p. 1197-1208.

Hanks, C.L., Lorenz, J., Teufel, L., and Krumhardt, A.P., 1997, Lithologic and structural controls on natural fracture distribution and behavior within the Lisburne Group, Northeastern Brooks Range and North Slope subsurface, Alaska: American Association of Petroleum Geologists Bulletin, v. 81, p. 1700-1720.

Hanks, C.L., Parris, T., and Wallace, W.K., 2006, Fracture paragenesis and microthermometry in Lisburne Group detachment folds: Implication for the thermal and structural evolution of the northeastern Brooks Range, Alaska: American Association of Petroleum Geologists Bulletin, v. 90, p. 1-20.

Hanks, C.L., Wallace, W.K., Atkinson, P.K., Brinton, J., Bui, T., Jensen, J., and Lorenz, J., 2004, Character, relative age and implications of fractures and other mesoscopic structures associated with detachment folds: an example from the Lisburne Group of the northeastern Brooks Range, Alaska: Bulletin of Canadian Petroleum Geology, v. 52, p. 121-138.

Hanks, C.L., Shimer, G.T., Oraki-Kohshour, I., Ahmadi, M., McCarthy, P.J, Dandekar, A., Mongrain, J., Wentz, R., 2014, Integrated reservoir characterization and simulation of a shallow, light oil, low temperature reservoir: Umiat Field, National Petroleum Reserve, Alaska: AAPG Bulletin, 2014.

Hayes, M.R., 2004, The influence of mechanical stratigraphy on the development of detachment folds and associated mesoscopic structures: an example from the Lisburne Group carbonates, Northeastern Brooks Range, Alaska [M.S. thesis]: Fairbanks, University of Alaska Fairbanks, 134 p.

Hayes, M.R., and Hanks, C.L., 2008, Evolving mechanical stratigraphy during detachment folding: Journal of Structural Geology, v. 30, pp. 548-564.

Helgeson, D.E., and Aydin, A. 1991, Characteristics of joint propagation across layer interfaces in sedimentary rocks: Journal of Structural Geology, v. 13, no. 8, p. 897.

Hennings, P.H., Olson, J.E., and Thompson, L.B., 2000, Combining outcrop data and three-dimensional structural models to characterize fractured reservoirs: an example from Wyoming: AAPG Bulletin, v. 84, p. 830-849.

Houseknecht, D.W., and Schenk, C.J., 2004, Sedimentology and sequence stratigraphy of the Cretaceous Nanushuk, Seabee, and Tuluvak formations exposed at Umiat Mountain, north-central Alaska: U.S. Geological Survey Professional Paper 1709-B, 18 p.

Houseknecht, D.W., Bird, K.J., and Schenk, C.J., 2009, Seismic analysis of clinoform depositional sequences and shelf-margin trajectories in Lower Cretaceous (Albian) strata, Alaska North Slope: Basin Research, v. 21, p. 644-654.

Houseknecht, D.W., Bird, K.J., and O'Sullivan, P., 2011, Constraining the age and magnitude of uplift in the northern National Petroleum Reserve in Alaska (NPRA): Apatite fission-track analysis of samples from three wells: U.S. Geological Survey Professional Paper 1784-A, 22 p.

Hubbert, M.K., 1940, The theory of ground-water motion: Journal of Geology, v. 48, no. 8, p. 785-944.

Hubbert, M.K., 1953, Entrapment of petroleum under hydrodynamic conditions: The Bulletin of American Association of Petroleum Geologists, v. 37, no. 8, p. 1954-2026.

Jones, P.B., 1982, Oil and gas beneath east-dipping under thrust faults in the Alberta Foothills, *in* Powers, R.B., ed., Studies of Cordilleran thrust belt: Rocky Mountain Association of Geologists, p. 61-74.

Kohshour, I.O., Ahmadi., M., and Hanks, C., 2013, Uncertainty assessment in geologic modeling and sensitivity analysis of static and dynamic models in Umiat: A frozen shallow oil accumulation in National Petroleum Reserve Alaska: Society of Petroleum Engineers Conference Paper, SPE Western Regional and AAPG Pacific Section Meeting, April 19-25, Monterey, CA, doi: 10.2118/165341-MS.

LePain, D.L., McCarthy, P.J., and Kirkham, R., 2009, Sedimentology, stacking patterns and depositional systems in the middle Albian-Cenomanian Nanushuk Formation in outcrop, central North Slope, Alaska: Division of Geological and Geophysical Surveys, 78 p.

Levi-Johnson, O., 2010, Petrophysical property modeling of Umiat field, a frozen reservoir [M.S. thesis]: Fairbanks, University of Alaska Fairbanks, 129 pp.

Lorenz, J.C., Teufel, L.W., and Warpinski, N.R., 1991, Regional fractures: A mechanism for the formation of regional fractures at depth in flat-lying reservoirs: American Association of Petroleum Geologists Bulletin, v. 75, p. 1714-1737.

Magoon, L.B., Lillis, P.G., Bird, K.E., Lampe, C., and Peters, K.E., 2003, Alaskan North Slope petroleum systems: USGS Open-File Report 03-324, 3 sheets.

Magoon, L.B., and Bird, K.E., 1985, Alaskan North Slope petroleum geochemistry for the Shublik Formation, Kingak Shale, Pebble Shale unit, and Torok Formation, *in* Magoon, L.B., and Claypool, G.E., eds., Alaska North Slope oil-rock correlation study: AAPG Studies in Geology, v. 20, p. 31-48.

McMechan, M.E., 1985, Low-taper triangle zone geometry: An interpretation for the Rocky Mountain foothills, Pine Pass-Peace River area, British Columbia: Bulletin of Canadian Petroleum Geology, v. 33, p. 31-38.

Molenaar, C.M., 1982, Umiat field, an oil accumulation in a thrust-faulted anticline, North Slope of Alaska, *in* Powers, R.B., ed., Geologic studies of the Cordilleran thrust belt: Rocky Mountain Association of Geologists, p. 537-548.

Molenaar, C.M., Egbert, R.M., and Krystinik, L.F., 1988, Depositional facies, petrography, and reservoir potential of the Fortress Mountain Formation (Lower Cretaceous), central North Slope, Alaska, *in* G. Frye, ed., Geology and exploration of the National Petroleum Reserve in Alaska, 1974–1982: U.S. Geological Survey Professional Paper 1399, p. 257-279.

Moore, T.E., Potter, C.J., O'Sullivan, P.B., Shelton, K.L., and Underwood, M.B., 2004, Two stages of deformation and fluid migration in the west-central Brooks Range fold and thrust belt, northern Alaska, *in* Swennen, F.R., and Granath, J.W., eds., Deformation, fluid flow, and reservoir appraisal in foreland basin fold and thrust belts: American Association of Petroleum Geologists Dedberg Series no. 1, p. 157-186.

Moore, T.E., Wallace, W.K., Bird, K.J., Karl, S.M., Mull, C.G., and Dillon, J.T., 1994, Geology of northern Alaska, *in* Plafker, G. and Berg, H.C., eds., The geology of North America, v. G-1, The geology of Alaska: Boulder, Colorado, Geological Society of America, p. 49-140.

Mull, C.G., 1982, Tectonic evolution and structural style of the Brooks Range and Arctic Slope, Alaska, *in* Powers, R.B., eds., Geology studies of the Cordilleran thrust belt: Rocky Mountain Association of Geologists, pp. 1-45.

Mull, C.G., Houseknecht, D.W., and Bird, K.J., 2003, Revised Cretaceous and Tertiary stratigraphic nomenclature in the Colville Basin, Northern Alaska: U.S. Geological Survey Professional Paper 1673, 51 p.

Mull, C. G., Houseknecht, D.W., Pessel, G.H., and Garrity, C.P., 2004, Geologic map of the Umiat quadrangle, Alaska: U.S. Geological Survey Scientific Investigations Map 2817-A, scale 1:250,000.

Narr, W., Schechter, D.W., and Thompson, L.B., 2006, Naturally fractured reservoir characterization: Society of Petroleum Engineers, 112 pp.

Narr, W., and Suppe, J., 1991, Joint spacing in sedimentary rocks: Journal of Structural Geology, v. 13, p. 1037-1048.

Nelson, R.A., 2009, Geologic analysis of naturally fractured reservoirs, 2nd ed.: Houston, Gulf Publishing, 332 pp.

O'Sullivan, P.B., 1996, Late Mesozoic and Cenozoic thermotectonic evolution of the Colville Basin, North Slope, Alaska, *in* Johnsson, M.J., and Howell, D.G., eds., Thermal evolution of sedimentary basins in Alaska: U.S. Geological Survey Bulletin 2142, p. 45-79.

O'Sullivan, P.B., Murphy, J.M., and Blythe, A.E., 1997, Late Mesozoic and Cenozoic thermotectonic evolution of the central Brooks Range and adjacent North Slope foreland basin, Alaska: Including fission-track results from the Trans-Alaska Crustal Transect (TACT): Journal of Geophysical Research, v. 102, p. 20, 821-845.

O'Sullivan, P.B., Moore, T.M., and Murphy, J.M., 1998, Tertiary uplift of the Mt. Doonerak antiform, central Brooks Range, Alaska: Apatite fission-track evidence from the Trans-Alaska Crustal Transect, *in* Oldow, J.S., Ave Lallemant, H.G., eds., Architecture of the central Brooks Range fold and thrust belt, arctic Alaska: Geological Society of America Special Paper 324, p. 179-193.

Potter, C.J., and Moore, T.E., 2003, Brookian structural plays in the National Petroleum Reserve, Alaska: U.S. Geological Survey Open-File Report 03-266, 49 p.

Price, N.J., 1966, Fault and joint development in brittle and semi-brittle rock: London, Pergamon Press, 176 p.

Price, N.J., and Cosgrove, J.W., 1990, Analysis of geological structures, Cambridge University Press, 502 p.

Priest, S.D., 1993, Discontinuity analysis for rock engineering, Chapman and Hall Press, 475 p.

Ramsay, J.G., and Huber, M.I., 1987, The techniques of modern structural geology, volume 2: Fold and fractures, p. 309-700. London, Academic Press.

Sanders, C., and Wallace, W.K., 2011, Structural geology of the Big Bend anticline, Brooks Range foothills, Alaska, *in* Hanks, C.L., ed., Producing light oil from a frozen reservoir: Reservoir and fluid characterization of Umiat field, National Petroleum Reserve, Alaska: Department of Energy, Annual report for DOE award DE-FC26-08NT0005641, Chapter 6, 33 p.

Shackleton, J.R., 2003, The relationship between fracturing, asymmetric folding, and normal faulting in Lisburne Group carbonates: Porcupine Lake valley, northeastern Brooks Range, Alaska [M.S. thesis]: Fairbanks, University of Alaska Fairbanks, 189 p.

Shackleton, J.R., Cooke, M.L., and Sussman, A.J., 2005, Evidence for temporally changing mechanical stratigraphy and effects on joint-network architecture: Geology, v. 33, p. 101-104.

Shimer, G.T., McCarthy, P.J., and Hanks, C.L., 2014, Sedimentology, stratigraphy, and reservoir properties of an unconventional reservoir in the Cretaceous Nanushuk Formation at Umiat Field, North Slope, Alaska: American Association of Petroleum Geologists Bulletin, v. 95, p. 1009-1037

Stearns, D.W., 1968, Certain aspects of fractures in naturally deformed rocks, *in* Reiker, R.E., National Science Foundation Advanced Science Seminar in Rock Mechanics: Special Report, Air Force Cambridge Research Laboratories, Bedford, MA, v. AD66993751, p. 97-118.

Stearns, D.W., and Friedman, M., 1972, Reservoirs in fractured rock: *in* Stratigraphic oil and gas fields: Classification, exploration methods, and case histories: American Association of Petroleum Geologists, Memoir 16, p. 82-106.

Szilard, R., 1974, Theory and analysis of plates: Classical and numerical methods: Prentice Hall.

Tanner, P.W., 1989, The flexural-slip mechanism: Journal of Structural Geology, v. 11, p. 635-655.

Wallace, W.K., 1997, Detachment folds and a passive-roof duplex: Examples from the northeastern Brooks Range, Alaska, *in* Solie, D.N., and Tannian, eds., Short notes on Alaskan geology 1993: Alaska Division of Geological and Geophysical Surveys Geologic Report 113, p. 81-99.

Wallace, W.K., 2009, Mechanical stratigraphy and the structural geometry and evolution of the central and eastern foothills of the Brooks Range, northern Alaska, *in* Hanks, C.L., ed., Unraveling the timing of fluid migration and trap formation in the Brooks Range foothills: A key to discovering hydrocarbons: National Energy Technology Laboratory, Department of Energy, Final report for DOE award DE-FC26-06NT41248, Chapter 2, 34 p.

Wallace, W.K., Duncan, A.S., Finzel, E.S., and Sanders, C., 2011, Geometry and evolution of folds in the central Brooks Range foothills, *in* Hanks, C.L., ed., Producing light oil from a frozen reservoir: Reservoir and fluid characterization of Umiat field, National Petroleum Reserve, Alaska: Department of Energy, Annual report for DOE award DE-FC26-08NT0005641, Chapter 5, 40 p.

Appendix A

FRACTURE TRANSECTS DATA TABLES FROM EACH FIELD LOCATION

All measurements were taken in centimeters.

Key for the data tables:

Distance from origin: Distance of fracture from zero on the measuring tape.

Spacing between fractures: Distance between adjacent fractures measured parallel to bedding.

Aperture: The width of the fracture opening measured normal to the fracture.

Fill: C for calcite fill, O for open, PC for partially filled with calcite.

Height: Vertical extent of the fracture normal to bedding.

Width: The length of the fracture parallel to bedding.

Mode: E = extensional, S = shear

Ind.: Indeterminate, missing, not exposed.

Table A1: Transect 1
Location: Big Bend south anticline

Fracture	Distance from Origin (cm)	Spacing Between Fractures (cm)	Strike	Dip	Dip Direction	Aperture (cm)	Fill: Calc or Qtz	Height (cm)	Width (cm)	Mode: Ext. or Shear
1	0		213	54	W	unknown	O	7.8	21.0	S
2	3	3	306	76	N	unknown	O	6.8	7.5	S
3	5	2	302	78	N	unknown	O	6.0	8.0	S
4	24	19	218	71	W	unknown	O	8.9	31.0	S
5	52	28	41	71	E	unknown	O	8.0	14.5	S
6	59	7	306	77	N	unknown	O	6.9	10.0	S
7	66	7	30	88	E	unknown	O	5.5	11.0	S
8	71	5	303	76	N	unknown	O	4.5	12.0	S
9	87	16	37	82	E	unknown	O	5.5	3.2	S
10	95	8	310	85	N	unknown	O	7.5	11.5	S
11	103	8	210	65	W	0.5	O	5.5	4.0	S
12	161	58	35	89	E	unknown	O	5.0	16.0	S
13	213	52	298	75	N	unknown	O	5.0	14.0	S
14	218	5	42	83	E	unknown	O	7.0	27.0	S
15	241	23	296	70	N	0.7	O	8.0	9.0	S
16	245	4	223	60	W	0.6	O	8.5	25.0	S
17	252	7	305	77	N	unknown	O	5.0	29.0	S
18	261	9	290	63	N	unknown	O	6.5	41.0	S
19	266	5	217	62	W	unknown	O	10.0	5.0	S
20	270	4	32	76	E	2.5	O	12.0	42.0	S
21	281	11	293	62	N	unknown	PC	7.0	27.0	E
22	311	30	205	70	W	unknown	O	10.0	52.0	S
23	316	5	295	83	N	unknown	O	4.5	4.0	S
24	318	2	205	70	W	unknown	O	10.0	12.0	S
25	319	1	305	67	N	0.5	O	10.0	6.5	S
26	323	4	300	77	N	unknown	O	10.0	66.0	S
27	356	33	210	65	W	unknown	O	10.0	25.0	S
28	385	29	42	90	vertical	unknown	O	9.0	33.0	S
29	429	44	206	75	W	unknown	O	9.0	36.0	S
30	468	39	20	90	vertical	1.5	O	10.0	6.0	S
31	479	11	42	79	E	0.3	O	11.0	32.0	S
32	504	25	39	90	vertical	2.0	O	10.0	4.0	S
33	524	20	41	86	E	unknown	O	10.0	27.0	S
34	529	5	295	72	N	1.0	O	9.0	1.0	S
35	535	6	295	81	N	unknown	O	8.0	1.0	S
36	537	2	296	80	N	1.0	O	9.0	20.0	S
37	549	12	38	61	E	unknown	O	10.0	37.0	S
38	557	8	121	90	vertical	unknown	O	11.0	5.0	S
39	572	15	36	67	E	unknown	O	11.0	44.0	S
40	593	21	38	82	E	unknown	O	11.0	41.0	S
41	628	35	226	63	W	unknown	O	11.0	24.0	S
42	647	19	115	90	vertical	unknown	O	10.0	43.0	S
43	1047	400	300	87	N	unknown	O	11.0	19.0	S
44	1054	7	107	82	S	unknown	O	12.0	8.0	S
45	1105	51	119	86	S	unknown	O	9.0	19.0	S
46	1136	31	266	66	NE	unknown	O	9.0	19.0	E
47	1178	42	92	66	S	0.3	O	12.0	1.0	E
48	1191	13	312	74	N	0.3	O	4.0	1.0	S
49	1229	38	295	62	N	unknown	O	11.0	37.0	S
50	1249	20	288	87	N	1.0	O	13.0	3.0	S
51	1314	65	127	90	vertical	5.0	O	16.0	26.0	S
52	1324	10	286	67	N	unknown	O	13.0	33.0	S
53	1344	20	120	83	S	0.6	O	9.0	3.0	S
54	1371	27	128	90	vertical	3.0	O	14.0	10.0	S
55	1392	21	296	85	N	unknown	O	12.0	19.0	S
56	1410	18	269	73	N	2.0	O	12.0	13.0	E
57	1420	10	319	68	N	unknown	O	10.0	20.0	S

Table A2: Transect 2
Location: Big Bend south anticline

Fracture	Distance from Origin (cm)	Spacing Between Fractures	Strike	Dip	Dip Direction	Aperture (cm)	Fill: Calc or Qtz	Height (cm)	Width (cm)	Mode: Ext. or Shear
1	0		215	76	W	2.1	O	100.0	3.0	S
2	12	12	299	76	N	unknown	O	300.0	12.0	S
3	20	8	297	83	N	unknown	O	12.0	17.0	S
4	24	4	221	67	W	unknown	O	300.0	100.0	S
5	29	5	39	90	vertical	unknown	O	300.0	97.0	S
6	35	6	135	90	vertical	2.2	O	10.0	3.0	S
7	49	14	129	90	vertical	1.8	O	1.0	4.0	S
8	60	11	42	90	vertical	unknown	O	10.5	38.0	S
9	97	37	214	79	W	0.3	O	4.0	1.0	S
10	100	3	117	82	S	unknown	O	13.5	37.5	S
11	110	10	213	79	W	unknown	O	31.0	1.5	S
12	132	22	216	49	W	unknown	O	200.0	71.0	S
13	140	8	131	80	S	unknown	O	12.0	25.0	S
14	143	3	115	90	vertical	unknown	O	29.0	4.5	S
15	175	32	218	66	W	unknown	O	200.0	100.0	S
16	187	12	231	78	W	1.0	O	100.0	16.0	S
17	193	6	109	65	S	unknown	O	100.0	44.0	S
18	195	2	219	71	W	unknown	O	10.0	19.0	S
19	204	9	220	86	W	unknown	O	14.5	19.0	S
20	221	17	222	79	W	0.1	O	14.0	0.5	S
21	221.5	0.5	121	81	S	unknown	O	100.0	40.0	S
22	254	33.5	60	90	vertical	1.0	O	300.0	17.0	S
23	272	18	234	79	W	unknown	O	12.5	6.0	S
24	292	20	239	70	W	0.3	O	6.0	4.0	S
25	355	63	221	86	W	unknown	O	28.0	17.0	S
26	355.5	0.5	119	86	S	unknown	O	12.0	25.0	S
27	374	19.5	213	82	W	unknown	O	300.0	122.0	S
28	378	4	126	89	S	unknown	O	10.0	12.0	S
29	396	18	316	74	N	unknown	PC	32.0	182.0	E
30	426	30	134	90	vertical	unknown	O	100.0	43.0	S
31	490	64	58	47	E	1.0	O	14.0	5.0	S
32	501	11	140	86	S	0.1	O	8.5	10.0	S
33	531	30	137	90	vertical	unknown	O	300.0	200.0	S
34	579	48	38	85	S	unknown	O	30.0	38.0	S
35	593	14	50	90	vertical	unknown	O	9.0	18.0	S
36	601	8	122	90	vertical	unknown	O	300.0	13.0	S
37	607	6	223	55	W	unknown	O	300.0	124.0	S
38	612	5	141	90	vertical	unknown	O	300.0	197.0	S
39	631	19	53	90	vertical	0.2	O	9.0	1.0	S
40	648	17	143	76	S	unknown	O	7.0	6.0	S
41	651	3	123	90	vertical	unknown	O	9.0	6.0	S
42	655	4	121	90	vertical	unknown	O	300.0	63.0	S
43	698	43	224	42	W	unknown	O	300.0	120.0	S
44	700	2	131	87	S	3.0	O	11.0	2.0	S
45	708	8	134	85	S	1.5	O	12.0	3.0	S
46	724	16	224	77	W	unknown	O	200.0	123.0	S
47	780	56	139	80	S	0.5	O	100.0	0.5	S
48	788	8	126	81	S	unknown	O	300.0	47.0	S
49	794	6	120	90	vertical	0.5	O	16.0	2.0	S
50	886	92	149	75	S	unknown	O	300.0	110.0	S
51	1054	168	224	82	W	unknown	O	200.0	44.0	S
52	1287	233	35	90	vertical	unknown	O	200.0	32.0	S
53	1301	14	212	68	W	unknown	O	21.0	37.0	S
54	1498	197	303	87	N	unknown	O	28.0	99.0	S
55	1591	93	124	90	vertical	unknown	O	21.0	18.0	S
56	1625	34	126	90	vertical	unknown	O	16.0	37.0	S

Table A3: Transect 3
Location: Big Bend south anticline

Fracture	Distance from Origin (cm)	Spacing Between Fractures	Strike	Dip	Dip Direction	Aperture (cm)	Fill: Calc or Qtz	Height (cm)	Width (cm)	Mode: Ext. or Shear
1	58		73	78	S	unknown	O	55.0	0.4	S
2	103	45	313	62	N	unknown	O	20.0	3.0	S
3	155	52	204	41	N	0.3	O	153.0	3.0	S
4	215	60	31	65	E	unknown	O	39.0	6.0	S
5	220	5	276	40	N	0.2	O	28.0	0.2	S
6	240	20	36	79	E	unknown	O	40.0	1.8	S
7	324	84	9	15	E	unknown	O	100.0	5.4	S
8	380	56	35	66	E	0.3	O	143.0	3.0	S
9	410	30	274	85	N	0.3	O	22.0	1.0	S
10	421	11	275	76	N	0.1	O	24.0	2.0	S
11	430	9	124	90	vertical	0.2	O	33.0	1.0	S
12	436	6	123	75	S	unknown	O	40.0	7.0	S
13	480	44	139	63	S	unknown	O	100.0	20.0	S
14	507	27	283	85	N	0.6	O	27.0	3.0	S
15	535	28	39	55	E	0.6	O	100.0	0.3	S
16	895	360	203	73	W	unknown	O	55.0	17.0	S
17	924	29	214	84	W	0.2	O	100.0	6.0	S
18	1060	136	266	43	N	1.0	O	200.0	5.0	S
19	1075	15	53	90	vertical	0.3	O	38.0	2.0	S
20	1165	90	294	65	N	0.4	O	140.0	3.0	S
21	1281	116	132	61	S	unknown	O	25.0	5.0	S
22	1500	219	36	51	E	unknown	O	100.0	13.0	S
23	1506	6	284	66	N	unknown	O	20.0	11.0	S
24	1529	23	293	52	N	0.2	O	49.0	4.0	S
25	1569	40	247	84	NW	0.1	O	153.0	0.5	S
26	1611	42	239	70	NW	0.1	O	75.0	0.5	S
27	1626	15	251	76	NW	0.1	O	13.0	0.2	S
28	1640	14	259	83	NW	0.2	O	5.0	0.5	S
29	1641	1	296	59	N	0.4	O	50.0	1.0	S
30	1670	29	275	85	N	1.0	O	38.0	6.0	S
31	1715	45	68	79	SE	0.5	O	30.0	5.0	S
32	1800	85	11	45	E	0.9	O	100.0	4.5	S
33	1860	60	296	72	N	unknown	O	45.0	7.0	S
34	1882	22	252	76	NW	unknown	O	16.0	4.0	S

Table A4: Transect 4
Location: Big Bend north anticline

Fracture	Distance from Origin (cm)	Spacing Between Fractures	Strike	Dip	Dip Direction	Aperture (cm)	Fill: Calc or Qtz	Height (cm)	Width (cm)	Mode: Ext. or Shear
1	0.0		49	56	E	unknown	O	100.0	15.0	S
2	151.0	151	64	58	E	unknown	O	110.0	9.0	S
3	300.0	149	130	69	SW	unknown	O	41.0	200.0	S
4	327.0	27	41	52	E	0.5	O	6.0	4.0	S
5	406.0	79	62	90	vertical	0.2	O	10.0	0.3	S
6	960.0	554	43	69	E	unknown	O	15.0	120.0	S
7	1100.0	140	61	56	E	unknown	O	82.0	16.0	S
8	1277.0	177	54	70	E	unknown	O	200.0	35.5	S
9	1295.0	18	57	60	E	unknown	O	13.0	24.0	S
10	1308.0	13	38	64	E	0.1	O	10.0	0.3	S
11	1334.0	26	45	84	E	0.3	O	9.0	0.1	S
12	1417.0	83	29	81	E	1.0	O	21.0	12.0	S
13	1460.0	43	55	90	vertical	unknown	O	14.0	45.0	S
14	1589.0	129	64	68	E	unknown	O	100.0	25.0	S
15	1593.0	4	56	71	E	unknown	O	12.0	22.0	S
16	1680.0	87	47	84	E	unknown	O	93.0	74.0	S
17	1772.0	92	62	79	E	0.5	O	7.5	2.0	S
18	1797.0	25	220	70	W	0.5	O	9.0	3.0	S
19	1841.5	44.5	44	90	vertical	0.3	O	4.0	2.0	S
20	1851.0	9.5	28	74	E	0.5	O	10.0	8.0	S
21	1915.0	64	37	75	E	unknown	O	36.0	49.0	S
22	2127.0	212	39	50	E	unknown	O	21.0	20.0	S
23	2146.0	19	55	56	E	unknown	O	200.0	74.0	S
24	2182.0	36	57	61	E	unknown	O	42.0	200.0	S
25	2200.0	18	44	62	E	unknown	O	10.0	0.4	S

Table A5: Transect 5
Location: Big Bend north anticline

Fracture	Distance from Origin (cm)	Spacing Between Fractures	Strike	Dip	Dip Direction	Aperture (cm)	Fill: Calc or Qtz	Height (cm)	Width (cm)	Mode: Ext. or Shear
1	0		64	77	E	unknown	O	31.0	67	S
2	41	41	58	64	E	unknown	O	12.0	113	S
3	77	36	75	51	E	unknown	O	9.0	43	S
4	200	123	65	77	E	unknown	O	8.0	10	S
5	504	304	123	90	vertical	unknown	O	22.0	0.5	S
6	527	23	79	90	vertical	0.1	O	24.0	0.2	S
7	551	24	61	90	vertical	0.4	O	66.0	0.5	S
8	675	124	79	90	vertical	0.2	O	52.0	0.1	S
9	722	47	126	81	S	unknown	O	87.0	6.0	S
10	744	22	103	90	vertical	0.5	O	83.0	0.5	S
11	790	46	47	74	E	unknown	O	13.0	83.0	S
12	825	35	64	47	E	unknown	O	39.0	13.0	S
13	854	29	48	64	E	unknown	O	100.0	6.0	S
14	884	30	41	69	E	0.5	O	100.0	6.0	S
15	973	89	228	73	N	unknown	O	4.5	15.0	S
16	983	10	139	80	S	unknown	O	5.4	9.0	S
17	991	8	141	83	E	unknown	O	11.3	5.0	S
18	1000.5	9.5	135	82	S	unknown	O	26.0	100.0	S

Table A6: Transect 6
Location: Big Bend north anticline

Fracture	Distance from Origin (cm)	Spacing Between Fractures	Strike	Dip	Dip Direction	Aperture (cm)	Fill: Calc or Qtz	Height (cm)	Width (cm)	Mode: Ext. or Shear
1	0		254	58	N	unknown	O	7.0	19.0	S
2	9	9	111	72	S	0.2	O	15.0	14.0	S
3	14	5	61	49	E	unknown	O	46.0	3.0	S
4	26	12	83	90	vertical	0.1	O	16.0	0.2	S
5	52	26	272	38	N	0.2	O	33.0	6.0	S
6	76	24	296	15	N	0.1	O	22.0	0.1	S
7	84	8	76	84	S	unknown	O	38.0	9.0	S
8	85	1	290	32	N	0.2	O	29.0	1.0	S
9	100	15	329	68	N	unknown	O	26.0	4.5	S
10	150	50	346	60	NE	unknown	O	27.0	200.0	S
11	154.5	4.5	84	69	S	unknown	O	100.0	9.0	S
12	159.5	5	82	59	S	unknown	O	100.0	4.5	S
13	197	37.5	94	80	S	0.3	O	91.0	7.0	S
14	251	54	104	90	vertical	0.1	O	34.0	0.2	S
15	289.5	38.5	27	67	E	unknown	O	500.0	14.0	S
16	321	31.5	115	90	vertical	0.1	O	17.0	0.2	S
17	335	14	86	90	vertical	0.2	O	9.0	1.0	S
18	360	25	116	82	S	0.2	O	53.0	1.0	S
19	361.5	1.5	62	62	S	0.2	O	100.0	1.0	S
20	366	4.5	161	55	S	unknown	O	100.0	19.0	S
21	385.5	19.5	93	67	S	unknown	O	100.0	3.5	S
22	421.5	36	119	81	S	11.0	O	33.0	6.5	S
23	436.5	15	92	65	S	0.2	O	34.0	4.5	S
24	487.5	51	96	90	vertical	unknown	O	41.0	5.0	S
25	550.5	63	99	90	vertical	0.3	O	100.0	20.0	S
26	607.3	56.8	76	67	S	unknown	O	7.5	5.0	S
27	668.2	60.9	110	73	S	unknown	O	300.0	34.0	S
28	742.5	74.3	94	90	vertical	2.0	O	100.0	76.0	S
29	878.2	135.7	129	50	S	unknown	O	100.0	72.0	S
30	993.2	115	79	70	S	unknown	O	2.0	23.0	S
31	1199.2	206	93	64	S	unknown	O	64.0	33.0	S

Table A7: Transect 7
Location: Colville incision

Fracture	Distance from Origin (cm)	Spacing Between Fractures	Strike	Dip	Dip Direction	Aperture (cm)	Fill: Calc or Qtz	Height (cm)	Width (cm)	Mode: Ext. or Shear
1	0		121	90	vertical	0.2	PC	100.0	7.0	E
2	133	133	184	75	W	0.4	P C	100.0	25.0	E
3	194	61	350	90	vertical	unknown	O	53.0	2.5	E
4	225	31	192	66	NE	0.5	O	100.0	10.0	E
5	246	21	11	79	E	1	O	100.0	20.2	E
6	436	190	4	90	vertical	unknown	O	100.0	22.0	E
7	437.6	1.6	20	84	E	0.1	C	47.0	6	E
8	443	5.4	16	90	vertical	0.1	C	27.0	2.1	E
9	499	56	24	90	vertical	0.3	PC	100.0	6.0	E
10	506	7	175	87	NE	0.3	O	100.0	2.0	E
11	527	21	357	90	vertical	unknown	O	100.0	4.0	E
12	555	28	9	90	vertical	0.3	O	30.0	4.0	E
13	569	14	322	72	SW	0.1	O	34.0	4.0	E
14	1010	441	359	86	W	unknown	O	100.0	31.2	E
15	1115	105	190	79	NE	unknown	O	90.0	52.0	E
16	1122	7	192	85	W	0.3	PC	28.0	22.0	E
17	1190	68	2	79	SW	0.2	O	27.0	8.0	E
18	1190.5	0.5	192	76	W	0.3	PC	70.0	5.1	E
19	1197	7.5	166	71	W	0.3	PC	109.0	8.5	E
20	1230	33	185	78	W	0.2	PC	105.0	2.5	E
21	1460	230	178	89	W	4.0	O	90.0	130.0	E
22	2309	849	172	73	W	unknown	O	85.0	6.0	E
23	2412	103	163	83	W	unknown	O	50.0	2.5	E
24	2440	28	2	90	vertical	0.3	O	18.0	4.0	E
25	2448	8	198	83	NW	0.2	O	30.0	2.0	E
26	2472	24	168	76	W	0.2	O	20.0	1.5	E
27	2487	15	192	84	W	0.1	O	6.5	0.2	E
28	2496	9	350	80	E	unknown	O	5.0	0.2	E
29	2521	25	349	79	E	0.1	O	18.0	2.5	E
30	2955	434	189	82	W	unknown	O	87.0	26.0	E
31	2957	2	1	89	E	unknown	O	8.0	0.3	E
32	2970	13	4	90	vertical	0.1	C	18.0	2.0	E
33	2971	1	4	68	E	0.1	O	25.0	9.0	E
34	2974	3	204	84	W	0.3	O	20.0	2.0	E
35	2985	11	359	89	E	0.05	C	28.0	2.0	E
36	3016	31	6	82	E	0.2	O	40.0	4.0	E
37	3065	49	7	82	E	0.1	C	45.0	9.0	E
38	3082	17	167	83	W	unknown	O	52.0	7.5	E
39	3109	27	2	90	vertical	0.1	C	36.0	12.0	E
40	3147	38	2	87	E	0.2	O	54.0	0.3	E
41	3156	9	354	81	E	0.5	PC	47.0	6.0	E
42	3211	55	7	90	vertical	1	PC	51.0	4.0	E
43	3231	20	4	86	E	0.2	O	48.0	0.2`	E
44	3249	18	197	76	W	0.2	O	50.0	0.2	E
45	3275	26	191	83	W	0.6	O	35.0	6.0	E
46	3317	42	175	86	W	unknown	O	37.0	3.0	E
47	3318	1	189	89	W	0.5	C	15.0	2.0	E
48	3390	72	356	89	E	0.2	O	17.0	5.0	E
49	3465	75	356	89	E	0.1	O	15.0	2.0	E
50	3596	131	17	87	E	unknown	O	40.0	23.0	E
51	3691	95	7	86	E	0.3	O	22.0	300.0	E
52	3855	164	206	86	W	unknown	O	26.0	9.0	E
53	3862	7	327	89	E	unknown	O	25.0	4.0	E
54	3864	2	31	90	vertical	unknown	O	26.0	4.0	E
55	3387	23	25	90	vertical	unknown	O	21.0	3.0	E
56	3906	19	191	88	W	unknown	O	40.0	29.0	E
57	3933	27	184	81	W	0.6	O	60.0	4.0	E
58	3976	43	344	78	E	unknown	O	60.0	8.0	E

Table A7 continued: Transect 7
Location: Colville incision

Fracture	Distance from Origin (cm)	Spacing Between Fractures	Strike	Dip	Dip Direction	Aperture (cm)	Fill: Calc or Qtz	Height (cm)	Width (cm)	Mode: Ext. or Shear
59	3999	23	11	88	E	1.0	O	70.0	9.0	E
60	4030	31	7	86	E	unknown	O	60.0	15.0	E
61	4037	7	206	65	W	0.2	O	24.0	1.0	E
62	4052	15	354	74	E	0.1	O	15.0	2.0	E
63	4057	5	14	71	E	unknown	O	20.0	2.0	E
64	4363	306	201	72	W	unknown	O	27.0	0.5	E
65	4370	7	162	75	W	unknown	O	100.0	7.0	E
66	4388	18	38	86	E	0.5	O	60.0	9.0	E
67	4464	76	21	86	E	unknown	O	76.0	10.0	E
68	4474	10	169	77	W	unknown	O	100.0	15.0	E
69	4487	13	19	77	E	0.2	O	100.0	7.0	E
70	4516	29	29	67	E	0.2	O	100.0	7.0	E
71	4560	44	195	78	W	0.2	O	100.0	11.0	E
72	4590	30	205	86	W	unknown	O	51.0	18.0	E
73	4658	68	168	81	W	0.4	O	100.0	4.0	E
74	4677	19	198	87	W	unknown	O	23.0	3.0	E
75	4747	70	24	82	E	unknown	O	30.0	6.0	E
76	4816	69	4	86	E	0.3	O	37.0	3.0	E
77	4852	19	185	84	W	0.3	O	18.0	1.0	E
78	4902	50	6	90	vertical	0.2	O	18.0	4.0	E
79	4916	14	22	81	E	unknown	O	37.0	15.0	E
80	4930	14	192	81	W	0.1	O	41.0	8.0	E
81	5139	209	170	82	NE	0.1	O	81.0	23.0	E
82	5152	13	194	79	W	unknown	O	23.0	12.0	E
83	5173	21	21	67	E	unknown	O	27.0	15.0	E
84	5184	11	190	90	vertical	0.3	O	100.0	9.0	E
85	5190	6	165	81	W	unknown	O	23.0	2.0	E
86	5196	6	171	81	W	unknown	O	16.0	7.0	E
87	5202	6	191	73	W	0.1	O	100.0	5.0	E
88	5215	13	313	75	E	0.1	O	6.0	2.0	E
89	5270	55	189	70	W	0.1	O	6.0	3.0	E
90	5295	25	184	78	W	0.2	O	100.0	9.0	E
91	5449	154	175	76	W	0.2	O	100.0	2.0	E
92	5533	84	4	89	E	0.2	C	29.0	2.0	E
93	5584	51	176	75	W	unknown	PC	200.0	50.0	E
94	5725	141	11	70	E	unknown	O	200.0	17.0	E
95	5738	13	356	82	E	0.2	O	74.0	12.0	E
96	5755	17	174	64	W	0.1	O	51.0	3.0	E
97	5937	182	358	86	E	0.2	O	50.0	2.0	E
98	6017	80	199	74	W	0.2	O	200.0	70.0	E
99	6071	54	205	73	W	0.1	O	200.0	64.0	E
100	6155	84	3	69	E	0.3	PC	200.0	31.0	E
101	6178	23	358	86	E	unknown	PC	123.0	23.0	E
102	6245	67	2	74	E	unknown	O	100.0	45.0	E
103	6265	20	22	70	E	unknown	PC	100.0	31.0	E
104	6290	25	19	79	E	0.3	PC	97.0	21.0	E
105	6308	18	5	90	vertical	0.1	O	86.0	21.0	E
106	6322	14	342	89	E	0.1	O	38.0	4.0	E
107	6336	14	24	81	E	0.1	C	100.0	10.0	E
108	6375	39	8	90	vertical	0.2	PC	68.0	0.3	E
109	6386	11	351	87	E	0.1	PC	100.0	39.0	E
110	6425	39	28	82	E	0.2	PC	100.0	7.0	E
111	6455	30	24	74	E	0.1	O	23.0	14.0	E
112	ind.	ind.	274	90	vertical	ind.	O	ind.	ind.	E
113	ind.	ind.	94	79	S	ind.	O	ind.	ind.	E
114	ind.	ind.	279	90	vertical	ind.	O	ind.	ind.	E
115	ind.	ind.	92	85	N	ind.	O	ind.	ind.	E
116	ind.	ind.	95	71	N	ind.	O	ind.	ind.	E

Table A7 continued: Transect 7
Location: Colville incision

Fracture	Distance from Origin (cm)	Spacing Between Fractures	Strike	Dip	Dip Direction	Aperture (cm)	Fill: Calc or Qtz	Height (cm)	Width (cm)	Mode: Ext. or Shear
117	ind.	ind.	92	83	N	ind.	O	ind.	ind.	E
118	ind.	ind.	91	82	N	ind.	O	ind.	ind.	E
119	ind.	ind.	94	89	S	ind.	O	ind.	ind.	E
120	ind.	ind.	96	89	S	ind.	O	ind.	ind.	E
121	ind.	ind.	97	82	N	ind.	O	ind.	ind.	E
122	ind.	ind.	92	83	S	ind.	O	ind.	ind.	E
123	ind.	ind.	92	90	vertical	ind.	O	ind.	ind.	E
124	ind.	ind.	97	81	N	ind.	O	ind.	ind.	E
125	ind.	ind.	274	90	vertical	ind.	O	ind.	ind.	E
126	ind.	ind.	99	86	S	ind.	O	ind.	ind.	E
127	ind.	ind.	97	87	S	ind.	O	ind.	ind.	E
128	ind.	ind.	94	88	S	ind.	O	ind.	ind.	E
129	ind.	ind.	97	88	S	ind.	O	ind.	ind.	E
130	ind.	ind.	94	82	S	ind.	O	ind.	ind.	E
131	ind.	ind.	95	86	S	ind.	O	ind.	ind.	E
132	ind.	ind.	96	84	S	ind.	O	ind.	ind.	E
133	ind.	ind.	93	73	N	ind.	O	ind.	ind.	E
134	ind.	ind.	92	86	N	ind.	O	ind.	ind.	E
135	ind.	ind.	95	79	S	ind.	O	ind.	ind.	E
136	ind.	ind.	98	81	S	ind.	O	ind.	ind.	E

Table A8: Transect 8
Location: Fossil Creek (south limb)

Fracture	Distance from Origin (cm)	Spacing Between Fractures	Strike	Dip	Dip Direction	Aperture (cm)	Fill: Calc or Qtz	Height (cm)	Width (cm)	Mode: Ext. or Shear
1	0		328	71	W	unknown	O	40.0	1.5	S
2	10.0	10	329	76	N	unknown	O	23.0	6.0	S
3	19	9	346	80	SW	unknown	O	44.0	44.0	E
4	21	2	272	61	N	unknown	O	40.0	20.0	E
5	26	5	351	77	NE	unknown	O	100.0	30.0	E
6	34	8	51	81	E	unknown	O	33.0	86.0	S
7	46	12	295	76	N	0.3	O	17.0	8.0	S
8	55	9	339	90	vertical	unknown	O	14.0	9.0	S
9	90	35	326	72	N	unknown	O	24.0	16.0	S
10	144	54	88	86	SE	unknown	O	43.0	72.0	E
11	166	22	293	90	vertical	unknown	O	45.0	36.0	S
12	176	10	351	82	NE	unknown	O	40.0	85.0	E
13	181	5	77	82	E	unknown	O	83.0	115.0	E
14	261	80	324	79	NE	unknown	O	43.0	39.0	S
15	285	24	248	65	NW	unknown	O	63.0	96.0	S
16	305	20	311	74	N	unknown	O	75.0	85.0	S
17	375	70	324	79	NE	unknown	O	100.0	86.0	S
18	376	1	239	90	vertical	unknown	O	100.0	66.0	S
19	411	35	139	85	S	unknown	O	13.0	9.0	S
20	417	6	298	89	N	0.2	O	36.0	6.0	S
21	424	7	46	70	E	unknown	O	100.0	140.0	S
22	433	9	142	86	SE	unknown	O	100.0	16.0	S
23	443	10	345	82	N	unknown	O	36.0	6.0	S
24	477	34	246	81	W	unknown	O	100.0	100.0	S
25	637	160	228	72	W	unknown	O	30.0	9.0	S
26	647	10	239	72	W	unknown	O	100.0	50.0	S
27	695	48	271	74	NW	unknown	O	100.0	16.0	E
28	709	14	89	81	SW	unknown	O	100.0	61.0	E
29	722	13	74	73	E	unknown	O	17.0	74.0	E
30	724	2	85	80	E	0.2	O	2.0	2.5	E

Table A9: GPS location, transect orientations, and bedding strike/dip for each transect location

Location	Transect	GPS Locations	Transect Orientation	Bedding Strike(s)	Bedding Dip(s)
		Lat/Lon			
Colville incision	8	69° 16' 21.0" N 152° 35’ 22.9" W	east-west	95	23° N
Fossil Creek	7	69° 13' 43.5" N 152° 27’ 55.3” W	north-south	110	14° SW
Big Bend north	6	69° 07' 04.8" N 151° 47' 18.8" W	northwest-southeast	168	44° S
	5	69° 07' 04.8" N 151° 47' 18.8" W	northwest-southeast	164	31° SW
	4	69° 07' 04.8" N 151° 47' 18.8" W	northeast-southwest	117	16° SW
	3	69° 07' 04.8" N 151° 47' 18.8" W	northwest-southeast	167	43° SW
Big Bend south	2	69° 04' 42.40" N 151° 56' 08.46" W	northwest-southeast	39	12° SE
	1	69° 04' 42.40" N 151° 56' 08.46" W	northwest-southeast	39	12° SE

Appendix B

RESULTS OF STATISTICAL TESTS PERFORMED ON FRACTURE SPACING

Results of statistical tests on fracture spacing in the outcrops at the Colville incision, Fossil Creek, and the Big Bend anticline are shown in Tables B1–B4. All tests are at the 95% confidence level (0.05). These tests were used to determine the similarity of median fracture spacing between fracture sets A, B, and C. The ANOVA test is a nonparametric test that was used to determine if fracture set A, B, and C are in fact different sets. The post hoc is also a non-parametric test used to determine what set is different compared to other sets.

Table B1: Descriptive statistics
Fracture sets A, B, and C

	N	Range	Minimum	Maximum	Mean	Std. Deviation	Variance	Skewness		Kurtosis	
	Statistic	Statistic	Statistic	Statistic	Statistic	Statistic	Statistic	Statistic	Std. Error	Statistic	Std. Error
Set A	30.00	2210.60	5.40	2216.00	254.80	504.83	254853.76	3.05	0.43	9.45	0.83
Set B	91.00	848.00	1.00	849.00	79.54	128.38	16480.81	3.55	0.25	15.76	0.50
Set C	222.00	553.50	0.50	554.00	43.64	66.74	4454.51	4.00	0.16	21.42	0.33
Valid N (listwise)	30.00										

Table B2: Kolmogorov-Smirnov Test
Fracture Sets A, B, and C

One-Sample Kolmogorov-Smirnov Test				
		Set A	**Set B**	**Set C**
N		30.00	91.00	222.00
Normal Parameters[a]	Mean	254.80	79.54	43.64
	Std. Deviation	504.83	128.38	66.74
Most Extreme Differences	Absolute	0.34	0.27	0.26
	Positive	0.34	0.27	0.23
	Negative	-0.31	-0.27	-0.26
Kolmogorov-Smirnov Z		1.86	2.58	3.86
Asymp. Sig. (2-tailed)		0.00	0.00	0.00
a. Test distribution is normal.				

Table B3: ANOVA Test and Test of Homogeneity of Variances
Fracture sets A, B, and C

ANOVA					
Fracture Sets A, B, C					
	Sum of Squares	df	Mean Square	F	Sig.
Between Groups	8.66	2	4.33	13.26	.00
Within Groups	110.72	339	.32		
Total	119.39	341			

Test of Homogeneity of Variances			
Fracture Sets A, B, C			
Levene Statistic	df1	df2	Sig.
1.91	2.00	339.00	0.15

Table B4: Post Hoc Test
Fracture sets A, B, and C

Multiple Comparisons							
Dependent Variable: Fracture Sets ABC LOG							
	(I) VAR00002	(J) VAR00002	Mean Difference (I-J)	Std. Error	Sig.	95% Confidence Interval	
						Lower Bound	Upper Bound
LSD	1	2	.2814*	.1203	.020	.045	.518
		3	.5083*	.1112	.000	.290	.727
	2	1	-.2814*	.1203	.020	-.518	-.045
		3	.2269*	.0712	.002	.087	.367
	3	1	-.5083*	.1112	.000	-.727	-.290
		2	-.2269*	.0712	.002	-.367	-.087
Bonferroni	1	2	.2814	.1203	.060	-.008	.571
		3	.5083*	.1112	.000	.241	.776
	2	1	-.2814	.1203	.060	-.571	.008
		3	.2269*	.0712	.005	.056	.398
	3	1	-.5083*	.1112	.000	-.776	-.241
		2	-.2269*	.0712	.005	-.398	-.056
*. The mean difference is significant at the 0.05 level.							